Heterogeneity of radial spokes structural components and associated enzymes in *Tetrahymena* cilia.

Running title: Heterogeneity of Tetrahymena radial spokes

Marta Bicka[1,2#], Corbin Black[3#], Avrin Ghanaeian[3#], Ewa Joachimiak[1], Anna Osinka[1], Sumita Majhi[1], Anna Konopka[4,5], Ewa Bulska[2,4], Khanh Huy Bui[3*], Dorota Wloga[1*]

1. Laboratory of Cytoskeleton and Cilia Biology, Nencki Institute of Experimental Biology of Polish Academy of Sciences, 3 Pasteur Street, 02-093 Warsaw, Poland
2. Faculty of Chemistry, University of Warsaw, 1 Pasteur Street, 02-093 Warsaw, Poland.
3. Department of Anatomy and Cell Biology, Faculty of Medicine and Health Sciences, McGill University, Montréal, QC, Canada.
4. Faculty of Chemistry, Biological and Chemical Research Centre, University of Warsaw, 101 Żwirki i Wigury Street, 02-089 Warsaw, Poland
5. Łukasiewicz Research Network - PORT Polish Center for Technology Development, 147 Stablowicka Street, 54-066 Wrocław, Poland

# equal contribution

*corresponding authors

Impact Statement

Identification of the subtypes of RS1 and RS2 spokes and RS1-3-specific RSPs. Discovery of the novel radial spoke structural components and RS-associated enzymes regulating ADP/ATP ratio and protein phosphorylation.

Keywords: radial spoke, label-free, TMT, mass spectrometry, cryo-ET, cilia, adenylate kinases, casein kinase, PKA

Abstract

Radial spokes (RS), the T-shaped, multiprotein complexes of motile cilia, transmit regulatory signals from the central apparatus to the outer doublet complexes, including inner dynein arms. In the vast majority of ciliated species, RSs assemble as repeats of triplets (RS1-RS2-RS3), and each spoke is associated with a different subset of inner dynein arms. Studies in *Chlamydomonas* and mice sperm flagella led to the identification of RS proteins (RSPs) and revealed that some structural components are either RS1- or RS2-specific. In contrast, the protein composition of RS3 remains largely unknown. We used the ciliate *Tetrahymena thermophila* to investigate the protein composition of individual RSs, including the poorly characterized RS3. The *Tetrahymena* genome encodes three RSP3 paralogs. Using engineered *RSP3* knock-out mutants and previously studied RS mutants with *CFAP61*, *CFAP91*, or *CFAP206* deletion and complementary approaches, including bioinformatics, total ciliome comparisons, and cryo-electron tomography with subtomogram averaging, we identified *Tetrahymena* RSP orthologs and solved the composition of individual RSs, showing their subunit heterogeneity. We found that RSP3 proteins are components of RS1 and RS2 but not RS3. Based on the presence of the RSP3 paralog, we distinguished sub-types of RS1 (RSP3A- or RSP3B-containing) and RS2 spokes (RSP3B- or RSP3C-containing). We identified novel RS-associated proteins, including several enzymes that may locally regulate ADP/ATP levels, GMP-recycling-related enzymes, and enzymes regulating phosphorylation levels. These discoveries will help to better understand the molecular mechanism(s) that regulate cilia beating and overall cilia metabolism.

Introduction

Motile cilia and homologous flagella are highly evolutionarily conserved, hair-like cell protrusions, supported by a microtubular skeleton, the axoneme, composed of nine peripheral doublets and two central singlets (9 x 2 + 2). The central microtubules, C1 and C2, together with attached complexes, the projections, form the central apparatus (CA), the structure believed to initiate signals required for planar cilia beating. Transient interactions between CA projections and outer doublet-docked radial spokes (RSs) enable transmission of regulatory signals to outer doublet complexes, including the nexin-dynein regulatory complex (N-DRC) and the motor protein-containing outer and inner dynein arms (ODAs and IDAs) (Grossman-Haham et al., 2021; Oda et al., 2014; Smith & Yang, 2004).

Radial spokes are T-shaped, approximately 40-nm long complexes with three morphologically distinct regions: an elongated elastic stalk docked to the axoneme, an orthogonal head, and a neck connecting the stalk and the head. Within the axonemal repeat unit, radial

66 spokes are arranged as triplets (RS1, RS2, RS3) within which the distance between the
67 neighboring spokes is specific to each spoke pair, enabling their identification (Goodenough &
68 Heuser, 1985). The architectures of RS1, RS2, and RS3 are not identical (Barber et al., 2012; Lin
69 et al., 2012, 2014; Pigino et al., 2011; Yoke et al., 2020). The most striking example of the RS
70 morphological diversity is a *Chlamydomonas* short, knob-like RS3, unfit to directly interact with
71 the CA (Lin et al., 2012; Pigino et al., 2011).

72 Pioneering studies using the *Chlamydomonas pf14* mutant carrying a mutation in the
73 *RSP3* gene (Williams et al., 1989) and lacking full-length spokes, RS1 and RS2, led to the
74 identification of radial spoke subunits, RSP1-RSP23 (Yang et al., 2001, 2006). The list of
75 *Chlamydomonas* RSPs was recently extended and most of the RSPs were assigned to RS1 and/or
76 RS2 spokes (Gui et al., 2021). The RS1 protein composition was also resolved for the murine
77 sperm axoneme (Zhang et al., 2022). However, despite the extensive research conducted using
78 diverse ciliated species, including *Chlamydomonas*, *Tetrahymena* (Urbanska et al., 2015;
79 Vasudevan et al., 2015), *Ciona intestinalis* (Padma et al., 2003; Satouh et al., 2005; Satouh &
80 Inaba, 2009), and mice (Guan et al., 2010; Zhang et al., 2021, 2022), the RS protein composition
81 is still not fully solved, especially that of RS3. The knob-like RS3 is present in the *pf14*
82 *Chlamydomonas* mutant (Lin et al., 2012; Pigino et al., 2011) and thus, its protein composition
83 was not resolved in earlier studies. In organisms where RS3 is a full-length spoke, its architecture
84 differs from that of RS1 and RS2 (Chen et al., 2023; Lin et al., 2012; Pigino et al., 2011). To date,
85 CFAP61 and CFAP251 are the only known RS3 components, building a part of the stalk and an
86 arch-like structure at the RS3 base, respectively (Urbanska et al., 2015). This raises a question
87 about the protein composition of this spoke.

88 The identification of RSPs and RSP-interacting proteins is crucial to understand the
89 mechanism(s) of signal transduction from the CA to dynein arms. Here, we used the existing
90 *Tetrahymena* knockout mutants with RS(s) defects (CFAP61-KO (Urbanska et al., 2015),
91 CFAP206-KO (Vasudevan et al., 2015), and CFAP91-KO) (Bicka et al., 2022), and newly
92 engineered mutants lacking RSP3 paralogs to decipher the protein composition of each RS in the
93 triplet by label-free and tandem mass tag (TMT) quantitative mass spectrometry of wild-type and
94 mutant ciliomes. Next, using co-immunoprecipitations and BioID, we verified that the identified
95 proteins are either the subunits of RS complexes or are present in their vicinity. These proteomic
96 approaches combined with cryo-electron tomography (cryo-ET) and subtomogram averaging
97 studies of the ultrastructural alterations in the RS mutants allowed us to assign with high
98 probability the substantial number of known RSPs and newly identified candidate proteins to
99 either RS1, RS2, or RS3. Importantly, among the newly identified proteins, we found not only

structural but also enzymatic proteins, including serine-threonine kinases, GMP recycling-related enzymes, adenylate kinases that dock to specific RSs, and an arginine kinase that locally controls the ATP level. We also noted a destabilization of some single-headed inner dynein arms in the analyzed RSP mutants.

As a result, we propose a model of the protein composition of *Tetrahymena* RSs showing both ubiquitous and RS-specific RSPs, new candidates of RS structural proteins, and RS-associated enzymes. The presence of spoke-specific RSPs agrees with structural differences among the individual RSs detected using cryo-ET (Lin et al., 2012; Pigino et al., 2011). Moreover, we found that in *Tetrahymena,* there are sub-types of RS1 and RS2 spokes, which further increases the heterogeneity of radial spokes. Together, obtained data contribute to a better understanding of the molecular mechanisms regulating planar cilia motion.

Results

Deletion of different RSP3 paralogs causes heterogeneous phenotypic and ultrastructural defects

The RSP3 dimer is the main component of RSs (Wirschell et al., 2008). It stretches from the RS base (N-terminal end) to the RS head (C-terminal end) and directly interacts with numerous RSPs (Gui et al., 2021; Oda et al., 2014). Comparative analyses of flagellar proteins purified from the wild-type and *pf14*, an RS1-RS2 spokes-less *Chlamydomonas* mutant (Yang et al., 2006) carrying a mutation in the *RSP3* gene (Williams et al., 1989) and cryo-EM studies combined with proteomics, and molecular modeling (Gui et al., 2021) yielded a model of RS1-RS2 protein composition in this green alga. We used a similar approach to decipher the protein composition of the *Tetrahymena* RSs. In contrast to *Chlamydomonas*, which has a single RSP3 gene, the *Tetrahymena* genome encodes three RSP3 proteins: RSP3A, RSP3B, and RSP3C (Figure 1A). RSP3C is unusual in having an N-terminal ARF (ADP-ribosylation factor) domain and a C-terminal region enriched in glutamic acids. Such unusual RSP3 orthologs were also found in the proteomes of *Paramecium*, *Ichthyophthirius*, and *Pseudocohnilembus* belonging to Oligohymenophorea.

Tetrahymena RSP3 proteins expressed as C-terminal 3xHA-tagged fusions under the control of native transcriptional promoters localize uniformly along the entire cilia length (Figure 1B-E). To explore whether the distribution of the three RSP3 paralogs differs between RS1, RS2, and RS3, we constructed knockout strains lacking single paralogs (Figure 2-figure supplement 1)

using a germ-line approach (Cassidy-Hanley et al., 1997; Dave et al., 2009). Compared to wild-type cells, RSP3 knockout cells swam significantly more slowly (Figure 2A-E). The loss of RSP3B had the most profound effect and reduced the swimming rate to ~12% of the wild-type rate while deletions of either *RSP3A* or *RSP3C* were less damaging (70% and 56% of the wild-type rate, respectively).

Tetrahymena cells are propelled by the forces generated by cilia beating as metachronal waves. The cilium beating cycle has two phases, the power and recovery strokes that occur in different planes in relation to the cell surface, perpendicular and parallel, respectively. During the power stroke the cilium is straight while during the recovery stroke it bends, and the bend position shifts from the cilium base to the tip as the recovery stroke progresses (Figure 2F) (Bazan et al., 2021; Bicka et al., 2022). Deletion of *RSP3A* did not apparently affect the ciliary waveform, beat amplitude (Figure 2F), and cilia metachrony (Figure 2-figure supplement 2). In contrast, cilia lacking RSP3B were beating in a less coordinated manner, with inconsistencies in the waveform and amplitude between neighboring cilia and between subsequent beating cycles performed by the same cilium (Figure 2F). Moreover, in the majority of RSP3B-KO cilia their distal part remained bent during the power stroke (Figure 2F). A delayed straightening of the distal end during the power stroke was also observed in cells lacking RSP3C. However, in contrast to RSP3B-KO mutant, in *RSP3C* knockout, cilia beat with metachrony and beating amplitude was only slightly reduced (Figure 2F and Figure 2-figure supplement 2).

Compared to cilia in wild-type cells, which beat with a frequency of 38.6+/-4.7 Hz, in *RSP3A* and *RSP3C* knockouts, the ciliary beating frequency was mildly reduced (on average 31.2+/-8.2 Hz and 31.9+/-5.7 Hz, respectively). In contrast, the loss of RSP3B reduced ciliary beating frequency nearly by half (25.6+/-5.8 Hz) (Figure 2G-H).

The differences in the RSP3 mutant phenotypes suggest that lack of the particular RSP3 paralogs likely results in different ultrastructural alterations. Indeed, cryo-ET and subtomogram averaging analyses of RSP knockout cilia revealed paralog-specific ultrastructural defects (Figure 3, Figure 3-figure supplement 1, and Figure 3-figure supplement 2). The RSP3A-KO mutant cilia frequently (~35% of the 96-nm axonemal units) lacked either the entire RS1 (~30%, n=639 units) or RS1 except for the RS1 base (~67%, n=1417) (Figure 3 and Figure 3-figure supplement 1). The RSP3B-KO cilia lacked the entire RS2 structure in all analyzed 96-nm axonemal repeats. Moreover, 77.5% of the axonemal repeats (n=1622) showed RS1 spoke defects and lacked either the entire RS1 (26%) or, more frequently, its distal fragment (51.5%) (Figure 3 and Figure 3-figure supplement 1). Surprisingly, RS2 was also impaired in the majority of RSP3C-KO

axonemal repeats, where it was either missing (20%) or only the RS2 base was well visible (62%). Thus, the RS2 head visible in the average image (Figure 3A) is due to the presence of intact RS2 spokes in 18% of the analyzed axonemal repeats (Figure 3 and Figure 3-figure supplement 1). Interestingly, in all RSP3 mutants, the RS3 structure was intact, strongly suggesting that neither of the RSP3 paralogs is a *Tetrahymena* RS3 component.

Taken together, the cryo-ET data suggest that in *Tetrahymena* there are at least two types of RS1 spokes: (i) RS1 type I containing RSP3A (spokes missing in RSP3A-KO cilia), making up approximately one-third of ciliary RS1 and (ii) RS1 type II, supported by RSP3B (missing in RSP3B-KO cilia), constituting approximately two-thirds of cilia RS1, and at least two types of RS2: (i) RS2 type I containing only RSP3B (3B-3B homodimer, intact RS2 spokes (18%) in RSP3C-KO cilia) and (ii) RS2 type II, having RSP3C in the stalk, likely as a heterodimer with RSP3B. However, we cannot exclude that some RS1 spokes can contain the RSP3A/RSP3B heterodimer or that RSP3A and RSP3B could partly substitute one another in the RS1 structure. Moreover, we cannot rule out that there is a minor fraction of RS2 containing the RSP3C homodimer. We must also keep in mind that in *Tetrahymena* the radial spokes' heads are connected and therefore the radial spokes may stabilize each other. Thus, some RS1 spokes could be destabilized in the RSP3B-KO mutant (secondary effect), as a moderate reduction in the level of RSP3A shown in global proteome comparisons (see below) coincided with the *RSP3B* deletion.

Identification of *Tetrahymena* radial spoke subunits by comparative mass spectrometry analyses of wild-type and RSP3 knockout ciliomes

To identify RS1, RS2, and RS3-specific components, we isolated cilia from wild-type cells, *RSP3* knockouts, and previously described *Tetrahymena* RSP knockouts: CFAP206-KO, missing either the entire RS2 or only its base, rarely accompanied by RS3 defects (Vasudevan et al., 2015), CFAP61-KO, lacking a part of the RS3 stalk (Urbanska et al., 2015), and CFAP91-KO frequently missing the RS3 and a part of the RS2 base (Bicka et al., 2022), and performed comparative proteomic mass spectrometry analyses using label-free and TMT 10-plex isobaric mass tagging approaches. The experiments were repeated three times to generate independent sets of data (at least 75% of proteins were present in all three replicas). Principal component analysis of the radial spokes mutant ciliomes using Ingenuity Pathway Analysis showed that the RSP3A-KO ciliome is most similar to the wild-type ciliome (Figure 4A). The changes in the protein levels were analyzed using Perseus software (v. 2.0.3) (Tyanova et al., 2016).

198 Approximately one-thousand ciliary proteins from wild-type cells and RSP mutants were
199 analyzed in LFQ experiments, while nearly four times more proteins were detected using the
200 TMT approach. To determine the significant differences in the abundance of ciliary proteins
201 between wild-type and knockout samples, we performed a t-test ($p < 0.05$) (Figure 4-Source Data
202 1', Figure 4-Source Data 2') and identified a number of proteins differentially abundant (with a
203 ±1.5-fold change) in knock-out mutants compared to the wild-type control. The obtained data are
204 graphically represented as Volcano plots -log (*P* value) *vs.* $\log_2$ (fold change of mutant/WT,
205 Figure 4A) and Venn diagrams (Figure 5). The analyses of the levels of the outer dynein arms,
206 two-headed, inner dynein arm IDAI1/f, tether/tetherhead complex, nexin-dynein regulatory
207 complex, and central apparatus components showed that these structures were generally
208 unaffected (Figure 4-Source Data 1', Figure 4-Source Data 2').

209 To support and validate the global proteome comparisons, we performed co-IP and BioID
210 assays followed by mass spectrometry analyses to identify ciliary proteins that either directly or
211 indirectly interact with well-evolutionarily conserved, HA-tagged RSPs (Figure 6-Source Data
212 1'), or are biotinylated in cilia of cells expressing RSPs fused with mutated biotin ligase, BirA*
213 (Figure 6-figure supplement 1, Figure 6-Source Data 2'). Next, we collated all proteomic data
214 with bioinformatics analyses and cryo-ET ultrastructural studies to assign known RSPs and newly
215 identified proteins to RS1, RS2, and RS3 spokes (Figure 6, Figure 6-figure supplement 3, and
216 Table 1).

217 *Localization of the RSP3 paralogs*

218 Changes in the RSPs levels in the analyzed mutants are presented in Figure 4-Source Data
219 1' and Figure 4-Source Data 2' and summarized in Figure 6, Figure 6-figure supplement 3, and
220 Table 1. Global mass spectrometry analyses of the RSP3A-KO, RSP3B-KO, and RSP3C-KO
221 axonemes confirmed that the protein encoded by the targeted gene was completely eliminated.
222 Moreover, the knockout of *RSP3A* or *RSP3C* did not affect the levels of other RSP3 paralogs
223 while in RSP3B-KO cilia the level of RSP3A was mildly reduced. The knockout of *CFAP61* has
224 no effect on the level of RSP3 paralogs while in CFAP91-KO and CFAP206-KO mutants, the
225 level of RSP3B and RSP3C were reduced, which agrees with the lack of RS2 spokes or part of
226 the RS2 base/stalk in these mutants (Bicka et al., 2022; Vasudevan et al., 2015). Thus, the
227 comparative mass spectrometry analyses of wild-type and mutant ciliomes support our hypothesis
228 that there are two types of RS1 spokes (with either RSP3A-RSP3A or RSP3B-RSP3B dimers).
229 The reduced RSP3A level in RSP3B-KO mutant cilia suggests either that in the absence of RS2,

230 some of the RSP3A-containing RS1 spokes are less stable or that some of RS1 spokes contain the
231 RSP3A-RSP3B heterodimer.

232 Based on the cryo-EM studies, we also hypothesized that the RS2 spokes contain either
233 the RSP3B-RSP3B homodimer or the RSP3B-RSP3C heterodimer (not excluding, however, the
234 possibility of the existence of the RSP3C-RSP3C homodimer). The comparative proteomic
235 analyses revealed that the level of RSP3B did not change in RSP3C-KO mutant cilia, suggesting
236 that in the absence of RSP3C, the RSP3B from the RSP3B-RSP3C heterodimer is still attached to
237 the axoneme without maintaining the T-shape RS2 structure (Figure 3-figure supplement 1).
238 However, the unaffected level of RSP3C (and RSP3C-associated RSPs, see Figure 6-figure
239 supplement 3) in RSP3B-KO mutant cilia missing all RS2 spokes is surprising. To sum up, we
240 found that RSP3B is a dominant *Tetrahymena* RSP3 paralog, roughly present in two-thirds of the
241 RS1 spokes and likely in all RS2 spokes.

242 The RSP3 dimer interacts with other RSPs, forming together the RS head, neck, and stalk
243 (Gui et al., 2021; Pigino et al., 2011; Yang et al., 2006). The bioinformatics analyses revealed
244 that the *Tetrahymena* genome encodes more than one ortholog of several RSPs (Table 1 and
245 Figure 6-figure supplement 3). Combined comparative ciliomes analyses, co-IP, and BioID
246 assays allowed us to assign the RSPs to individual RSs (Figure 6 and Tables 1 and 2). Of note,
247 the level of proteins that are the subunits of both RS1 and RS2 spokes in the RSP3A-KO mutant
248 can be below the significance threshold (a ±1.5-fold change), as only one-third of RS1 contains
249 the RSP3A paralog. Such proteins were assigned to RS1 based on the BioID data.

250 *The components of the Tetrahymena radial spoke stalk*

251 RSP8 and RSP14 are ARM-like (armadillo-like) motif-containing proteins. The level of
252 RSP8 was significantly reduced in mutants with RS2 defects (RSP3B-KO, RSP3C-KO, and
253 CFAP206-KO) but not in RSP3A-KO cilia, which lack a substantial portion of RS1 spokes. In
254 contrast, the level of RSP14 was reduced in mutants with RS1 defects, RSP3A-KO (RS1 type I)
255 and RSP3B-KO (RS1 type II), but was unchanged in RSP3C-KO or CFAP206-KO mutants with
256 only RS2 defects. The reduced level of RSP8 in mutants lacking RS2 and RSP14 in mutants
257 missing RS1 agrees with the BioID assays showing the biotinylation of RSP8 in cells expressing
258 RSP3B, RSP3C, or CFAP206 BirA* fusions and biotinylation of RSP14 in cells expressing either
259 RSP3A-HA-BirA* or RSP3B-HA-BirA*. Thus, RSP14 and RSP8 are RS1 and RS2 proteins,
260 respectively, which agrees with recent studies in *Chlamydomonas* (Gui et al., 2021) and murine
261 sperm axonemes (Zhang et al., 2022).

262 RSP7 and RSP11 form a heterodimer near RSP14 or RSP8 (Gui et al., 2021). The
263 *Chlamydomonas* RSP7, in addition to the RIIa domain (dimerization-anchoring domain of
264 cAMP-dependent PK regulatory subunit) at its N-terminus, also has several EF hand motifs in the
265 middle and C-terminal regions. A search of the *Tetrahymena* proteome using *Chlamydomonas*
266 RSP7 as a query revealed two proteins with a weak similarity to *Chlamydomonas* RSP7, RSP7A,
267 the 39 kDa protein containing N-terminal RIIa and C-terminal calmodulin-binding motif (IQ,
268 isoleucine, glutamine) and 66 kDa RSP7B with an AKA28 (A-kinase anchoring protein) domain
269 and two EF hands. The level of RSP7A was significantly reduced only in RSP3B-KO cells, but
270 RSP7A was biotinylated in cells expressing either of the RSP3 paralogs as BirA* fusions. In
271 contrast, the level of RSP7B was reduced in cilia lacking CFAP91. Accordingly, RSP7B was
272 poorly biotinylated in cells expressing RSP3 paralogs as BirA* fusions but detected by a higher
273 number of peptides among proteins biotinylated in CFAP61-HA-BirA* cilia, leading to the
274 conclusion that this is likely an RS3-associated protein. In *Tetrahymena,* RSP11 is a small (7.9
275 kDa) basic protein (pI = 9) with a predicted RIIa domain and limited similarity to
276 *Chlamydomonas* RSP11. The level of RSP11 was reduced in all RSP3 mutants.

277 RSP15/LRRC34 (leucine-reach repeat-containing) protein was previously described as an
278 RS2-specific protein in *Chlamydomonas* (Gui et al., 2021). Indeed, the *Tetrahymena* RSP15
279 ortholog was nearly completely eliminated or significantly reduced in mutants with RS2 defects,
280 in agreement with its RS2 localization.

281 In early radial spoke studies (Yang et al., 2001, 2006), the name RSP20 was assigned to
282 calmodulin and RSP22 to LC8 (cytoplasmic dynein light chain 2). In *Chlamydomonas* flagella,
283 calmodulin binds to FAP253 between RS1 and RS1-docked IDAs (Gui et al., 2021). In
284 *Tetrahymena,* the level of calmodulin RSP20/CaM1 was reduced in mutants with RS2 defects
285 (RSP3B-KO and RSP3C-KO) and was biotinylated in cells expressing RSP3B-HA-BirA*,
286 suggesting an association of CaM1 with RS2 and perhaps RSP3B-containing RS1. On the other
287 hand, the RS1 base containing CFAP253 is preserved in RSP3A-KO mutants, and thus, we
288 cannot exclude the possibility that CaM1 is also an RS1 type I protein. Interestingly, the so-called
289 calmodulin 7-2 was moderately reduced in cells with *RSP3A* or *RSP3C* deletion, suggesting that
290 this calmodulin-type protein is the RS1 type I (RSP3A-containing) and RS2 type II (RSP3C-
291 containing) component.

292 In *Chlamydomonas* flagella, RSP22/LC8 is associated with RS1 (four homodimers) and
293 RS2 (two homodimers) (Gui et al., 2021). *Chlamydomonas* RSP22/LC8 is most similar to
294 *Tetrahymena* LC8, a protein reduced in RSP3B-KO cilia. Based on BioID assays, this protein is

295 likely positioned in the vicinity of all RSP3 orthologs, CFAP206, and CFAP91, suggesting an
296 association with both RS1 and RS2. It was recently proposed that RS stalks dock to the LC8
297 multimers (Gui et al., 2021). Thus, it is possible that some RSP22/LC8 multimers remain
298 associated with the axoneme in *Tetrahymena* RSP3A and RSP3C mutants. Indeed, the
299 subtomogram average of *Tetrahymena* RSP3A-KO and RSP3C-KO cilia revealed that the spoke
300 base remained associated with tubule A (Figure 3 and Figure 3-figure supplement 1), which
301 explains why the level of LC8 was not reduced in these mutants.

302 Recent studies have led to the identification of additional RSPs. FAP207, a MORN motif-
303 containing protein, localizes at the RS1 and RS2 base, and the IQ motif-containing FAP253,
304 orthologous to *Ciona* CMUB116 (Zhu et al., 2017) and murine IQUB (Zhang et al., 2022), is an
305 RS1 adaptor protein (Gui et al., 2021; Zhang et al., 2022). *Tetrahymena* CFAP253 and
306 *Chlamydomonas* FAP253 are smaller than their mammalian orthologs and lack the ubiquitin
307 homolog domain predicted in IQUB. The level of *Tetrahymena* CFAP253 was unaltered in all
308 studied mutants, but CFAP253 was biotinylated in cells expressing RSP3A or RSP3B fused with
309 BirA*. Thus, CFAP253 is likely an RS1 adaptor also in *Tetrahymena* cilia. The *Tetrahymena*
310 genome also encodes one ortholog of FAP207 (Table 1 and Figure 6-figure supplement 3). The
311 level of *Tetrahymena* CFAP207 was significantly reduced in cells with RS2 defects (except for
312 RSP3C-KO cilia, where the RS2 base is present) but not in RSP3A-KO cilia (the RS1 base is also
313 maintained in RSP3A-KO cilia).

314 *The components of the Tetrahymena radial spoke head*

315 The RS head consists of two identical lobes connected by an RSP16 dimer. In
316 *Chlamydomonas,* each lobe is composed of RSP4 and RSP6 (paralogous proteins), RSP5, RSP9,
317 the MORN motif-containing RSP1 and RSP10, a fragment of the neck protein, RSP2, and a C-
318 terminus of RSP3 (Gui et al., 2021; Pigino et al., 2011; Yang et al., 2006). The *Tetrahymena*
319 genome encodes three paralogs of RSP4/RSP6: RSP4A, RSP4B, and RSP4C, and single
320 orthologs of RSP1, RSP9, and RSP10. The identification of RSP1 and RSP10 orthologs was
321 possible only by a combination of bioinformatics and proteomic data, as the *Tetrahymena*
322 genome encodes 129 proteins containing MORN motifs (Habicht et al., 2015). Only two of those
323 proteins, named here RSP1 and RSP10, were identified among proteins that co-
324 immunoprecipitated with HA-tagged RSP4 and were biotinylated in BioID assays. A blastp
325 search with *Chlamydomonas* RSP1 or RSP10 as a query revealed that *Tetrahymena* RSP1 and
326 RSP10 are more similar to *Chlamydomonas* RSP10 than RSP1.

327 The levels of RSP1, RSP9, and RSP10 were significantly reduced only in RSP3B-KO
328 lacking all RS2 and two-thirds of RS1. The levels of several other MORN domain proteins,
329 similar to RSP1/10, were also altered in the ciliomes of the analyzed mutants, but none of them
330 was detected in either co-IP or BioID assays (Figure 6-figure supplement 3). Thus, it is unlikely
331 that these other MORN domain-containing proteins are RS head components.

332 The loss of RSP3B coincided with the reduced levels of RSP4A and RSP4C, while the
333 level of RSP4B was reduced in cilia of *RSP3C* and *CFAP91* knockout mutants. Moreover,
334 RSP4A and RSP4C were biotinylated in RSP3A-HA-BirA*- and RSP3B-HA-BirA*-expressing
335 cells, while RSP4B was biotinylated in RSP4A-HA-BirA*-expressing cells. We propose that the
336 head of RSs containing either RSP3A or RSP3B as a stalk component is composed of RSP:1, 4A,
337 4C, 9, and 10, while RS2 spokes containing RSP3C likely have RSP4B instead of RSP4C in the
338 head. These conclusions must be considered with caution, as in *Tetrahymena,* the RS heads are
339 connected (Lin et al., 2012; Pigino et al., 2011), and thus, a subunit of one spoke expressed as a
340 BirA* ligase fusion could biotinylate proteins not only within the same spoke head but also of the
341 adjacent spoke.

342 A search of the predicted *Tetrahymena* proteome with *Chlamydomonas* RSP5 aldo-keto
343 reductase as a query failed to identify an ortholog. Among proteins annotated as aldo-keto
344 reductases in the Tetrahymena Genome Database (TGD), thirteen were found in our *Tetrahymena*
345 ciliomes, and four were significantly reduced in the *RSP3* knockouts. However, these proteins did
346 not co-precipitate with RSPs and were not biotinylated in cilia of *Tetrahymena* cells expressing
347 RSP-BirA* fusions (Table 1 and Figure 6-figure supplement 3). The human genome also lacks
348 *RSP5*. It is likely that RSP5 is a *Chlamydomonas* and related algae-specific protein.

349 *The components of the Tetrahymena radial spoke neck*

350 In *Chlamydomonas*, the V-shaped radial spoke neck is composed of RSP2, RSP12,
351 RSP16, RSP23/FAP67, FAP198, and FAP385 (Gui et al., 2021). *Tetrahymena* has single
352 orthologs of RSP2 and RSP23, two paralogs of RSP16, (RSP16A and RSP16B), CFAP198,
353 (CFAP198A and CFAP198B), and RSP12 (RSP12A and RSP12B), but lacks FAP385.

354 *Tetrahymena* and *Chlamydomonas* RSP2 and RSP23/FAP67B proteins are similar only
355 within the N-terminal regions containing DPY-30 and NDK (nucleoside diphosphate kinase)
356 domains, respectively. RSP2 is likely a component of RS1 and RS2, as its level was reduced in
357 both RSP3A and RSP3B knockouts (Tables 1 and 2). The level of RSP23/CFAP67B was not
358 significantly altered in the analyzed mutants, but it was identified in co-IP and BioID assays. In
359 addition to RSP23/CFAP67B, the *Tetrahymena* genome encodes CFAP67A

360 (TTHERM_00266490), with a high similarity to *Chlamydomonas* RSP23. CFAP67A was
361 detected neither in co-IP nor BioID assays. Based on recent single-particle cryo-EM and
362 molecular modeling studies, FAP67 (likely CFAP67A) is an A-tubule MIP protein (Kubo et al.,
363 2023). Thus, we propose that RSP23/CFAP67B is, similar to in *Chlamydomonas*, an RS1 and
364 RS2 component.

365 The level of RSP16A was significantly reduced in cells with deletion of *RSP3A* or *RSP3B,*
366 while the RSP16B level was diminished in cells with deletion of *RSP3C*, *CFAP206,* and
367 *CFAP91*. The presence of RSP16A and 16B in RS1 and RS2 is also supported by BioID data.

368 *Chlamydomonas* FAP198 docks near RSP14/RSP8 stalk proteins (Gui et al., 2021). In
369 *Tetrahymena,* the level of CFAP198A was significantly reduced in *RSP3A* and *RSP3B* knockouts,
370 while CFAP198B was reduced in cells with *RSP3C* deletion, suggesting that CFAP198A is a
371 component of RS1 and RSP3B-containing RS2, while CFAP198B is a subunit of RSP3C-
372 containing RS2. Importantly, both CFAP198A and B were identified in co-IP (CFAP198A) and
373 BioID assays (both paralogs).

374 The *Tetrahymena* genome encodes 15 proteins similar to RSP12, the peptidyl-prolyl cis-
375 trans isomerase. Among the seven that were identified in the *Tetrahymena* ciliome, two are
376 RSP12 candidates. TTHERM_01018330 (RSP12A) could be an RS2 component, as its level was
377 reduced in cilia with RS2 defects (RSP3B-KO, RSP3C-KO, CFAP206-KO). RSP12A was also
378 reduced in CFAP91-KO cells; however, it is not clear whether the detected reduction is due to
379 RS2 elimination or RS3 defects. The level of the isomerase encoded by TTHERM_00466090
380 (putative RSP12B) was reduced in cells lacking RSP3A or RSP3B. Both proteins were detected
381 in BioID assays by a very limited number of peptides.

382

383 **New radial spoke candidate proteins**

384 The global comparative proteomic analyses led to the identification of several proteins,
385 the candidate RSPs or proteins positioned in the RS vicinity (Table 1 and Figure 6-figure
386 supplement 3). The levels of two tetratricopeptide repeat (TPR)-containing proteins, TtTPR1 and
387 TtTPR2, were reduced in mutants lacking RS2, TtTPR1 in *RSP3C* knockout and TtTPR2 in
388 *RSP3B* knockout. TtTPR1 was found among biotinylated proteins in the BioID assays, while
389 TtTPR2 appeared once in a co-IP. Kelch repeat-containing proteins are involved in various
390 biological processes (Gupta & Beggs, 2014). The level of Kelch repeat-containing protein 1
391 (Kelch1) was diminished in the CFAP91-KO mutant. In agreement, the BioID and co-IP data also

392 suggest that Kelch1 is an RS3 protein. Kelch2 was reduced in *RSP3B* and *CFAP206* knockouts,
393 suggesting its association with RS2 spoke.

394 The levels of two leucine-rich repeat-containing (LRRC) proteins similar to LRRC23,
395 LRRC23-like 1 and LRRC23-like 2, were reduced in CFAP91-KO cilia but unchanged in *RSP3*
396 mutants, suggesting their association with RS3 spoke. The level of LRRC23-like 2 was also
397 reduced in the CFAP61-KO mutant lacking only a fragment of the RS3 stalk but having a neck
398 and a head. Thus, LRRC23-like 2 could be a component of the RS3 stalk. It was recently reported
399 that LRRC23 is a subunit of the RS3 head in human and mouse sperm (Hwang et al., 2023).
400 Thus, LRRC23-like 1 is likely a conserved component of RS3. The level of another LRRC
401 protein, TTHERM_01084360, was reduced in cilia lacking RSP3B, CFAP206 or CFAP91,
402 suggesting its presence in the RS2 vicinity. Interestingly, a protein with similarity to human
403 LRRC45 (TTHERM_01220370) was found in both RSP precipitates and among biotinylated
404 proteins, but its level in RSP mutant cilia was similar to that in the wild type, suggesting that
405 LRRC45 is not a component of the RSs but is positioned in the RS vicinity.

406 We also found that the level of TTHERM_00557860 protein with the coiled-coil domain,
407 orthologous to human CCDC104/FAP36/BARTL1, recently shown to be an Arl3-binding protein
408 in the primary cilia (Lokaj et al., 2015), was also altered in RS mutants. The putative CCDC104
409 ortholog was poorly biotinylated in BioID assays, and its role or precise localization in cilia
410 requires further analyses.

411

412 **Radial spoke-associated proteins with enzymatic activity**

413 *ATP homeostasis*

414 The ultrastructural defects in RS mutant cilia are accompanied by changes in the levels of
415 a number of enzymes (Table 1 and Figure 6-figure supplement 3), suggesting that RSs serve as
416 enzyme docking sites. Dynein arm motor activity requires a constant supply of ATP and its
417 uniform distribution within the entire cilium. ATP is both delivered to cilia from the cell body by
418 diffusion and produced within cilia (Villar et al., 2017). The levels of several enzymes involved
419 in ATP homeostasis were altered in radial spoke mutants.

420 Enolase 1 (ENO1) and pyruvate kinase 1 (PYK1) are glycolytic enzymes that catalyze
421 two final steps resulting in ATP synthesis. The levels of both enzymes were reduced in *RSP3B*
422 and *CFAP61* knock-outs (ENO1 also in CFAP91-KO). Intriguingly, the reduction of the ENO1
423 and PYK1 levels was also reported in the *Tetrahymena* central apparatus mutants, with the

424 deletion of either *SPEF2A* or *CFAP69* genes encoding subunits of the C1b projection
425 (Joachimiak et al., 2021).

426 Adenylate kinases and phosphagen kinases can serve as ATP-shuttles and locally control
427 ATP levels. Phosphagen kinases (creatine kinase in vertebrates, arginine kinase in *Tetrahymena*)
428 catalyze the reversible transfer of the phosphate group from ATP to a guanidine substrate. The
429 *Tetrahymena* genome encodes two arginine kinases, AK1 and AK2 (Michibata et al., 2014; Uda
430 et al., 2006). The levels of ~40 kDa AK1 and ~80 kDa AK2 were reduced in RS mutants except
431 for RSP3A-KO. ENO1, PYP1, AK1, and AK2 were not identified in co-IP or BioID assays.

432 Adenylate kinases reversibly catalyze the ATP+AMP↔ADP reaction and thus locally
433 control the ATP level and maintain the homeostasis of adenine nucleotides (Dzeja & Terzic, 2009).
434 The levels of at least six adenylate kinases (types 1, 7, 8, and 9) were changed in the cilia of
435 *Tetrahymena* RS mutants. Importantly, adenylate kinases were also found among proteins that
436 either co-immunoprecipitated with RSPs and/or were biotinylated in cilia of cells expressing
437 RSPs fused with mutated BirA* ligase. Thus, adenylate kinases are likely radial spoke-associated
438 proteins, while changes in the levels of arginine kinase 2, ENO1 and PYK1 may reflect more
439 general changes in cilia physiology.

440 The level of AK8B adenylate kinase was dramatically reduced in RSP3A-KO cilia, while
441 kinases AK7B and AK9 (and to a lesser extent, AK7A) were nearly completely eliminated in
442 cilia of the CFAP91-KO mutant but unaltered in RSP3 mutants. Thus, RS1 is likely the main
443 docking site for AK8B, while AK7A, AK7B, and AK9 preferentially associate with the RS3
444 spoke or its vicinity. AK1 and AK8A are likely associated with RSP3B-containing spokes, as
445 their levels were significantly reduced in cilia of RSP3B-KO but not RSP3A-KO or RSP3C-KO
446 mutants. With the exception of AK7B, AK8B, and AK9, which were either completely missing
447 or substantially reduced in the analyzed mutants, the levels of other adenylated kinases were only
448 moderately reduced, suggesting that in addition to radial spokes, AK1, AK7A, and AK8A likely
449 associate with other ciliary structures.

450 *cGMP-related enzymes*

451 Of the two *Tetrahymena* guanylate kinases, GK1 is present in the *Tetrahymena* ciliome.
452 Guanylate kinase catalyzes the transfer of phosphate from ATP to GMP, producing GDP and
453 ADP. The phosphorylation of GDP to GTP is catalyzed by nucleoside-diphosphate kinases
454 (NDK), and GTP can be converted to cGMP by guanylate cyclase, while 3'5'-cyclic nucleotide
455 phosphodiesterase (PDE) hydrolyzes cGMP (Muthaiyan Shanmugam et al., 2018; Wyatt, 2015;
456 Wyatt et al., 1998). The levels of GK1 and PDE (similar to AK9) were dramatically reduced in

457 CFAP91-KO cilia (PDE also in CFAP61-KO) but not in RSP3 mutants. Moreover, GK1 co-
458 immunoprecipitated with an RS3 base protein, CFAP251. Thus, GK1 and PDE are likely RS3-
459 associated enzymes, and cGMP could play a role in signal transduction in the vicinity of RS3.
460 The RSP23 protein contains NDK domains (Patel-King et al., 2004); however, its level did not
461 significantly change in the analyzed mutants. Interestingly, we identified another protein
462 containing an NDK domain (TTHERM_000160999) whose level was reduced in cilia lacking
463 RSP3B or RSP3C.

464 Early analyses of ciliary beating using another ciliate, *Paramecium,* as a model showed
465 that cyclic nucleotide monophosphate-driven chemical signaling controls ciliary beating (Bonini &
466 Nelson, 1988; Hemmersbach et al., 1998; Noguchi et al., 2004). Thus, the immobility of the CFAP91-
467 KO mutants might be caused not only by the lack of RS3 and some IDAs (Bicka et al., 2022) but
468 also by the perturbation of guanidine nucleotide homeostasis.

469

470 *Serine/threonine protein kinases*

471 Comparative global proteomic analyses also revealed that the levels of three
472 serine/threonine kinases, casein kinase 1 (CK1), calcium/calmodulin-dependent protein kinase,
473 and cAMP-dependent protein kinase (PKA), were altered in radial spoke mutants. In
474 *Chlamydomonas,* CK1 docks to outer doublets and regulates the phosphorylation of IC138, the
475 IDAI1/f intermediate chain (Yang & Sale, 2000). In *Tetrahymena*, the level of CK1 was reduced in
476 CFAP91-KO and CFAP61-KO cilia, suggesting its association with RS3 spoke. The presence of
477 CK1 in the RS3 vicinity was confirmed by co-IP and BioID studies; however, it is unlikely that
478 RSs are the sole CK1 docking site.

479 The RSP3 protein has an AKAP domain (A-kinase anchoring domain) (Gaillard et al.,
480 2001) and thus locally regulates PKA localization and activity by restricting access to substrates.
481 In *Chlamydomonas,* disruption of the RSP3 AKAP domain affects the activity of cAMP-
482 dependent protein kinase (PKA) and causes abnormal flagellar motility (Gaillard et al., 2006).
483 PKA functions as a tetramer composed of two regulatory and two catalytic subunits (Scott &
484 Pawson, 2009). The levels of two PKA catalytic subunits, TTHERM_00433420 and
485 TTHERM_00658860, and a regulatory subunit (TTHERM_00623090) were reduced in RS2
486 mutants.

487 The level of calcium/calmodulin-dependent protein kinase was apparently diminished in
488 mutants with RS2 defects and in CFAP91-KO cilia, suggesting a role of RS2 and perhaps RS3 in
489 calcium/calmodulin-dependent signaling.

490 Interestingly, at least some RSPs are present in cilia in more than one isoform (2-
491 dimensional analyses of the HA-tagged RSPs, Figure 6-figure supplement 2 and) (Bicka et al.,
492 2022)). It is tempting to speculate that some RSPs undergo phosphorylation and that the
493 phosphorylation status controls other protein binding and/or signal transduction.

494

495 **Radial spoke defect-related instability of inner dynein arms**

496 Single-headed inner dynein arms (IDA) are docked in pairs at the radial spoke base,
497 dynein a and b at RS1, c and e at RS2, and d and g at RS3. They are composed of IDA type-
498 specific dynein heavy chain (DYH), actin, and centrin (dyneins b, e, g) or light chain protein, p28
499 (dyneins a, c, d) (Yamamoto et al., 2021). The comparative global proteomic analyses revealed
500 that the deletion of genes encoding the components of the RS stalk also affected the levels of
501 some IDAs (Table 2). The level of DYH9 was reduced in RSP3A-KO cells, while the levels of
502 DYH10, 12, and 25 were decreased in the RSP3B-KO mutant, which coincides with the lack of
503 dynein c density in the 96-nm subtomogram averaged map of RSP3B-KO cilia. The levels of
504 DYH10, 12, and 25 were also reduced in CFAP206-KO, specifically missing dynein c
505 (Vasudevan et al., 2015), and in CFAP91-KO mutants (Bicka et al., 2022), further supporting the
506 assumption that these dynein heavy chains are the components of dynein c. The most frequent
507 ultrastructural defect in *Tetrahymena* CFAP91-KO mutant cilia is a lack of RS3. As we
508 previously reported, in addition to DYH10, 12, and 25, the levels of DYH16, 22, and 24 are
509 moderately reduced in CFAP91-KO cilia (Bicka et al., 2022), suggesting that these dynein heavy
510 chains are components of IDAd or IDAg.

511 *Tetrahymena* has three orthologs of the single-headed IDA light chain protein p28: p28A,
512 p28B, and p28C (Subramanian et al., 2016). The level of p28B was reduced in cells lacking
513 RSP3B and CFAP206, which agrees with p28B being a dynein c subunit (Yamamoto et al.,
514 2021). In CFAP91-KO cilia, not only was the level of p28B reduced (Bicka et al., 2022) but also
515 that of p28A, suggesting that p28A is a main component of dynein d (Yamamoto et al., 2021).
516 The above data provide further experimental evidence regarding the protein composition of
517 single-headed IDAs and show a heterogeneity of the protein composition of IDAs of a particular
518 type (three different dynein heavy chains can be a component of IDAc). This raises a question
519 about the biological significance of such diversity. Interestingly, in both RS2 mutants (RSP3B-
520 KO and CFAP206-KO), only dynein c is missing (Vasudevan et al., 2015) and this work),
521 suggesting differences in the docking of dynein c and dynein e at the RS2 base.

522

523 **Discussion**

524 Radial spokes are important links in the signal transduction chain from the central
525 apparatus to the dynein arms. Here, using bioinformatics, proteomic and cryo-ET approaches, we
526 were able to define a large part of the protein composition of the individual RSs in the ciliate
527 *Tetrahymena* (Figure 6). In contrast to other studied organisms assembling motile cilia or
528 flagella, the genome of *Tetrahymena* encodes more than one ortholog of several RSP genes
529 (RSP3, RSP4/6, RSP7, RSP12, RSP16, CFAP198). This finding agrees with the *Tetrahymena*
530 genome analyses revealing duplication of some genes encoding proteins involved in sensing or
531 structural complexity (Eisen et al., 2006).

532 Immunofluorescence analyses revealed that *Tetrahymena* RSP3 and RSP4/6 paralogs are
533 uniformly distributed along the entire cilium length. However, they are components of RSs of a
534 specific type. Strikingly, in *Tetrahymena,* the differences in protein composition are not only
535 between RS1, RS2, and RS3 spokes, as was shown earlier in *Chlamydomonas* (Gui et al., 2021)
536 and mouse sperm axonemes (Zhang et al., 2022) but also within the group of RS1 and RS2
537 spokes. *Tetrahymena* likely has at least two types of RS1 (type I containing RSP3A and type II
538 having RSP3B homodimers) and likely two types of RS2 spokes (type I containing RSP3B
539 homodimer and type II with RSP3B-RSP3C heterodimer). At the moment, we cannot exclude the
540 possibility that the RSP3A and RSP3B proteins also form heterodimers and that RSP3C can form
541 homodimers. Interestingly, deletion of CFAP206 has a stronger impact on the level of RSP3C
542 than RSP3B, while the level of CFAP206 is unaltered in RSP3C-KO but significantly reduced in
543 RSP3B-KO, suggesting that RSP3C docks to CFAP206, which in turn binds to RSP3B. We have
544 also found that some RSPs associate with a specific RSP3 paralog, further increasing RS
545 diversity and suggesting co-evolution of some RSPs. Thus, the *Tetrahymena* cilium is a mosaic
546 of RS1 and RS2 spokes composed of different RSP3 paralogs. At present, the significance of RS1
547 and RS2 heterogeneity is unknown.

548 The RS head transiently interacts with CA projections. These interactions can be
549 mechano-chemical (Oda et al., 2014) and electrostatic in nature (Grossman-Haham et al., 2021).
550 The very C-terminal end of RSP3C, compared to the RSP3A and RSP3B proteins, is enriched in
551 glutamic acid residues that increase the RS head surface negative charge. If the RSP3C C-
552 terminal end, similar to the *Chlamydomonas* RSP3 tail, is a part of the radial spoke head, its
553 presence increases the negative charge of the head surface and thus might strengthen the
554 electrostatic interactions with CA projections. Thus, the incorporation of RSP3C into the RS2
555 structure could locally strengthen the interactions between the RS and the CA projection(s).

556 Interestingly, the N-terminal part of RSP3C is also unusual in having an ARF domain, which
557 could play a role in signaling.

558 The analyses of the proteins biotinylated in cells expressing RSPs-BirA* fusions revealed
559 the presence of several CA proteins (Figure 6-Source Data 2'), suggesting close proximity
560 between the projections and the RSs. In particular, numerous peptides were those of two proteins,
561 CFAP46 and CFAP54, the components of the C1d projection, which is surprising, as C1d is not
562 the longest projection. This unexpected result calls for further studies.

563 The presented proteomic data clearly indicate that the lack of specific RSP3 protein
564 causes not only destabilization of certain RSs but also affects the stability of specific IDAs, the
565 receivers and effectors of transduced regulatory signals and perhaps other minor
566 structures/linkers/proteins positioned in the RS vicinity. In cells with knocked out *RSP3B*, only
567 one of two IDAs docked at the RS2 base, IDAc, is missing. These data strongly suggest that the
568 docking of two IDAs, IDAc and IDAe, at the RS2 base is different. Moreover, comparative
569 proteomic analyses of wild-type and RSP3B-KO cilia enabled the identification of dynein heavy
570 chains that are components of IDAc.

571 The global comparative analyses of wild-type and RS mutant ciliomes led to another
572 interesting discovery – the identification of several enzymes that likely dock to specific RSs.
573 Among them are (i) adenylate kinases that together with arginine kinase locally regulate ATP
574 homeostasis, (ii) enzymes involved in GMP recycling, and (iii) serine-threonine kinases that
575 could play a role in the control/regulation of RS-mediated signal transduction. Thus, the
576 phenotypic outcome of the deletion of genes encoding RS structural proteins is not simply a
577 consequence of the radial spokes ultrastructural alterations but also of the alterations of the IDAs,
578 linkers, and changes of the level of nucleotide, Ca2+/calmodulin, and protein phosphorylation-
579 mediated signaling as well as the accessibility of the ATP-stored energy.

580

581 **Materials and Methods**

582 **Cell growth conditions and phenotypic analyses**

583 *Tetrahymena* cells were grown to the mid-log phase with shaking (80-110 rpm) at 30 °C. Wild-
584 type cells and motile mutants were cultured in a standard SPP medium (Gorovsky et al., 1975),
585 while mutants with major ciliary defects were grown in a rich MEPP medium (Orias & Rasmussen,
586 1976), both supplied with an antibiotic-antimycotic mix (Sigma-Aldrich, St. Louis, MO, USA) at
587 1:100 (SPP) or 1:50 (MEPP). The measurements of the cell swimming rate and the analyses of

588 cilia beating (amplitude, waveform and frequency) were described in detail (Bicka et al., 2022).
589 Briefly, for swimming rate analyses, cells at a density of 10^4 cells/mL were viewed and recorded
590 at room temperature using a Zeiss Discovery V8 Stereo microscope (Zeiss, Oberkochen,
591 Germany) equipped with a Zeiss Plans 10_ FWD 81 mm objective, and an Axiocam 506 camera
592 and ZEN2 (blue edition) software. The length of the trajectories was measured using ImageJ
593 software. To analyze cilia beating, cells at a density of 10^5 cells/mL were cultured at room
594 temperature for 3 hours, and beating cilia were recorded using a Phantom Miro C110 high-speed
595 camera (Vision Research, Wayne, NJ, USA) mounted on an AXIO Imager M2 microscope
596 (Zeiss, Germany) with either a 40 x oil immersion lens (analyses of cilia beating frequency) or a
597 63x oil immersion lens (numerical aperture 1.4, analyses of ciliary waveform). Videos were
598 recorded at 900 frames/s and analyzed using ImageJ as described (Bicka et al., 2022).

599 **Knock-ins and knock-outs**

600 Engineering and phenotypic analyses of *Tetrahymena* mutants with deleted *CFAP61* (Urbanska
601 et al., 2015), *CFAP206* (Vasudevan et al., 2015), or *CFAP91* (Bicka et al., 2022) were described.
602 The RSP3 genes' fragments used to obtain knock-out and knock-in transgenes were amplified by
603 PCR with the addition of restriction sites using high-fidelity polymerase and the appropriate
604 primers listed in Table S1. To delete fragments of the RSP3 genes, approximately 1.2-1.5 kb
605 fragments positioned upstream and downstream of the targeted gene fragment were amplified and
606 cloned subsequently on both sites of the neo4 resistance cassette (Mochizuki, 2008).
607 Approximately 60 µg of plasmid was digested with ApaI and SacII to separate the transgene from
608 the plasmid backbone, precipitated onto gold particles and used to transform conjugating
609 *Tetrahymena* cells. Transformed cells were processed as described (Cassidy-Hanley et al., 1997;
610 Dave et al., 2009). The deletion of the targeted fragments was confirmed by PCR.

611 To express RSP proteins as fusions with C-terminal either -3HA or –HA-BirA* tag under
612 the control of a respective gene promoter, approximately 1 kb fragments of the open reading
613 frame without the stop codon and 1 kb fragment of the 3'UTR were amplified and cloned into
614 CFAP44-3HA-neo4 or CFAP44-HA-BirA*-neo4 plasmids, respectively (Urbanska et al., 2018)
615 to replace CFAP44 gene fragments. On average, 10-15 µg of plasmid was linearized with MluI
616 and XhoI, precipitated onto gold, and used to transform CU428 cells.

617 **Immunofluorescence**

618 To localize HA-tagged RSPs, cells from the overnight culture were fixed on coverslips with a
619 mix of 0.25% Triton-X-100 and 4% PFA in a PHEM buffer. After drying and blocking, cells
620 were stained overnight with a mix of primary antibodies, monoclonal anti-HA antibody

621 (BioLegend, San Diego, CA, USA) diluted 1:300 and 6-11 B1 (Sigma-Aldrich), an anti-
622 acetylated α-tubulin antibody (1:2000) at 4 °C. After washing with PBS, samples were stained for
623 1.5 h at RT with a mix of the secondary antibodies, anti-mouse or anti-rabbit IgG, conjugated
624 with either Alexa-488 or Alexa-555 (Invitrogen, Eugene, OR, USA) diluted 1:300. Coverslips
625 were mounted in Fluoromount-G (Southern Biotech., Birmingham, AL, USA). Cells were
626 recorded using either a Zeiss LSM780 (Carl Zeiss Jena, Germany) or a Leica TCS SP8 (Leica
627 Microsystems, Wetzlar, Germany) confocal microscope.

628 **Cryo-ET preparation**

629 The axonemes for cryo-ET were cross-linked with glutaraldehyde (final concentration 0.15%) for
630 40 min on ice and quenched with 35 mM Tris pH 7.5. The axoneme solution at 3.6 mg/mL was
631 mixed with 5 (Cytodiagnostics) or 10 (Aurion) nm gold beads in a 1:1 ratio for a final axoneme
632 concentration of 1.8 mg/mL. Inside the Vitrobot Mk IV (Thermo Fisher) chamber, 4 µl of
633 crosslinked axoneme sample was applied to negatively glow discharged (10 mA, 10 s) C-Flat
634 Holey thick carbon grids (Electron Microscopy Services #CFT312-100). The sample was
635 incubated at 23 °C and 100% humidity for 45 seconds on the grid, followed by 8 seconds of
636 blotting with force 0 and plunge frozen in liquid ethane.

637 **Cryo-ET acquisition and reconstruction**

638 Tilt series were collected using the dose-symmetric scheme from -60 to 60 degrees with an
639 increment of 3 degrees at 2.12 Å per pixel using a Titan Krios equipped with Gatan K3 and
640 BioQuantum energy filter. The acquisition was performed using SerialEM (Mastronarde, 2005).
641 The defocus for each tilt series ranges from -2.5 to -6 µm. The total dose for each tilt series is 120
642 to 160 e- per Å2. For each view, a movie of 10-13 frames was collected. Motion correction of
643 each view was performed with Alignframes (Mastronarde & Held, 2017). Tomograms were
644 reconstructed using IMOD (Kremer et al., 1996).

645 **Subtomogram Averaging**

646 CTF estimation for each tilt series was performed with WARP (Tegunov & Cramer, 2019). The
647 doublet microtubule for subtomogram averaging was picked using IMOD by tracing the line
648 along the microtubules (Kremer et al., 1996). Subtomogram averaging of the 4-times binned 96
649 nm repeating unit of WT and mutant strains was performed using the "axoneme align" program
650 (Bui & Ishikawa, 2013). The subtomogram coordinates and alignment parameters were converted
651 to Relion 4.0 for local refinement and classification (Kimanius et al., 2021). The resolutions for
652 the 96-nm repeating unit of the axoneme of wild type, *RSP3A-KO*, *RSP3B-KO*, and *RSP3C-KO*

653 are 18, 20, 22, and 17 Å, respectively. Axonemal repeats from *RSP3A* and *RSP3B* mutants
654 showed strong heterogeneity in the occurrence of RS1 and RS2. To analyze the heterogeneity of
655 the mutant strains, three-dimensional (3D) classification without alignment was performed in
656 Relion by masking RS2 and RS1. The axoneme of the *RSP3C* mutant strain showed
657 heterogeneity in the RS2 head and neck region. Therefore, unsupervised 3D-classification by
658 masking the head and neck region was performed with three classes.

659 For visualization, tomograms were CTF deconvolved and missing wedge corrected using IsoNet
660 (Liu et al., 2022). The UCSF ChimeraX package was used for the visualization of subtomogram
661 averages, surface rendering, segmentation, and fitting (Pettersen et al., 2021).

662 **Deciliation and Western Blot**

663 All buffers used in biochemical studies were supplied with protease inhibitors (cOmplete, EDTA-
664 free protease inhibitor cocktail, Roche Diagnostics GmbH, Mannheim, Germany). To purify cilia,
665 cells from the overnight, mid-log phase culture were collected, rinsed with Tris-HCl buffer, pH
666 7.4, resuspended in a deciliation buffer (10 mM Tris-HCl, pH 7.4, 10 mM $CaCl_2$, 50 mM
667 sucrose), and deciliated by a pH shock (Wloga et al., 2008). Deciliation was monitored under a
668 microscope. Samples containing intact non-moving cells were spun down twice at 1680 x g for 5
669 min to remove cell bodies, and cilia were collected by centrifugation at 23,300 x g for 30 min.
670 Next, cilia were suspended in 10 mM Tris-HCl buffer (pH 7.4) with protease inhibitors, and the
671 protein concentration was estimated using Pierce™ BCA Protein Assay Kit (Thermo Scientific,
672 Bartlesville, OK, USA).

673 For Western blot analyses, 30 µg of ciliary proteins were loaded on the gel. After transfer to
674 nitrocellulose, HA-tagged fusion proteins were detected using monoclonal anti-HA antibodies
675 diluted 1:2000, followed by washing (4 x 10 min, TBST) with an incubation with HRP-
676 conjugated secondary antibodies, 1: 10 000 in 5% milk/TBSP (Jackson ImmunoResearch, West
677 Grove, PA, USA). HA-tagged proteins were detected using a Westar Supernova kit (Cyanagen,
678 Italy). Two-dimensional electrophoresis was performed as described (Bicka et al., 2022).

679 **Co-immunoprecipitation and proximity labeling (BioID) assays**

680 For co-immunoprecipitation assay, 200 ml of cells (3 x 10^5 cells/ml) expressing -3HA
681 tagged radial spoke proteins under the control of a native promoter and wild-type cells (control),
682 all at mid-log phase, were spun down and washed with 10 mM Tris-HCl buffer (pH 7.4). After
683 deciliation, collected cilia were suspended in 10 mM Tris-HCl buffer (pH 7.4) and combined with
684 an equal volume of 2% NP-40 and 1.2 M NaCl in 80 mM Tris-HCl buffer, pH 7.5, with protease

685 inhibitors. After a 15 min incubation on ice, axonemes were pelleted at 20,000 × *g* and treated
686 with 0.5 M KI, 30 mM NaCl, 5 mM MgSO4, 0.5 M EDTA, 1 mM dithiothreitol, and 10 mM
687 HEPES, pH 7.5. After 30 min on ice, the axonemes were centrifuged (16,000 × *g* for 15 min at 4
688 °C), and the collected supernatant was diluted with 50 mM Tris–HCl, pH 7.4 (1:9). The axonemal
689 proteins were incubated overnight with anti-HA magnetic beads with bound anti-HA antibodies
690 (Thermo Fisher Scientific, Waltham, MA) at 4 °C. The bead-bound proteins were analyzed by
691 SDS–PAGE and silver staining and identified by mass spectrometry.

692 The proximity-labeling assay (Roux et al., 2012) was performed as described in detail
693 (Joachimiak et al., 2021). Briefly, 200 ml of cells (3 x 10^5 cells/ml) expressing RSP-HA-BirA*
694 and wild-type cells (control) at mid-log phase were spun down and suspended in 200 mL of 10
695 mM Tris-HCl buffer (pH 7.4). After approximately 18 h, Tris buffer was supplied with biotin (50
696 µM final concentration), and the cells were cultured for 4 h at 30 °C. After deciliation, collected
697 cilia were suspended in axoneme stabilization buffer (20 mM potassium acetate, 5 mM MgSO4,
698 0.5 mM EDTA, 20 mM HEPES, pH 7.5 with protease inhibitors) supplied with 0.2% NP-40, and
699 after 5 min, the axonemes were spun down (30 min at 23,300x g at 4 °C) and suspended in lysis
700 buffer (50 mM Tris–HCl, pH 7.4, 0.4% SDS, 0.5 M NaCl, 1 mM DTT with protease inhibitors).
701 After an hour, samples were spun down (8000x g at 4 °C), and the supernatant was diluted with
702 50 mM Tris–HCl, pH 7.4 (1:3). The biotinylated proteins were incubated overnight with
703 streptavidin-coupled Dynabeads (Dynabeads M-280 Streptavidin, Thermo Fisher Scientific,
704 Waltham, MA) at 4 °C. The bead-bound biotinylated proteins were analyzed by Western blotting
705 using HRP-streptavidin diluted 1:40 000 in 3% BSA/TBST (Thermo Fisher Scientific, Rockford,
706 IL, USA) and identified by mass spectrometry.

707 **Differential Quantitative Cilia Proteome Analyses**

708 *Sample Preparation*

709 Cilia purified from 5x10^7 cells were resuspended in axoneme stabilization buffer
710 containing 0.2% NP-40 and incubated for 5 min on ice to remove the ciliary membrane.
711 Axonemes were lysed for 1 hour at RT with lysis buffer (1% SDS, 50 mM Tris–HCl, pH 7.4),
712 and protein concentrations were determined by a Pierce™ BCA Protein Assay Kit (Thermo
713 Scientific, Bartlesville, OK, USA). Three hundred micrograms of protein was precipitated using a
714 ReadyPrep 2-D Cleanup Kit (Bio-Rad Laboratories, USA) at −20 °C overnight. Next, samples
715 were centrifuged at 20,000× g for 30 min at 4 °C (5804/5804 R Centrifuge, Eppendorf, USA),
716 and supernatants were discarded. Protein pellets were dissolved in 0.1% RapiGest and 500
717 mmol/L TEAB and then incubated at 850 rpm for 45 min at 37 °C (Eppendorf Comfort

718 Thermomixer, Eppendorf, USA). Proteins were digested by trypsin (Trypsin Gold, Mass
719 Spectrometry Grade, Promega; protein:enzyme (w/w) ratio – 100:1, at 37 °C for 16 h) according
720 to a standard protein digestion protocol including reduction (by 1,4-dithiothreitol) and alkylation
721 (by iodoacetamide). The digestion reaction was stopped by the addition of 55% trifluoroacetic
722 acid (final concentration of 5%), samples were centrifuged at 20,000× g for 30 min at 4 °C to
723 precipitate RapiGest, and pellets were discarded. Supernatants containing the obtained peptides
724 were purified using Pierce™ Peptide Desalting Spin Columns (Thermo Scientific, Bartlesville,
725 OK, USA) according to the manufacturer's protocol, dried in a vacuum concentrator at RT
726 (SpeedVac Concentrator Plus, Eppendorf, USA) and stored at -80 °C for further analysis.

727 *LC–MS/MS analysis of labeled peptides (TMT analysis)*

728 Desalted peptides were dissolved in 100 µl of 100 mmol/l TEAB solution, and peptide
729 concentrations were determined using the Pierce™ Quantitative Fluorescent Peptide Assay
730 (Thermo Scientific, USA). Next, a TMT labeling reaction was performed according to the
731 procedure provided by the manufacturer. Briefly, a volume of sample containing 30 µg of
732 peptides was labeled with a corresponding tandem mass tag. The labeling reaction was carried
733 out for 1 h at room temperature and quenched with 5% hydroxylamine. Additionally, a test
734 sample was prepared to check the efficiency of labeling. Labeled peptides were purified and
735 fractionated using liquid chromatography at high pH. Separation was carried out for 26 minutes
736 at a flow rate of 0.8 ml/min using a UPLC system (Acquity UPLC Class H system, Waters). The
737 mobile phases consisted of water (A), acetonitrile (B) and 100 mmol/L ammonia solution (C).
738 The percentage of phase C was kept constant at 10% throughout the separation. Fractions were
739 collected every 1 minute, starting from the second minute of the run. The peptide elution was
740 monitored spectrophotometrically at 214 nm. Twenty-four fractions were collected and combined
741 to obtain 12 measurement samples. Samples were dried in a vacuum concentrator at room
742 temperature. Peptides were resuspended in 100 µl of 5% acetonitrile and 0.1% formic acid.

743 Peptides were analyzed on the Evosep One system (Evosep Biosystems, Odense,
744 Denmark) coupled to an Orbitrap Exploris 480 mass spectrometer (Thermo Fisher Scientific,
745 USA) according to (Bekker-Jensen et al., 2020). One µg of peptides was loaded onto Evotips
746 C18 trap columns (Evosep Biosystems, Odense, Denmark) according to the manufacturer's
747 protocol with some modifications. Chromatographic separation of peptides was carried out using
748 a mobile phase flow rate of 500 nl/min in gradient elution mode for 44 min on an EV1106
749 analytical column (Dr. Maisch C18 AQ, particle size 1.9 µm, 150 µm x 150 mm, Evosep
750 Biosystems, Odense, Denmark). The following gradient elution was used: 0 min – 1% B, 120 min

751 – 35% B, 121 min – 95% B, 124 min – 1% B, 127 min – 95% B, 130 min – 1% B. The eluted
752 peptides were ionized in the positive ion mode in the nano-ESI source with a capillary voltage of
753 2.1 kV and the temperature of transfer capillary 275 °C. Survey scans from 300 *m/z* to 1700 *m/z*
754 were acquired by an Orbitrap mass analyzer at a resolving power of 60 000. The resolving power
755 in the MS2 spectrum measurement mode was 30 000 with the TurboTMT function set to TMT
756 Reagents. HCD-MS/MS spectra (normalized collision energy of 30%) were generated for 25
757 multiply charged precursor ions from each survey scan. A precursor fit filter was applied to
758 reduce peptide co-fragmentation. Dynamic exclusion was set to 20 s, and the precursor ion
759 intensity threshold was set to $5x10^3$.

760 *LC-MS/MS analysis of non-labeled peptides (label-free analysis)*

761 Desalted peptides were resuspended in 100 µl of 5% acetonitrile and 0.1% formic acid. Next,
762 peptide samples were analyzed on the Evosep One system (Evosep Biosystems, Odense,
763 Denmark) coupled to an Orbitrap Exploris 480 mass spectrometer (Thermo Fisher Scientific,
764 USA) according to (Bekker-Jensen et al., 2020) with some modifications. Chromatographic
765 separation and mass spectrometry detection were conducted as described in a previous article
766 (Bicka et al., 2022).

767 *Data analysis*

768 MS data were analyzed with FragPipe (v. 17.1) (Nesvilab, University of Michigan, Ann Arbor,
769 MI) with MSFragger (v. 3.4) (Kong et al., 2017) and Philosopher (v. 4.2.1) (da Veiga Leprevost
770 et al., 2020). ProteoWizard's MSConvert (v. 3.0.1908) (Palo Alto, CA) (Chambers et al., 2012)
771 was used to convert the raw MS data to mzML format. The *Tetrahymena thermophila* UniProt
772 database (canonical and isoform sequences; 27,027 entries) was searched using the following
773 search parameters: (i) digestion enzyme-trypsin/P, up to two missed cleavage sites were allowed,
774 (ii) precursor and fragment ion mass tolerance ±10.0 ppm and ±20 ppm, respectively, (iii) fixed
775 modifications: carbamidomethyl (C), (iv) variable modifications: oxidation (M), deamidation (N),
776 (Q). For TMT samples, additional fixed modification was used (v) TMT modification of lysine
777 (+229.16293) and variable modification (vi) TMT modification of N-termini of protein and
778 peptide (+229.16293). Proteins and peptides were identified using the target-decoy approach with
779 a reversed database. The peptide mass range was set from 500 Da to 5 000 Da. The results were
780 processed with FDR (false discovery rate) set to 1% at the PSM, peptide and protein levels.
781 Quantitative analysis was performed using IonQuant (label-free quantitation) and TMT Integrator
782 (TMT-based quantitation). Statistical analysis was performed with Perseus (v. 2.0.3) (Max Planck
783 Institute of Biochemistry, Martinsried, Germany). In label-free quantitation, missing values were

replaced based on quantile regression imputation of left-censored data (QRILC) (Rudolph & Cox, 2019). Student T-test was used for statistical analysis. Proteins were considered to be differentially expressed if the difference in abundance was statistically significant (FDR adjusted p-value < 0.05) and the fold change was equal to or higher than 1.5.

Reagent availability. All plasmids and *Tetrahymena* mutants are available on request. LFQ and TMT mass spectrometry data are provided as Figure 4-Source Data 1' and Figure 4-Source Data 2'. The list of all protein identified in co-IP and BioID experiments are provided as Figure 6-Source Data 1' and Figure 6-Source Data 2'. Nucleotide sequences of the primers used to amplified PCR fragments are provided in Table S1.

Acknowledgment: We thank Dr. Jacek Gaertig for critical reading of the manuscript. The immunofluorescence confocal imaging was performed in the Laboratory of Imaging Tissue Structure and Function, Nencki Institute of Experimental Biology, PAS. The mass spectrometry analyses were done in cooperation with the Mass Spectrometry Laboratory, Institute of Biochemistry and Biophysics, PAS, Warsaw, Poland. The authors have no competing financial interests to declare.

Funding: This work was supported by:

- the National Science Centre, Poland Grants, OPUS13 2017/25/B/NZ3/01609 to Dorota Wloga
- the National Science Centre, Poland Grants, OPUS15 2018/29/B/NZ3/02443 to Ewa Joachimiak
- Natural Sciences and Engineering Research Council of Canada (RGPIN-2022-04774) to Khanh Huy Bui
- Project No. POWR.03.02.00-00-I007/16-00 implemented under the Operational Program Knowledge Education Development 2014–2020 co-financed from the European Social Fund Project NCBiR No. PBS3/A8/36/2015.

The funders had no role in study design, data collection and interpretation, or the decision to submit the work for publication.

Competing interest: The authors declare that no competing interests exist.

Author contributions:

Marta Bicka, Investigation, Validation, Formal analysis, Visualization

Corbin Black, Investigation,

818 Avrin Ghanaeian, Formal analysis, Investigation, Writing – review & editing, Visualization
819 Ewa Joachimiak, Methodology, Investigation, Validation, Formal analysis, Visualization,
820 Funding acquisition, Writing—Review and Editing
821 Anna Osinka, Investigation, Visualization
822 Sumita Majhi, Investigation,
823 Anna Konopka, Methodology, Validation, Resources, Supervision
824 Ewa Bulska, Supervision, Resources , funding acquisition, writing - review & editing
825 Khanh Huy Bui, Investigation, Supervision, Resources, Funding acquisition, Writing – review &
826 editing
827 Dorota Wloga, Conceptualization, Investigation, Validation, Visualization, Resources, Formal
828 analysis, Supervision, Funding acquisition, Project administration, Writing – original draft,
829 Writing – review and editing
830
831

832 **References**

833 Barber, C. F., Heuser, T., Carbajal-González, B. I., Botchkarev, V. V., & Nicastro, D. (2012). Three-
834 dimensional structure of the radial spokes reveals heterogeneity and interactions with dyneins in
835 Chlamydomonas flagella. *Molecular Biology of the Cell*, *23*(1), 111–120.
836 https://doi.org/10.1091/mbc.E11-08-0692

837 Bazan, R., Schröfel, A., Joachimiak, E., Poprzeczko, M., Pigino, G., & Wloga, D. (2021). Ccdc113/Ccdc96
838 complex, a novel regulator of ciliary beating that connects radial spoke 3 to dynein g and the nexin
839 link. *PLoS Genetics*, *17*(3). https://doi.org/10.1371/journal.pgen.1009388

840 Bekker-Jensen, D. B., Martínez-Val, A., Steigerwald, S., Rüther, P., Fort, K. L., Arrey, T. N., Harder, A.,
841 Makarov, A., & Olsen, J. V. (2020). A Compact Quadrupole-Orbitrap Mass Spectrometer with FAIMS
842 Interface Improves Proteome Coverage in Short LC Gradients. *Molecular & Cellular Proteomics :*
843 *MCP*, *19*(4), 716–729. https://doi.org/10.1074/MCP.TIR119.001906

844 Bicka, M., Joachimiak, E., Urbanska, P., Osinka, A., Konopka, A., Bulska, E., & Wloga, D. (2022). Cfap91-
845 Dependent Stability of the RS2 and RS3 Base Proteins and Adjacent Inner Dynein Arms in
846 Tetrahymena Cilia. *Cells*, *11*(24), 4048. https://doi.org/10.3390/CELLS11244048

847 Bonini, N. M., & Nelson, D. L. (1988). Differential regulation of Paramecium ciliary motility by cAMP and
848 cGMP. *The Journal of Cell Biology*, *106*(5), 1615–1623. https://doi.org/10.1083/JCB.106.5.1615

849 Bui, K. H., & Ishikawa, T. (2013). 3D structural analysis of flagella/cilia by cryo-electron tomography.
850 *Methods in Enzymology*, *524*, 305–323. https://doi.org/10.1016/B978-0-12-397945-2.00017-2

851 Cassidy-Hanley, D., Bowen, J., Lee, J. H., Cole, E., VerPlank, L. A., Gaertig, J., Gorovsky, M. A., & Bruns, P.
852 J. (1997). Germline and somatic transformation of mating Tetrahymena thermophila by particle
853 bombardment. *Genetics*, *146*(1), 135–147. https://doi.org/10.1093/GENETICS/146.1.135

854 Chambers, M. C., MacLean, B., Burke, R., Amodei, D., Ruderman, D. L., Neumann, S., Gatto, L., Fischer, B.,
855 Pratt, B., Egertson, J., Hoff, K., Kessner, D., Tasman, N., Shulman, N., Frewen, B., Baker, T. A.,

Brusniak, M. Y., Paulse, C., Creasy, D., … Mallick, P. (2012). A cross-platform toolkit for mass spectrometry and proteomics. *Nature Biotechnology*, *30*(10), 918–920. https://doi.org/10.1038/NBT.2377

Chen, Z., Greenan, G. A., Shiozaki, M., Liu, Y., Skinner, W. M., Zhao, X., Zhao, S., Yan, R., Yu, Z., Lishko, P. V., Agard, D. A., & Vale, R. D. (2023). In situ cryo-electron tomography reveals the asymmetric architecture of mammalian sperm axonemes. *Nature Structural & Molecular Biology*, *30*(3). https://doi.org/10.1038/S41594-022-00861-0

Dave, D., Wloga, D., & Gaertig, J. (2009). Manipulating ciliary protein-encoding genes in Tetrahymena thermophila. *Methods in Cell Biology*, *93*, 1–20. https://doi.org/10.1016/S0091-679X(08)93001-6

da Veiga Leprevost, F., Haynes, S. E., Avtonomov, D. M., Chang, H. Y., Shanmugam, A. K., Mellacheruvu, D., Kong, A. T., & Nesvizhskii, A. I. (2020). Philosopher: a versatile toolkit for shotgun proteomics data analysis. *Nature Methods*, *17*(9), 869–870. https://doi.org/10.1038/S41592-020-0912-Y

Dzeja, P., & Terzic, A. (2009). Adenylate kinase and AMP signaling networks: metabolic monitoring, signal communication and body energy sensing. *International Journal of Molecular Sciences*, *10*(4), 1729–1772. https://doi.org/10.3390/IJMS10041729

Eisen, J. A., Coyne, R. S., Wu, M., Wu, D., Thiagarajan, M., Wortman, J. R., Badger, J. H., Ren, Q., Amedeo, P., Jones, K. M., Tallon, L. J., Delcher, A. L., Salzberg, S. L., Silva, J. C., Haas, B. J., Majoros, W. H., Farzad, M., Carlton, J. M., Smith, R. K., … Orias, E. (2006). Macronuclear genome sequence of the ciliate Tetrahymena thermophila, a model eukaryote. *PLoS Biology*, *4*(9), 1620–1642. https://doi.org/10.1371/JOURNAL.PBIO.0040286

Gaillard, A. R., Diener, D. R., Rosenbaum, J. L., & Sale, W. S. (2001). Flagellar radial spoke protein 3 is an A-kinase anchoring protein (AKAP). *The Journal of Cell Biology*, *153*(2), 443–448. https://doi.org/10.1083/JCB.153.2.443

Gaillard, A. R., Fox, L. A., Rhea, J. M., Craige, B., & Sale, W. S. (2006). Disruption of the A-kinase anchoring domain in flagellar radial spoke protein 3 results in unregulated axonemal cAMP-dependent protein kinase activity and abnormal flagellar motility. *Molecular Biology of the Cell*, *17*(6), 2626–2635. https://doi.org/10.1091/MBC.E06-02-0095

Goodenough, U. W., & Heuser, J. E. (1985). Substructure of inner dynein arms, radial spokes, and the central pair/projection complex of cilia and flagella. *The Journal of Cell Biology*, *100*(6), 2008–2018. https://doi.org/10.1083/JCB.100.6.2008

Gorovsky, M. A., Yao, M. C., Keevert, J. B., & Pleger, G. L. (1975). Isolation of micro- and macronuclei of Tetrahymena pyriformis. *Methods in Cell Biology*, *9*(0), 311–327. https://doi.org/10.1016/S0091-679X(08)60080-1

Grossman-Haham, I., Coudray, N., Yu, Z., Wang, F., Zhang, N., Bhabha, G., & Vale, R. D. (2021). Structure of the radial spoke head and insights into its role in mechanoregulation of ciliary beating. *Nature Structural & Molecular Biology*, *28*(1), 20–28. https://doi.org/10.1038/S41594-020-00519-9

Guan, J., Ekwurtzel, E., Kvist, U., Hultenby, K., & Yuan, L. (2010). DNAJB13 is a radial spoke protein of mouse “9+2” axoneme. *Reproduction in Domestic Animals = Zuchthygiene*, *45*(6), 992–996. https://doi.org/10.1111/J.1439-0531.2009.01473.X

Gui, M., Ma, M., Sze-Tu, E., Wang, X., Koh, F., Zhong, E. D., Berger, B., Davis, J. H., Dutcher, S. K., Zhang, R., & Brown, A. (2021). Structures of radial spokes and associated complexes important for ciliary

motility. *Nature Structural & Molecular Biology*, *28*(1), 29. https://doi.org/10.1038/S41594-020-00530-0

Gupta, V. A., & Beggs, A. H. (2014). Kelch proteins: emerging roles in skeletal muscle development and diseases. *Skeletal Muscle*, *4*(1). https://doi.org/10.1186/2044-5040-4-11

Habicht, J., Woehle, C., & Gould, S. B. (2015). Tetrahymena Expresses More than a Hundred Proteins with Lipid-binding MORN Motifs that can Differ in their Subcellular Localizations. *The Journal of Eukaryotic Microbiology*, *62*(5), 694–700. https://doi.org/10.1111/JEU.12216

Hemmersbach, R., Voormanns, R., Bromeis, B., Schmidt, N., Rabien, H., & Ivanova, K. (1998). Comparative studies of the graviresponses of Paramecium and Loxodes. *Advances in Space Research*, *21*(8–9), 1285–1289. https://doi.org/10.1016/S0273-1177(97)00400-6

Hwang, J. Y., Chai, P., Nawaz, S., Choi, J., Lopez-Giraldez, F., Hussain, S., Bilguvar, K., Mane, S., Lifton, R. P., Ahmad, W., Zhang, K., & Chung, J.-J. (2023). LRRC23 loss-of-function impairs radial spoke 3 head assembly and causes defective sperm motility underlying male infertility. *BioRxiv : The Preprint Server for Biology*. https://doi.org/10.1101/2023.02.25.530050

Joachimiak, E., Osinka, A., Farahat, H., Świderska, B., Sitkiewicz, E., Poprzeczko, M., Fabczak, H., & Wloga, D. (2021). Composition and function of the C1b/C1f region in the ciliary central apparatus. *Scientific Reports*, *11*(1). https://doi.org/10.1038/s41598-021-90996-9

Kimanius, D., Dong, L., Sharov, G., Nakane, T., & Scheres, S. H. W. (2021). New tools for automated cryo-EM single-particle analysis in RELION-4.0. *The Biochemical Journal*, *478*(24), 4169–4185. https://doi.org/10.1042/BCJ20210708

Kong, A. T., Leprevost, F. V., Avtonomov, D. M., Mellacheruvu, D., & Nesvizhskii, A. I. (2017). MSFragger: ultrafast and comprehensive peptide identification in mass spectrometry-based proteomics. *Nature Methods*, *14*(5), 513–520. https://doi.org/10.1038/NMETH.4256

Kremer, J. R., Mastronarde, D. N., & McIntosh, J. R. (1996). Computer visualization of three-dimensional image data using IMOD. *Journal of Structural Biology*, *116*(1), 71–76. https://doi.org/10.1006/JSBI.1996.0013

Kubo, S., Black, C. S., Joachimiak, E., Yang, S. K., Legal, T., Peri, K., Khalifa, A. A. Z., Ghanaeian, A., McCafferty, C. L., Valente-Paterno, M., De Bellis, C., Huynh, P. M., Fan, Z., Marcotte, E. M., Wloga, D., & Bui, K. H. (2023). Native doublet microtubules from Tetrahymena thermophila reveal the importance of outer junction proteins. *Nature Communications*, *14*(1), 2168. https://doi.org/10.1038/S41467-023-37868-0

Lin, J., Heuser, T., Carbajal-González, B. I., Song, K., & Nicastro, D. (2012). The structural heterogeneity of radial spokes in cilia and flagella is conserved. *Cytoskeleton (Hoboken, N.J.)*, *69*(2), 88–100. https://doi.org/10.1002/CM.21000

Lin, J., Yin, W., Smith, M. C., Song, K., Leigh, M. W., Zariwala, M. A., Knowles, M. R., Ostrowski, L. E., & Nicastro, D. (2014). Cryo-electron tomography reveals ciliary defects underlying human RSPH1 primary ciliary dyskinesia. *Nature Communications*, *5*. https://doi.org/10.1038/NCOMMS6727

Liu, Y. T., Zhang, H., Wang, H., Tao, C. L., Bi, G. Q., & Zhou, Z. H. (2022). Isotropic reconstruction for electron tomography with deep learning. *Nature Communications*, *13*(1). https://doi.org/10.1038/S41467-022-33957-8

Mastronarde, D. N. (2005). Automated electron microscope tomography using robust prediction of specimen movements. *Journal of Structural Biology*, *152*(1), 36–51. https://doi.org/10.1016/J.JSB.2005.07.007

Mastronarde, D. N., & Held, S. R. (2017). Automated tilt series alignment and tomographic reconstruction in IMOD. *Journal of Structural Biology*, *197*(2), 102–113. https://doi.org/10.1016/J.JSB.2016.07.011

Michibata, J., Okazaki, N., Motomura, S., Uda, K., Fujiwara, S., & Suzuki, T. (2014). Two arginine kinases of Tetrahymena pyriformis: characterization and localization. *Comparative Biochemistry and Physiology. Part B, Biochemistry & Molecular Biology*, *171*(1), 34–41. https://doi.org/10.1016/J.CBPB.2014.03.008

Muthaiyan Shanmugam, M., Bhan, P., Huang, H.-Y., Hsieh, J., Hua, T.-E., Wu, G.-H., Punjabi, H., Lee Aplícano, V. D., Chen, C.-W., & Wagner, O. I. (2018). Cilium Length and Intraflagellar Transport Regulation by Kinases PKG-1 and GCK-2 in Caenorhabditis elegans Sensory Neurons. *Molecular and Cellular Biology*, *38*(7). https://doi.org/10.1128/MCB.00612-17

Noguchi, M., Kurahashi, S., Kamachi, H., & Inoue, H. (2004). Control of the ciliary beat by cyclic nucleotides in intact cortical sheets from Paramecium. *Zoological Science*, *21*(12), 1167–1175. https://doi.org/10.2108/ZSJ.21.1167

Oda, T., Yanagisawa, H., Yagi, T., & Kikkawa, M. (2014). Mechanosignaling between central apparatus and radial spokes controls axonemal dynein activity. *The Journal of Cell Biology*, *204*(5), 807–819. https://doi.org/10.1083/JCB.201312014

Orias, E., & Rasmussen, L. (1976). Dual capacity for nutrient uptake in Tetrahymena. IV. Growth without food vacuoles and its implications. *Experimental Cell Research*, *102*(1), 127–137. https://doi.org/10.1016/0014-4827(76)90307-4

Padma, P., Satouh, Y., Wakabayashi, K. ichi, Hozumi, A., Ushimaru, Y., Kamiya, R., & Inaba, K. (2003). Identification of a novel leucine-rich repeat protein as a component of flagellar radial spoke in the ascidian Ciona intestinalis. *Molecular Biology of the Cell*, *14*(2), 774–785. https://doi.org/10.1091/mbc.02-06-0089

Patel-King, R. S., Gorbatyuk, O., Takebe, S., & King, S. M. (2004). Flagellar radial spokes contain a Ca2+-stimulated nucleoside diphosphate kinase. *Molecular Biology of the Cell*, *15*(8), 3891–3902. https://doi.org/10.1091/MBC.E04-04-0352

Pettersen, E. F., Goddard, T. D., Huang, C. C., Meng, E. C., Couch, G. S., Croll, T. I., Morris, J. H., & Ferrin, T. E. (2021). UCSF ChimeraX: Structure visualization for researchers, educators, and developers. *Protein Science : A Publication of the Protein Society*, *30*(1), 70–82. https://doi.org/10.1002/PRO.3943

Pigino, G., Bui, K. H., Maheshwari, A., Lupetti, P., Diener, D., & Ishikawa, T. (2011). Cryoelectron tomography of radial spokes in cilia and flagella. *Journal of Cell Biology*, *195*(4), 673–687. https://doi.org/10.1083/jcb.201106125

Roux, K. J., Kim, D. I., Raida, M., & Burke, B. (2012). A promiscuous biotin ligase fusion protein identifies proximal and interacting proteins in mammalian cells. *The Journal of Cell Biology*, *196*(6), 801–810. https://doi.org/10.1083/JCB.201112098

Rudolph, J. D., & Cox, J. (2019). A Network Module for the Perseus Software for Computational Proteomics Facilitates Proteome Interaction Graph Analysis. *Journal of Proteome Research*, *18*(5),

979 2052–2064.
980 https://doi.org/10.1021/ACS.JPROTEOME.8B00927/SUPPL_FILE/PR8B00927_SI_004.TXT

981 Satouh, Y., & Inaba, K. (2009). Proteomic characterization of sperm radial spokes identifies a novel spoke
982 protein with an ubiquitin domain. *FEBS Letters*, *583*(13), 2201–2207.
983 https://doi.org/10.1016/j.febslet.2009.06.016

984 Satouh, Y., Padma, P., Toda, T., Satoh, N., Ide, H., & Inaba, K. (2005). Molecular characterization of radial
985 spoke subcomplex containing radial spoke protein 3 and heat shock protein 40 in sperm flagella of
986 the ascidian Ciona intestinalis. *Molecular Biology of the Cell*, *16*(2), 626–636.
987 https://doi.org/10.1091/mbc.E04-09-0784

988 Scott, J. D., & Pawson, T. (2009). Cell Signaling in Space and Time: Where Proteins Come Together and
989 When They're Apart. *Science (New York, N.Y.)*, *326*(5957), 1220.
990 https://doi.org/10.1126/SCIENCE.1175668

991 Smith, E. F., & Yang, P. (2004). The radial spokes and central apparatus: mechano-chemical transducers
992 that regulate flagellar motility. *Cell Motility and the Cytoskeleton*, *57*(1), 8–17.
993 https://doi.org/10.1002/CM.10155

994 Subramanian, A., Kabi, A., Gray, S. F., & Pennock, D. (2016). p28 dynein light chains and ciliary motility in
995 Tetrahymena thermophila. *Cytoskeleton (Hoboken, N.J.)*, *73*(4), 197–208.
996 https://doi.org/10.1002/CM.21295

997 Tegunov, D., & Cramer, P. (2019). Real-time cryo-electron microscopy data preprocessing with Warp.
998 *Nature Methods*, *16*(11), 1146–1152. https://doi.org/10.1038/S41592-019-0580-Y

999 Tyanova, S., Temu, T., Sinitcyn, P., Carlson, A., Hein, M. Y., Geiger, T., Mann, M., & Cox, J. (2016). The
1000 Perseus computational platform for comprehensive analysis of (prote)omics data. *Nature Methods*,
1001 *13*(9), 731–740. https://doi.org/10.1038/NMETH.3901

1002 Uda, K., Fujimoto, N., Akiyama, Y., Mizuta, K., Tanaka, K., Ellington, W. R., & Suzuki, T. (2006). Evolution
1003 of the arginine kinase gene family. *Comparative Biochemistry and Physiology. Part D, Genomics &*
1004 *Proteomics*, *1*(2), 209–218. https://doi.org/10.1016/J.CBD.2005.10.007

1005 Urbanska, P., Joachimiak, E., Bazan, R., Fu, G., Poprzeczko, M., Fabczak, H., Nicastro, D., & Wloga, D.
1006 (2018). Ciliary proteins Fap43 and Fap44 interact with each other and are essential for proper cilia
1007 and flagella beating. *Cellular and Molecular Life Sciences*, *75*(24), 4479–4493.
1008 https://doi.org/10.1007/s00018-018-2819-7

1009 Urbanska, P., Song, K., Joachimiak, E., Krzemien-Ojak, L., Koprowski, P., Hennessey, T., Jerka-Dziadosz,
1010 M., Fabczak, H., Gaertig, J., Nicastro, D., & Wloga, D. (2015). The CSC proteins FAP61 and FAP251
1011 build the basal substructures of radial spoke 3 in cilia. *Molecular Biology of the Cell*, *26*(8), 1463–
1012 1475. https://doi.org/10.1091/MBC.E14-11-1545

1013 Vasudevan, K. K., Song, K., Alford, L. M., Sale, W. S., Dymek, E. E., Smith, E. F., Hennessey, T., Joachimiak,
1014 E., Urbanska, P., Wloga, D., Dentler, W., Nicastro, D., & Gaertig, J. (2015). FAP206 is a microtubule-
1015 docking adapter for ciliary radial spoke 2 and dynein c. *Molecular Biology of the Cell*, *26*(4), 696–
1016 710. https://doi.org/10.1091/MBC.E14-11-1506

1017 Villar, P. S., Delgado, R., Vergara, C., Reyes, J. G., & Bacigalupo, J. (2017). Energy Requirements of Odor
1018 Transduction in the Chemosensory Cilia of Olfactory Sensory Neurons Rely on Oxidative
1019 Phosphorylation and Glycolytic Processing of Extracellular Glucose. *The Journal of Neuroscience :*

1020 *The Official Journal of the Society for Neuroscience*, *37*(23), 5736–5743.
1021 https://doi.org/10.1523/JNEUROSCI.2640-16.2017

1022 Williams, B. D., Velleca, M. A., Curry, A. M., & Rosenbaum, J. L. (1989). Molecular cloning and sequence
1023 analysis of the Chlamydomonas gene coding for radial spoke protein 3: flagellar mutation pf-14 is
1024 an ochre allele. *The Journal of Cell Biology*, *109*(1), 235–245. https://doi.org/10.1083/JCB.109.1.235

1025 Wirschell, M., Zhao, F., Yang, C., Yang, P., Diener, D., Gaillard, A., Rosenbaum, J. L., & Sale, W. S. (2008).
1026 Building a radial spoke: flagellar radial spoke protein 3 (RSP3) is a dimer. *Cell Motility and the*
1027 *Cytoskeleton*, *65*(3), 238–248. https://doi.org/10.1002/CM.20257

1028 Wloga, D., Rogowski, K., Sharma, N., Van Dijk, J., Janke, C., Eddé, B., Bré, M. H., Levilliers, N., Redeker, V.,
1029 Duan, J., Gorovsky, M. A., Jerka-Dziadosz, M., & Gaertig, J. (2008). Glutamylation on alpha-tubulin is
1030 not essential but affects the assembly and functions of a subset of microtubules in Tetrahymena
1031 thermophila. *Eukaryotic Cell*, *7*(8), 1362–1372. https://doi.org/10.1128/EC.00084-08

1032 Wyatt, T. A. (2015). Cyclic GMP and Cilia Motility. *Cells*, *4*(3), 315–330.
1033 https://doi.org/10.3390/CELLS4030315

1034 Wyatt, T. A., Spurzem, J. R., May, K., & Sisson, J. H. (1998). Regulation of ciliary beat frequency by both
1035 PKA and PKG in bovine airway epithelial cells. *The American Journal of Physiology*, *275*(4).
1036 https://doi.org/10.1152/AJPLUNG.1998.275.4.L827

1037 Yamamoto, R., Hwang, J., Ishikawa, T., Kon, T., & Sale, W. S. (2021). Composition and function of ciliary
1038 inner-dynein-arm subunits studied in Chlamydomonas reinhardtii. *Cytoskeleton (Hoboken, N.J.)*,
1039 *78*(3), 77–96. https://doi.org/10.1002/CM.21662

1040 Yang, P., Diener, D. R., Rosenbaum, J. L., & Sale, W. S. (2001). Localization of calmodulin and dynein light
1041 chain LC8 in flagellar radial spokes. *The Journal of Cell Biology*, *153*(6), 1315–1325.
1042 https://doi.org/10.1083/JCB.153.6.1315

1043 Yang, P., Diener, D. R., Yang, C., Kohno, T., Pazour, G. J., Dienes, J. M., Agrin, N. S., King, S. M., Sale, W. S.,
1044 Kamiya, R., Rosenbaum, J. L., & Witman, G. B. (2006). Radial spoke proteins of Chlamydomonas
1045 flagella. *Journal of Cell Science*, *119*(Pt 6), 1165–1174. https://doi.org/10.1242/JCS.02811

1046 Yang, P., & Sale, W. S. (2000). Casein kinase I is anchored on axonemal doublet microtubules and
1047 regulates flagellar dynein phosphorylation and activity. *The Journal of Biological Chemistry*, *275*(25),
1048 18905–18912. https://doi.org/10.1074/JBC.M002134200

1049 Yoke, H., Ueno, H., Narita, A., Sakai, T., Horiuchi, K., Shingyoji, C., Hamada, H., & Shinohara, K. (2020).
1050 Rsph4a is essential for the triplet radial spoke head assembly of the mouse motile cilia. *PLoS*
1051 *Genetics*, *16*(3). https://doi.org/10.1371/JOURNAL.PGEN.1008664

1052 Zhang, X., Sun, J., Lu, Y., Zhang, J., Shimada, K., Noda, T., Zhao, S., Koyano, T., Matsuyama, M., Zhou, S.,
1053 Wu, J., Ikawa, M., & Liu, M. (2021). LRRC23 is a conserved component of the radial spoke that is
1054 necessary for sperm motility and male fertility in mice. *Journal of Cell Science*, *134*(20).
1055 https://doi.org/10.1242/jcs.259381

1056 Zhang, X., Xiao, Z., Zhang, J., Xu, C., Liu, S., Cheng, L., Zhou, S., Zhao, S., Zhang, Y., Wu, J., Wang, Y., & Liu,
1057 M. (2022). Differential requirements of IQUB for the assembly of radial spoke 1 and the motility of
1058 mouse cilia and flagella. *Cell Reports*, *41*(8). https://doi.org/10.1016/J.CELREP.2022.111683

1059 Zhu, X., Liu, Y., & Yang, P. (2017). Radial Spokes-A Snapshot of the Motility Regulation, Assembly, and
1060 Evolution of Cilia and Flagella. *Cold Spring Harbor Perspectives in Biology*, *9*(5).
1061 https://doi.org/10.1101/CSHPERSPECT.A028126

1062

1063 **Figure legends**

1064 **Figure 1.** Localization of RSP3 fusion proteins. (A) Domain organization of RSP3 paralogs
1065 predicted by SMART (http://smart.embl-heidelberg.de/). (B) Western blot analyses of ciliary
1066 proteins isolated from cells expressing RSP3 paralogs as C-terminal 3-HA tagged proteins under
1067 the control of native promoters. A star indicates a band corresponding to the position of fusion
1068 proteins, RSP3A-3HA, RSP3B-3HA, and RSP3C-3HA. (C-E) Ciliary localization of the RSP3
1069 paralogs expressed as C-terminally -3HA tagged fusions under the control of the respective
1070 native promoters localize along the entire cilia length except for the ciliary tip. (C) RSP3A-3HA,
1071 (D) RSP3B-3HA, and (D) RSP3C-3HA labeled with a mix of anti-HA and anti-acetylated tubulin
1072 antibodies to visualize the entire cilia. To the right, the magnified fragments of the cells as
1073 indicated by the white insets, stained with anti-HA (red), anti-acetylated α-tubulin (green), and
1074 merged images (red and green). Below are images showing both channels but with some shifts to
1075 better visualize the presence of the RSP3 paralogs along the entire cilia. Note that all RSP3
1076 paralogs localize along the entire cilia length except for a ciliary tip.

1077 **Figure 2.** Knockout of particular RSP3 paralogs affects cilia beating to different extents. (A-D)
1078 WT (A), RSP3A-KO (B), RSP3B-KO (C), and RSP3C-KO (D) trajectories recorded for 3 sec
1079 using a high-speed video camera. The cell swimming paths are indicated by the parallel colored
1080 lines. Bar = 500 µm. (E) A comparison of the length of trajectories recorded for 3 sec. The red
1081 bar position to the right represents the standard deviation. The wild-type cells swam on average
1082 388+/-32 µm/s (n= 100), and the swimming speeds of the RSP3A-KO, RSP3B-KO, and RSP3C-
1083 KO mutants were reduced to 272+/-27 µm/s (n=100), 48+/-9 µm/s (n=82), and 217+/-25 µm/s
1084 (n=101), respectively. Statistical significance was calculated using student t-test. (F) Drawings
1085 showing examples of the most frequently observed subsequent positions of a cilium of WT and
1086 RSP3 knockout cells. The ciliary waveform and amplitude in the RSP3B-KO mutant can vary
1087 both in the case of neighboring cilia and during subsequent cycles of the same cilium. (G) Graph
1088 showing a range of cilia beating frequencies in wild-type and RSP3 knockout mutants. The red
1089 bar represents the standard deviation. Statistical significance was calculated using student t-test.
1090 (H) Examples of the kymographs used to calculate cilia beating frequency.

1091 **Figure 2-figure supplement 1**. Alterations in *RSP3A*, *RSP3B*, and *RSP3C* loci in engineered
1092 *Tetrahymena* knockout mutants. (A1, B1, C1) Schematic representations of the *RSP3A* (A),
1093 *RSP3B* (B), and *RSP3C* (C) loci in the wild-type genome (WT, upper gray bar) and obtained
1094 knockout cells (RSP3-KO, lower gray bar) with the size of the fragment of the open reading

1095 frame removed in the knockout cells indicated and the position of the annealing of primers (blue
1096 and red arrows) used to test changes in the analyzed loci marked. Numbers near the blue arrows
1097 indicate the distance of the primer annealing site from the neo4 cassette that replaced the
1098 removed fragment of the open reading frame in mutated loci. Note that the primer represented by
1099 a red arrow recognizes the nucleotide sequence deleted in mutant cells. Numbers above the gray
1100 bars representing the open reading frame indicate the distance between either the start or stop
1101 codons and the neo4 cassette insertion site. (A2, B2, C2) A table showing the expected size of the
1102 PCR products obtained using genomic DNA purified from wild-type (WT) and knockout cells
1103 (KO) and primers as indicated. (A3, B3, C3) PCR analyses of the RSP3 loci *RSP3A* (A3), *RSP3B*
1104 (B3), and *RSP3C* (C3) in independently obtained RSP3 mutants using either both primers
1105 annealing outside the neo4 cassette or one of the primers recognizing the deleted gene fragment
1106 as indicated in A1, B1, and C1, respectively.
1107

1108 **Figure 2-figure supplement 2**. Knockout of RSP3B affects cilia beating synchrony. Examples of
1109 the kymographs showing cilia beating synchrony.

1110

1111 **Figure 3.** Cryo-ET and subtomogram averaging analyses of the ciliary ultrastructure of wild-type
1112 cells and RSP3 knockout mutants. (A) Subtomogram averages of WT, RSP3A-KO, RSP3B-KO
1113 and RSP3C-KO mutants. RS1: green; RS2: red; RS3: blue. Inner dynein arms (IDAs): light pink,
1114 N-DRC: yellow, CCDC96-CCDC113 complex: dark pink. The black arrow in the RSP3B-KO
1115 subtomogram points to the place corresponding to the position of IDAc in the WT cilia. (B)
1116 Tomographic slices from WT, RSP3A-KO, RSP3B-KO and RSP3C-KO cilia showing the
1117 heterogeneity of RS distributions. Scale bar: 50 nm.

1118

1119 **Figure 3-figure supplement 1.** Consensus subtomogram averages and three-dimensional
1120 classification of the radial spokes in *Tetrahymena* RSP3 knockout mutants. In RSP3A-KO mutant
1121 cilia, RS1 is missing in ~35% of 96-nm axonemal units. The analyses of n=2099 axonemal
1122 repeats with RS1 defects revealed either the lack of the entire RS1 (~30%, n=639 units) or RS1
1123 except for the RS1 base (~67%, n=1417). Three percent of the recorded repeats were not
1124 classified due to the low number of particles. In RSP3B-KO mutant cilia, all analyzed axonemal
1125 repeats (n=2092) lacked RS2. Additionally, 77.5% of the axonemal repeats (n=1622) had RS1
1126 spokes defects. The RS1 spokes were either completely missing (51.5%, n=1078) or only their
1127 base was well visible (26%, n=544). Among the collected n=2790 axonemal repeats of RSP3C-

1128 KO mutant cilia, 173 axonemal repeats (7%) were unclassified. The analyses of the remaining
1129 n=2617 axomenal repeats revealed that ~20% (n=527) lacked the entire RS2. The 3D
1130 classification of the remaining 80% of repeats using the RS2 mask covering an RS2 head and
1131 stalk showed that the remaining units grouped into two categories: (i) with an intact RS2 structure
1132 (~18%, n=469) and (ii) with a well-visible RS2 base (~62%, n=1621).
1133
1134 **Figure 3-figure supplement 2.** Data collection and analysis parameters for cryo-ET and
1135 subtomogram averaging.
1136
1137 **Figure 4.** Graphical illustration of quantitative proteomics data. (A) Principal component analysis
1138 (PCA) score plot from fold-change values of the differentially expressed proteins showing similar
1139 grouping of ciliomes identified by mass spectrometry using either LFQ (graphs to the left) or
1140 TMT (graphs to the right) strategy based on two independent variables. The analyzed ciliary
1141 protein samples were color-coded as follows: WT - red, RSP3A-KO - green, RSP3B-KO - blue,
1142 and RSP3C-KO – orange. (B) Volcano plots of wild-type and RS mutant ciliary proteins
1143 identified by mass spectrometry using either LFQ (graphs to the left) or TMT (graphs to the right)
1144 strategy (N=3) showing changes in mutant ciliomes. FDR=0.05. Proteins Red dots represent
1145 proteins that are at a significantly lower level in RSP mutants compared to wild-type cells, while
1146 blue dots represent proteins that are more abundant in mutant cilia. Names are provided for
1147 known RSP proteins. The statistical significance of the difference in protein enrichment between
1148 wild-type and RS mutant ciliomes calculated using Student's t-test.
1149
1150 **Figure 5.** Venn diagrams indicating the overlap of differentially expressed proteins between
1151 different radial spoke mutants as estimated by global ciliomes obtained either by LFQ or TMT
1152 approaches. (A) Comparison of the total number of proteins identified using LFQ and TMT
1153 approaches (B-E). The overlap of proteins that were either reduced (to the left) or elevated (to the
1154 right) in different radial spoke mutants as detected using (B) TMT and (C-E) LFQ methods.
1155 Images were prepared in Adobe Photoshop based on data sorted using the Excel program.
1156
1157 **Figure 6**. A schematic summary of the radial spoke protein composition in *Tetrahymena* cilia
1158 prepared based on collected ultrastructural and proteomic data. (A) A summary of the RSP3
1159 paralog-dependent types of RS1 and RS2 spokes. RSP3A-RSP3B heterodimer-containing RS1
1160 and RSP3C-RSP3C-homodimer-containing RS2 are less probable. (B-D) Graphical presentation
1161 of the radial spokes composition, (B) RS1 containing either RSP3A or RSP3B homodimers, (C)

1162 RS2 containing either RSP3B homodimer or RSP3B-RSP3C heterodimer, (D) RS3. Names of the
1163 RS-specific RSPs existing in *Tetrahymena* as a single ortholog are in light blue; names of the RS-
1164 type specific RSP paralogs are in red; new candidate proteins are in orange; RS-associated
1165 enzymes are in blue. Note that in the case of RS2-type II (RSP3C-containing), RSPs were
1166 reduced in RSP3C-KO cilia and thus likely bind with RSP3C. DYH- dynein heavy chains.
1167
1168 **Figure 6-figure supplement 1.** (A-I) Immunofluorescence confocal images of *Tetrahymena* cells
1169 expressing RSP proteins as C-terminal –HA-BirA* fusions under the control of respective native
1170 promoters detected using anti-HA antibodies. (A) RSP3A-HA-BirA*, (B) RSP3B-HA-BirA*, (C)
1171 RSP3C-HA-BirA*, (D) RSP4A-HA-BirA*, (E) RSP4B-HA-BirA*, (F) RSP4C-HA-BirA*, (G)
1172 CFAP206-HA-BirA*, (H) CFAP61-HA-BirA*, (I) CFAP91-HA-BirA*. (J-M) Western blot
1173 analyses of the ciliary proteins isolated from *Tetrahymena* cells expressing RSP proteins as –HA-
1174 BirA* fusions under the control of respective native promoters. A star indicates a band
1175 corresponding to the position of fusion proteins. (J) Western blot-based identification of the RSP-
1176 HA-BirA* fusion proteins. (K-M) Western blot-based analyses of the biotinylated ciliary proteins
1177 in either WT cells or cells expressing RSP-HA-BirA* under the control of the respective native
1178 promoter, all grown for 4 hrs in a 10 mM Tris-HCl buffer (pH 7.4) supplemented with biotin,
1179 detected using HRP-conjugated streptavidin.
1180
1181 **Figure 6-figure supplement 2**. Two-dimensional analyses of the RSP isoforms. The radial
1182 spokes proteins were expressed as C-terminal 3HA fusions under the control of the respective
1183 native proteins. The isoelectric focusing of the ciliary proteins (30 µg) was performed using 7 cm
1184 4-7 or 3-10 ready strips. The theoretical pI and Mw values were calculated using
1185 https://web.expasy.org/compute_pi/. The RSP isoforms were detected using anti-HA antibodies.
1186
1187 **Figure 6-figure supplement 3**. Identification of Tetrahymena RSP orthologs
1188 .
1189 **Figure 6-figure supplement 3-Table 1A.** List of *Tetrahymena thermophila* radial spoke proteins
1190 identified in Tetrahymena Genome Database (TGD, https://tet.ciliate.org) using *Chlamydomonas*
1191 RSP proteins as baits. In the case of multiple hits (see details in **Table S1B**), it was analyzed if
1192 identified *Tetrahymena* RSP orthologs are present in the *Tetrahymena* ciliomes (Figure 4-Source
1193 Data 2'), co-immunoprecipitate with known RSPs (Figure 6-Source Data 1'), or are biotinylated
1194 in cilia of cells expressing RSP proteins fused with mutated BirA* ligase (Figure 6-Source Data
1195 2'). The identification of *Tetrahymena* orthologous proteins was verified by a reverse blast search

1196 against *Chlamydomonas reinhardtii* proteins (https://blast.ncbi.nlm.nih.gov). Domains were
1197 identified using SMART (http://smart.embl-heidelberg.de/) and InterProScan
1198 (https://www.ebi.ac.uk/interpro) programs.

1199 **Figure 6-figure supplement 3-Table 1B.** *Tetrahymena* RSP orthologs identified with multiple
1200 hits in TGD. In cases when numerous proteins were identified with similar scores in blastp search
1201 of *Tetrahymena* total proteome (TGD) using *Chlamydomonas* RSP as a bait, it was analyzed
1202 which of those proteins are present in *Tetrahymena* ciliome (Tables S3 and S4) and either co-
1203 immumoprecipitate (co-IP, Table S5) with known RSPs or are biotinylated (BioID, Table S6) in
1204 cells expressing known RS proteins as fusions with mutated BirA* ligase. Arrows indicate if
1205 there was a significant change (↑ increase or ↓ decrease) in the protein level in studied knock-out
1206 mutants (based on TMT analyses, Table S4). ns – change not significant, nd – protein not
1207 detected in the *Tetrahymena* ciliome.

1208

1209 **Figure 6-figure supplement 3-Table 2.** Comparative analyses of the levels of the radial spoke
1210 proteins in wild-type cells and radial spoke mutants

1211

1212 **Figure 6-figure supplement 3-Table 3.** Comparative analyses of the levels of potential radial
1213 spoke-associated proteins in wild-type cells and radial spoke mutants

1214

1215 **Figure 6-figure supplement 3-Table 4.** Comparative analyses of the levels of proteins with an
1216 enzymatic activities in radial spoke mutants

1217

1218 **Table 1**

1219 RSP proteins assigned to particular radial spoke types based on bioinformatics, proteomic, and
1220 cryo-EM data.

1221

RS1 3A-3A	**based on**	**RS1 3B-3B**	**based on**	**RS2 3B-3B**	**based on**	**RS2 3B-3C**	**based on**	**RS3**	**based on**
					RS head				
RSP1	BioID: 3A, co-IP: 3A	**RSP1**	3B-KO ↓ BioID: 3B, 4A, 4C	**RSP1**	3B-KO ↓ BioID: 3B, 4A, 4C	**RSP1**	3B-KO ↓ BioID: 3B, 4A, 4C	**LRRC23like 1?**	91-KO ↓ but 3B-KO ↑ 3C-KO ↑ Hwang et al., 2023
RSP4A	BioID	**RSP4A**	3B-KO ↓ BioID	**RSP4A**	3B-KO ↓ BioID	**RSP4A**	BioID		
RSP4C	BioID	**RSP4C**	3B-KO ↓ BioID	**RSP4C**	3B-KO ↓ BioID	**RSP4B**	3C-KO ↓ BioID		
RSP9	BioID	**RSP9**	3B-KO ↓ BioID	**RSP9**	3B-KO ↓ BioID	**RSP9**	BioID		
RSP10	BioID	**RSP10**	3B-KO ↓	**RSP10**	3B-KO ↓	**RSP10**	BioID		

			BioID		BioID				
				RS neck					
RSP2	3A-KO ↓ BioID: 3A, co-IP: 3A, 4A, 4C	**RSP2**	3B-KO ↓ BioID: 3B, 4A, 4C co-IP: 4A, 4C	**RSP2**	3B-KO ↓ BioID: 3B, 4A, 4C co-IP: 4A, 4C	**RSP2**	3B-KO ↓ BioID: 3B, 4A, 4C co-IP: 4A, 4C		
RSP12B	3A-KO ↓	**RSP12B**	3B-KO ↓	**RSP12A**	3B-KO ↓	**RSP12A**	3C-KO ↓		
RSP16A	3A-KO ↓ BioID	**RSP16A**	3B-KO ↓ BioID	**RSP16A**	3B-KO ↓ BioID	**RSP16B**	3C-KO ↓ BioID		
RSP23 **CFAP67B**	coIP	**RSP23** **CFAP67B**	coIP BioID	**RSP23** **CFAP67B**	coIP BioID	**RSP23** **CFAP67B**	coIP BioID		
CFAP198A	3A-KO ↓ BioID	**CFAP198A**	3B-KO ↓ BioID	**CFAP198A**	3B-KO ↓ BioID	**CFAP198B**	3C-KO ↓ BioID: CFAP206		
				RS stalk and base					
RSP3A	3A-KO ↓	**RSP3B**	3B-KO ↓	**RSP3B**	3B-KO ↓	**RSP3C**	3C-KO ↓		
RSP7A	BioID: 3A	**RSP7A**	3B-KO ↓ BioID	**RSP7A**	3B-KO ↓ BioID	**RSP7A**	BioID:3C	**RSP7B**	91-KO ↓ BioID:CFAP61
RSP11	3A-KO ↓	**RSP11**	3B-KO ↓	**RSP11**	3B-KO ↓	**RSP11**	3C-KO ↓	**CFAP61**	91-KO ↓ Urbanska et al., 2015
RSP14	3A-KO ↓	**RSP14**	3B-KO ↓	**RSP8**	3B-KO ↓	**RSP8**	3C-KO ↓	**CFAP251**	91-KO ↓ Urbanska et al., 2015
				RSP15	3B-KO ↓	**RSP15**	3C-KO ↓		
RSP20 ? **CaM1**		**RSP20** **CaM1**	3B-KO ↓ BioID:3B Gui et al., 2021	**RSP20** **CaM1**	3B-KO ↓ BioID:3B	**RSP20/CaM1**	3C-KO ↓		
CaM **7-2**	3A-KO ↓					**CaM 7-2**	3C-KO ↓		
RSP22/LC8	RS1 base in stable in 3A-KO coIP:3A BioID:3A	**RSP22/LC8**	3B-KO ↓	**RSP22/LC8**	3B-KO ↓	**RSP22/LC8**	RS2 base in stable in 3C-KO		
				CFAP206	3B-KO ↓ Vasudevan et al., 2015	**CFAP206**	Vasudevan et al., 2015		
CFAP207?	RS1 base in stable in 3A-KO	**CFAP207**	3B-KO ↓	**CFAP207**	3B-KO ↓ CFAP206-KO↓	**CFAP207**? ?	RS2 base in stable in 3A-KO		
CFAP253	BioID:3A	**CFAP253**	BioID:3B						
				New RS candidate proteins					
				TtTPR2	3B-KO ↓	**TtTPR1**	3C-KO ↓		
				Kelch motif-containing 2	3B-KO ↓			**Kelch motif-containing 1**	91-KO ↓
				LRR-containing	3B-KO ↓			**LRR-containing**	61-KO ↓ 91-KO ↓
								LRRC23-like2	61-KO ↓ 91-KO ↓
				RS associated enzymes					
AK8B	3A-KO ↓	**AK1**	3B-KO ↓	**AK1?**	3B-KO ↓ (not in CFAP206-KO)			AK7A	91-KO ↓
		AK8A		**AK8A?**	3B-KO ↓ (not in CFAP206-KO)			AK7B	91-KO ↓
				NDK	3B-KO ↓	**NDK**	3C-KO ↓	AK9	91-KO ↓
								GK1	91-KO ↓
				PKA	3B-KO ↓	**PKA**	3C-KO ↓	PDE	61-KO ↓ 91-KO ↓
				Ca/CaM-dependent kinase	3B-KO ↓	**Ca/CaM-dependent kinase**	3C-KO ↓	Casein kinase	61-KO ↓ 91-KO ↓ BioID

Table 2

Comparative analyses of the levels of inner dynein arms (IDAs) components in RSP3 mutants

Protein name	Numer in TGD	RSP3A-KO/WT				RSP3B-KO/WT				RSP3C-KO/WT			
		LFQ		TMT		LFQ		TMT		LFQ		TMT	
		q-value	difference	q-value	difference	q-value	difference	q-value	difference	q-value	difference	q-value	difference
DYH6	TTHERM_00688470	0,427619	-0,63	0,97248	0,00	0,829776	-0,11	0,0333644	0,19	0,42251	-0,58	0,22074	0,14
DYH7	TTHERM_00912290	0,63228	-0,26	0,92333	0,01	0,889118	0,06	0,0436144	0,17	0,552849	-0,36	0,25214	0,14
DYH8	TTHERM_00531870	nd		0,35423	-0,09	nd		0,794792	0,02	nd		0,05891	0,27
DYH9	TTHERM_00947430	**0,212183**	**-2,35**	**0,01518**	**-0,47**	0,19376	-1,15	0,138485	-0,11	0,202845	-2,54	0,13222	-0,19
DYH10	TTHERM_00420340	nd		0,24242	-0,12	nd		**0,0211327**	**-0,26**	nd		0,78056	-0,03
DYH11	TTHERM_00252430	0,278289	-1,14	0,64207	0,04	0,079717	-1,13	0,695276	-0,02	0,207409	-1,33	0,61464	-0,05
DYH12	TTHERM_00919540	0,391149	-0,81	0,77556	-0,03	**0,016857**	**-3,02**	**0,0024172**	**-0,39**	0,216267	-1,14	0,89791	-0,01
DYH14	TTHERM_00492830	0,627178	-0,26	0,86334	-0,02	0,81443	0,11	0,0682636	0,15	0,604414	-0,28	0,36991	0,10
DYH15	TTHERM_00433800	0,509668	-0,39	0,53573	0,06	0,98351	-0,01	0,035494	0,19	0,58223	-0,33	0,13251	0,19
DYH16	TTHERM_00558640	0,500578	-0,41	0,49759	0,06	0,663928	-0,19	0,0255092	0,21	0,478641	-0,44	0,13177	0,20
DYH17	TTHERM_00850620	nd		0,16265	-0,15	nd		0,322829	-0,06	nd		0,56919	0,06
DYH19	TTHERM_01027670	0,59496	-0,32	0,13983	0,16	0,650933	-0,20	0,0160624	0,26	0,456762	-0,57	0,1503	0,17
DYH20	TTHERM_00821980	nd		0,27734	-0,11	nd		0,546651	0,04	nd		0,04042	0,29
DYH22	TTHERM_00565600	0,739417	-0,17	0,89428	0,01	0,80461	-0,12	0,0433816	0,18	0,728791	-0,18	0,63557	0,05
DYH23	TTHERM_00355100	nd		0,568953	-0,05	nd		0,716902	0,02	nd		0,36156	0,12
DYH24	TTHERM_00193520	0,454189	-0,60	0,04083	0,26	0,0565	-1,13	0,261682	0,07	0,306765	-0,88	0,23358	0,15
DYH25	TTHERM_00774810	0,497702	-0,46	0,29773	0,11	**2,36E-05**	**-4,25**	**0,004094**	**-0,77**	0,227139	-1,28	0,19224	-0,16
p28A	TTHERM_00841210	0,62273	0,34	0,13922	0,17	0,140637	-1,09	0,574056	0,04	0,529654	-0,45	0,28815	0,11
p28B	TTHERM_00319990	0,918872	0,05	0,71511	0,04	**0,186438**	**-0,70**	**0,0378964**	**-0,20**	0,546171	-0,42	0,43061	0,11
p28C	TTHERM_01129720	0,931915	0,05	0,8939	0,013	0,978215	-0,016	0,0700761	0,16	0,478333	-0,44	0,59091	0,07

Significant changes are marked in red; TGD – Tetrahymena Genome Database; LFQ – label-free quantification, TMT- tandem mass tag 10-plex isobaric mass tagging approaches. Proteins listed as DYH13 (TTHERM_001104900) and DYH18 (TTHERM_00047540) in the TGD were not identified (nd, not detected) in the analyzed ciliomes.

Supplementary Tables

Table S1. List of primers used in this study. The nucleotide sequences recognized by the restriction endonucleases are in bold.

Source data

Figure 2-Source data1'. The analyses of the swimming rate of wild-type and RSP3 mutant cells

Figure 2-Source data2'. The analyses of the cilia beating frequency in wild-type and RSP3 mutant cells.

Figure 4-Source data1'. LFQ-based identification of proteins with altered (reduced or elevated) levels in radial spoke mutants.

1244 **Figure 4-Source data2'.** Tandem Mass Tag (TMT)-based identification of proteins with altered
1245 (reduced or elevated) levels in radial spoke mutants.
1246
1247 **Figure 6-Source data1'.** Mass spectrometry analysis of the ciliary proteins that co-
1248 immunoprecipitated with RSP3A-3HA, RSP4A-3HA, RSP4B-3HA, or RSP4C-3HA, all
1249 expressed at native levels. The radial spoke proteins are highlighted: RS head (dark blue), RS
1250 neck (yellow), RS stalk (green and light green), former CSC complex components and CFAP206
1251 (violet), new RS components identified by Gui et al., 2021 (light brown), new putative RS
1252 components (pink), adenylate kinases (dark yellow), other enzymes (orange), and central
1253 apparatus components (cyan).
1254
1255 **Figure 6-Source data2'.** Mass spectrometry analysis of proteins biotinylated in cells expressing
1256 RSP3A, RSP3B, RSP3C, RSP4A, RSP4B, RSP4C, CFAP61, CFAP91, or CFAP206 with a C-
1257 terminal –HA-BirA* tag under the control of the respective native promoters. The radial spoke
1258 proteins are highlighted: RS head (dark blue), RS neck (yellow), RS stalk (green and light green),
1259 former CSC complex components and CFAP206 (violet), new RS components identified by Gui
1260 et al., 2021 (light brown), new putative RS components (pink), adenylate kinases (dark yellow),
1261 other enzymes (orange), central apparatus components (cyan).

Figure 1

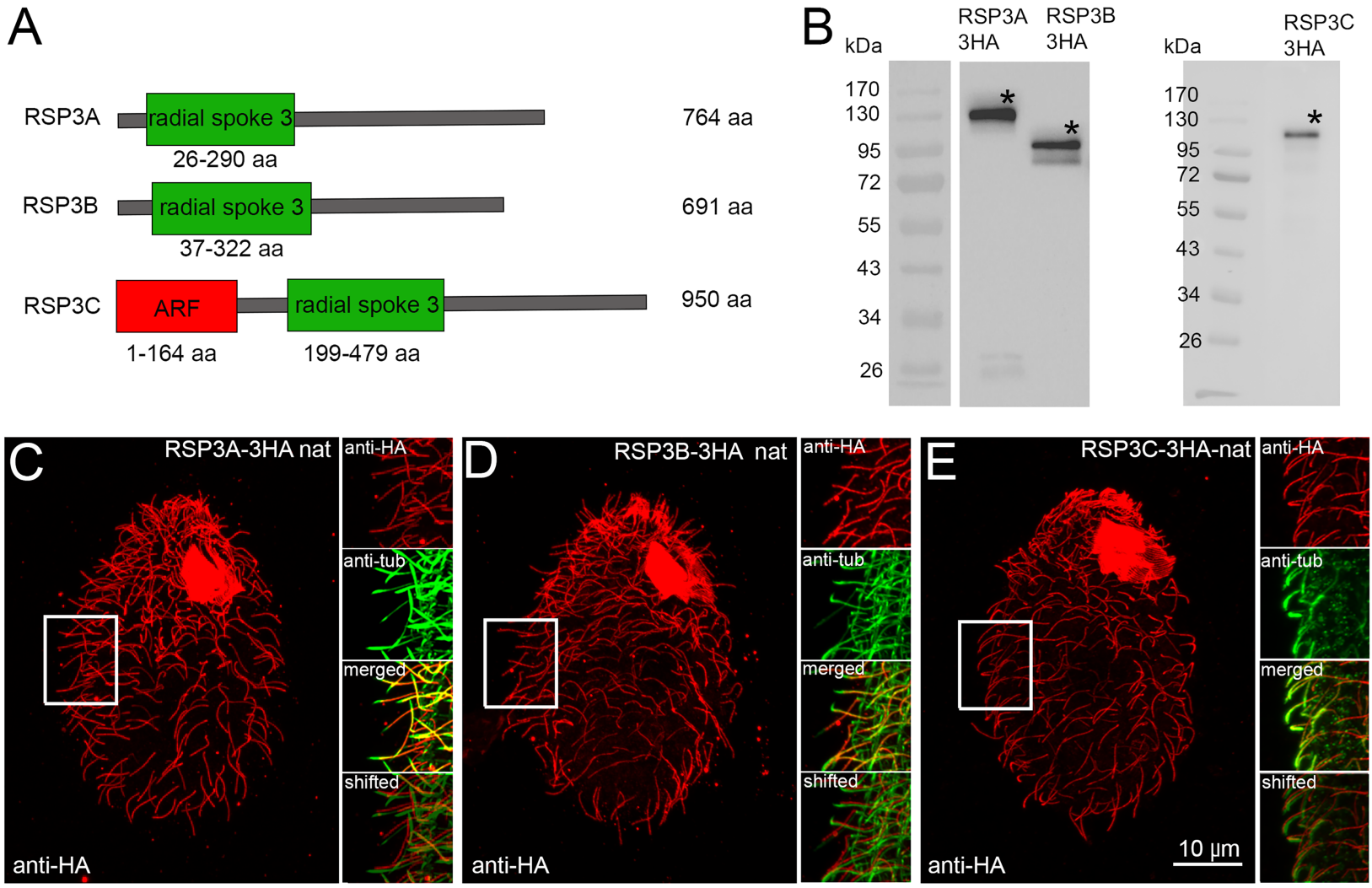
A
RSP3A
radial spoke 3
26-290 aa
764 aa
RSP3B
radial spoke 3
37-322 aa
691 aa
RSP3C
ARF
radial spoke 3
1-164 aa
199-479 aa
950 aa
B
kDa
RSP3A 3HA
RSP3B 3HA
170
130
95
72
55
43
34
26
kDa
RSP3C 3HA
170
130
95
72
55
43
34
26
C
RSP3A-3HA nat
anti-HA
anti-tub
merged
shifted
anti-HA
D
RSP3B-3HA nat
anti-HA
anti-tub
merged
shifted
anti-HA
E
RSP3C-3HA-nat
anti-HA
anti-tub
merged
shifted
anti-HA
10 µm

Figure 2

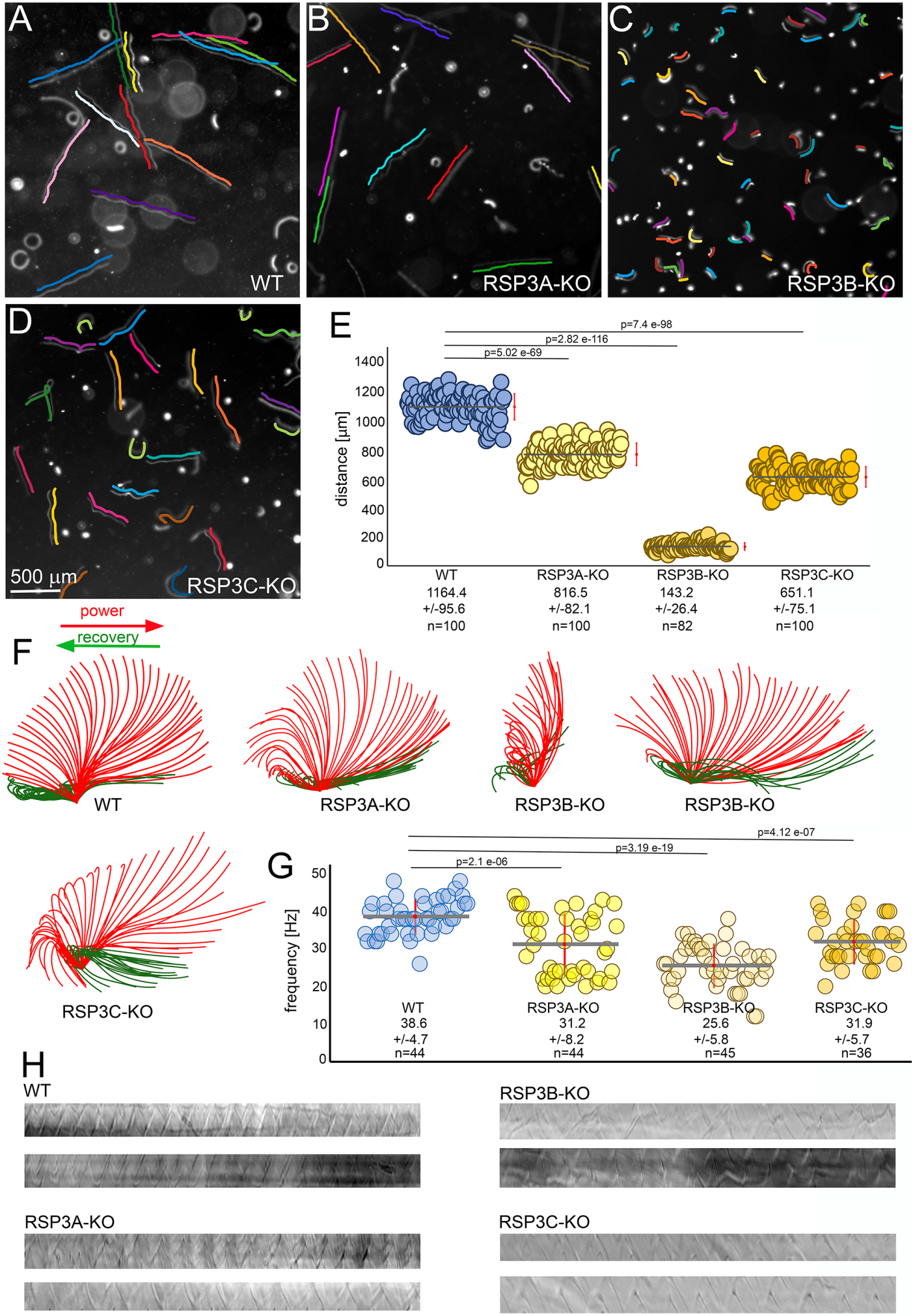
A
WT
B
RSP3A-KO
C
RSP3B-KO
D
500 µm
RSP3C-KO
E
p=7.4 e-98
p=2.82 e-116
p=5.02 e-69
distance [µm]
1400
1200
1000
800
600
400
200
0
WT
1164.4
+/-95.6
n=100
RSP3A-KO
816.5
+/-82.1
n=100
RSP3B-KO
143.2
+/-26.4
n=82
RSP3C-KO
651.1
+/-75.1
n=100
power
recovery
F
WT
RSP3A-KO
RSP3B-KO
RSP3B-KO
RSP3C-KO
G
p=4.12 e-07
p=3.19 e-19
p=2.1 e-06
frequency [Hz]
50
40
30
20
10
0
WT
38.6
+/-4.7
n=44
RSP3A-KO
31.2
+/-8.2
n=44
RSP3B-KO
25.6
+/-5.8
n=45
RSP3C-KO
31.9
+/-5.7
n=36
H
WT
RSP3B-KO
RSP3A-KO
RSP3C-KO

Figure 2-figure supplement 1

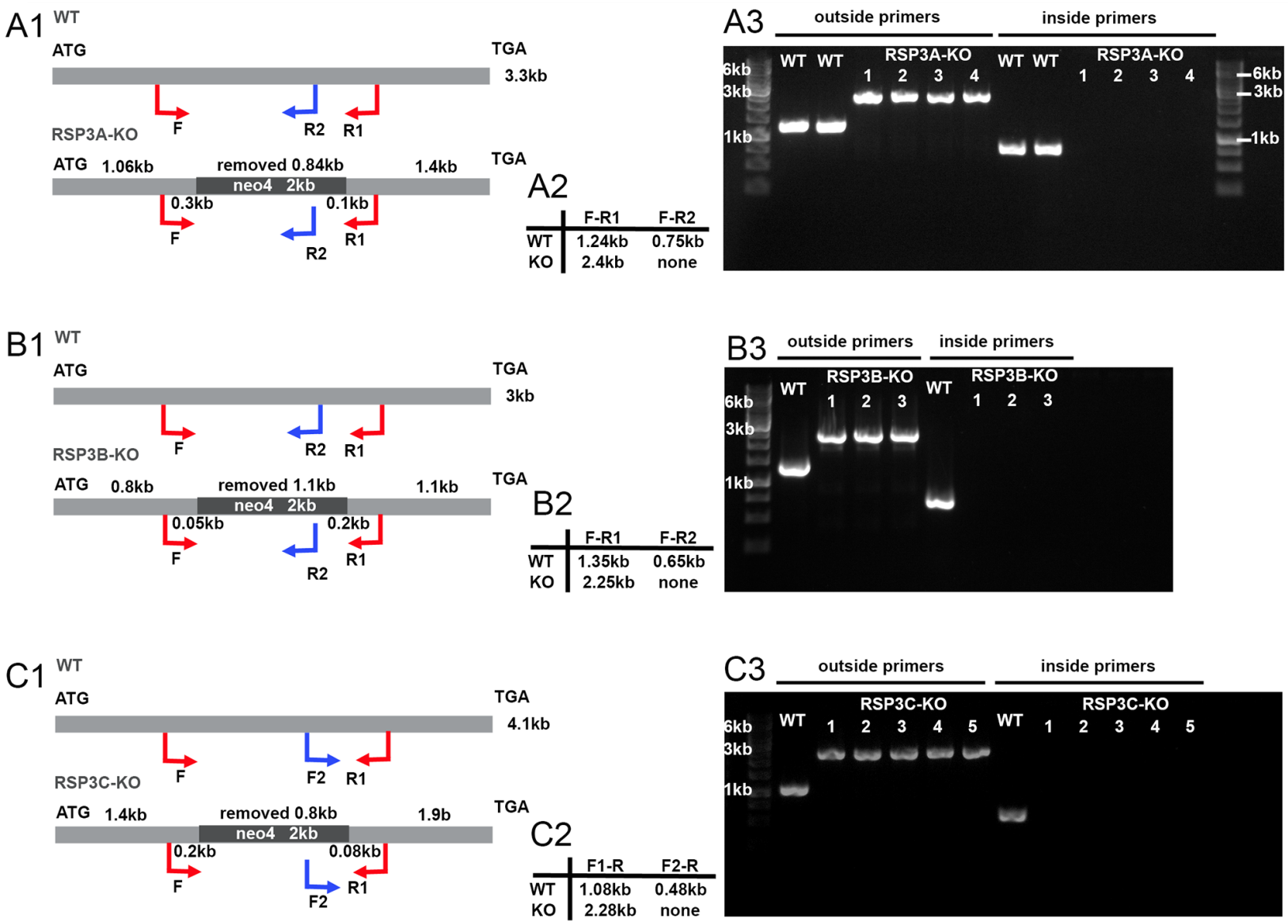

Figure 2-figure supplement 2

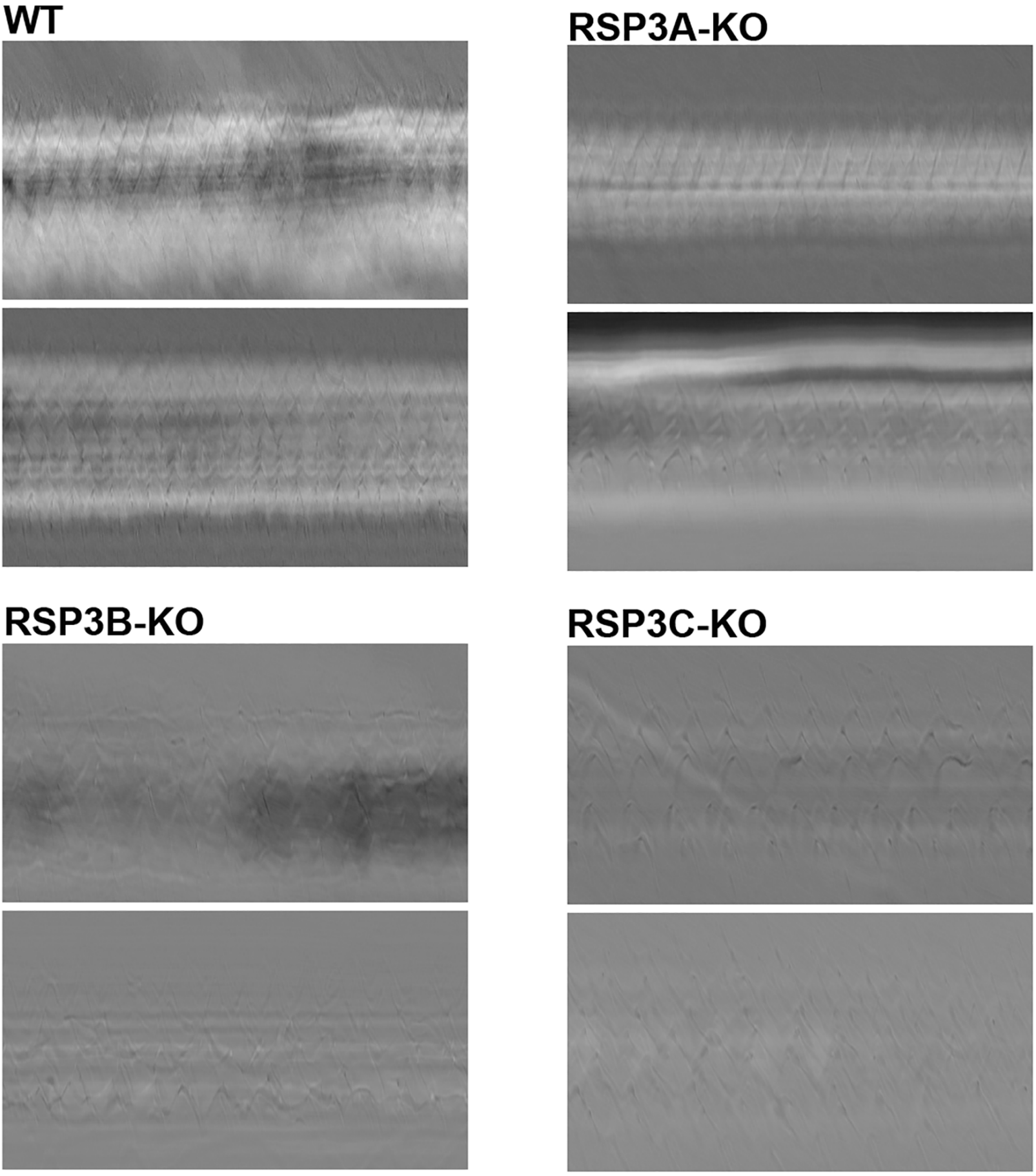

Figure 3

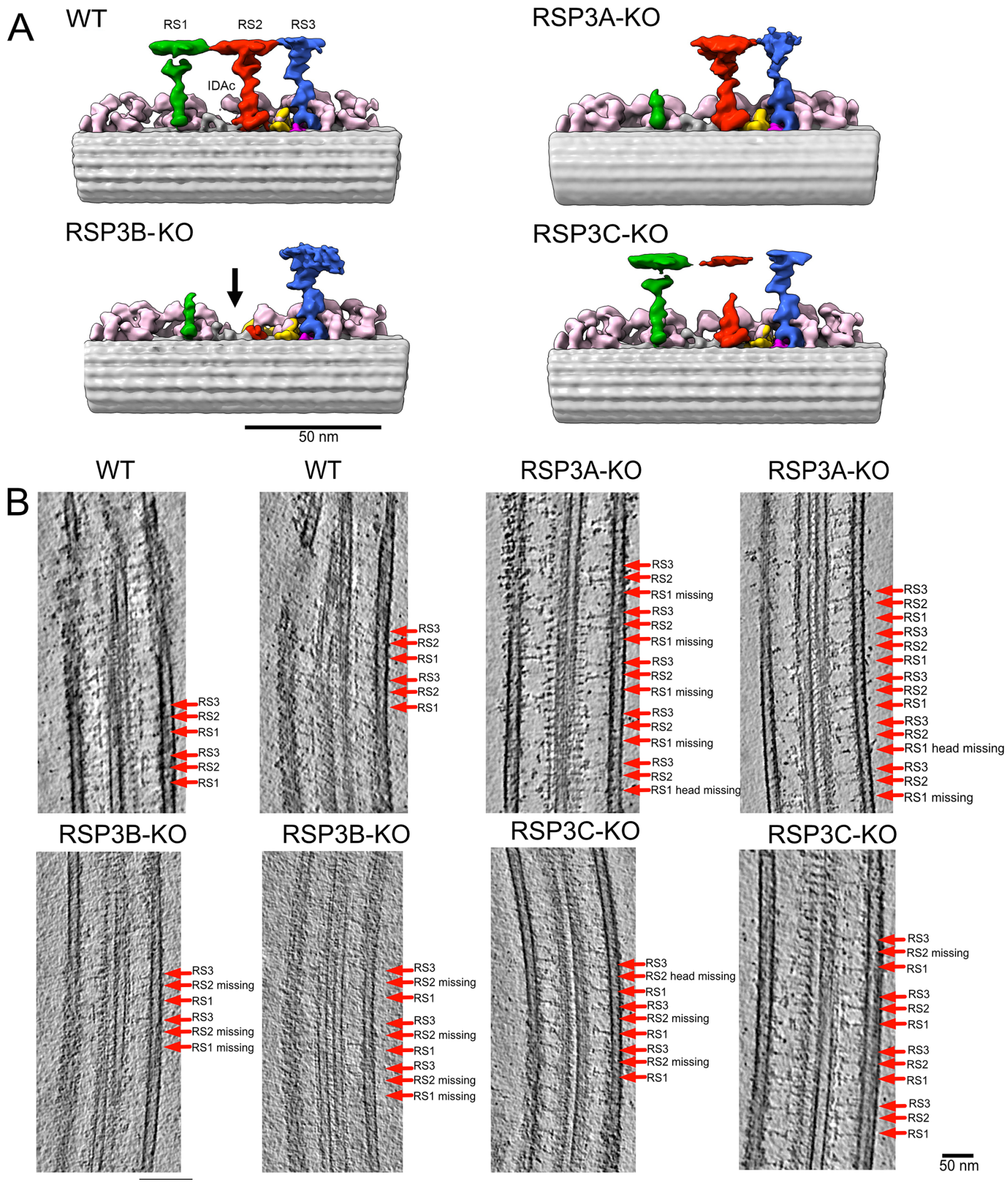
A
WT
RS1
RS2
RS3
IDAc
RSP3A-KO
RSP3B-KO
RSP3C-KO
50 nm
B
WT
RS3
RS2
RS1
RS3
RS2
RS1
WT
RS3
RS2
RS1
RS3
RS2
RS1
RSP3A-KO
RS3
RS2
RS1 missing
RS3
RS2
RS1 missing
RS3
RS2
RS1 missing
RS3
RS2
RS1 missing
RS3
RS2
RS1 head missing
RSP3A-KO
RS3
RS2
RS1
RS3
RS2
RS1
RS3
RS2
RS1
RS3
RS2
RS1 head missing
RS3
RS2
RS1 missing
RSP3B-KO
RS3
RS2 missing
RS1
RS3
RS2 missing
RS1 missing
RSP3B-KO
RS3
RS2 missing
RS1
RS3
RS2 missing
RS1
RS3
RS2 missing
RS1 missing
RSP3C-KO
RS3
RS2 head missing
RS1
RS3
RS2 missing
RS1
RS3
RS2 missing
RS1
RSP3C-KO
RS3
RS2 missing
RS1
RS3
RS2
RS1
RS3
RS2
RS1
RS3
RS2
RS1
50 nm

Figure 3-figure supplement 1

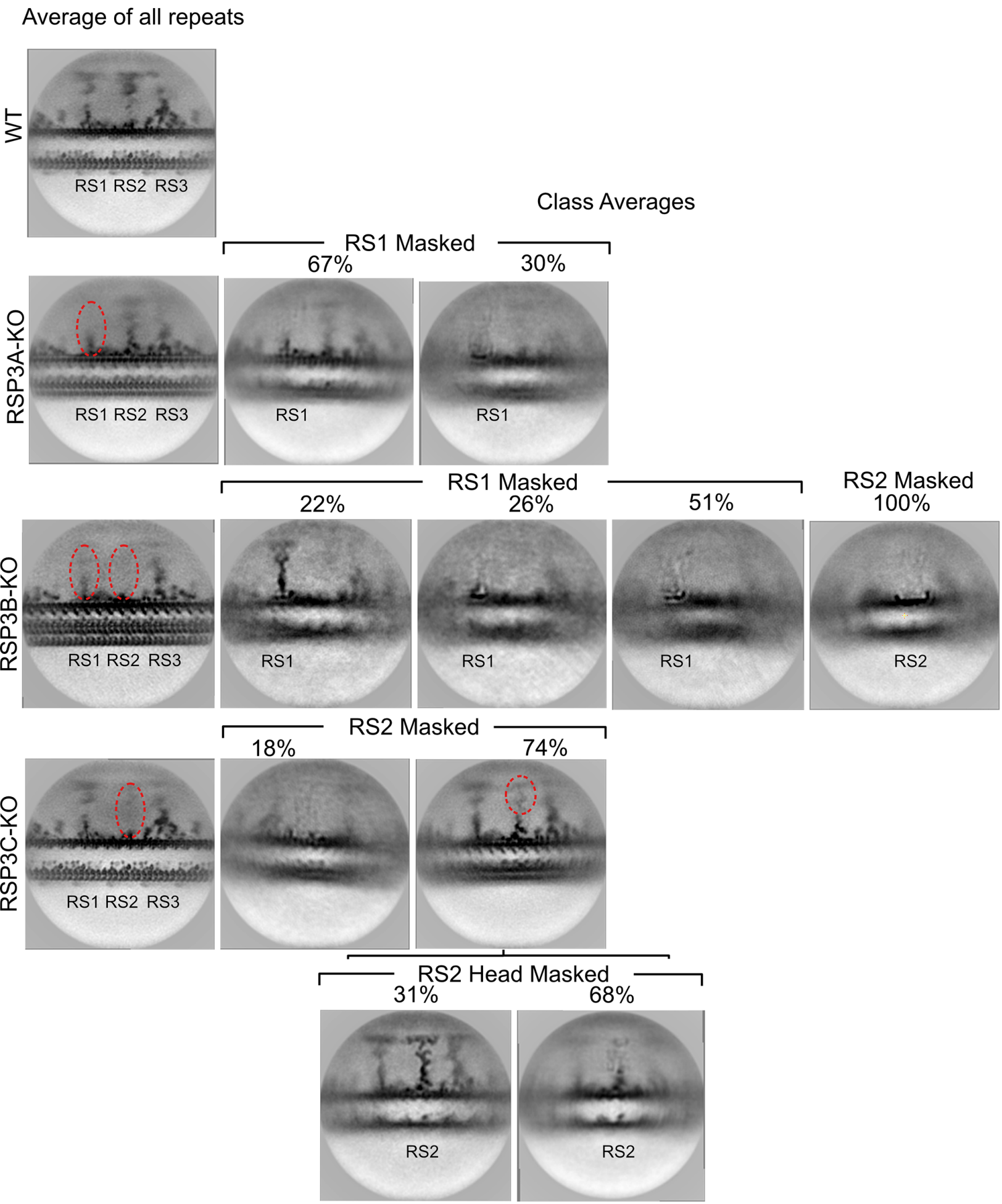

Figure 3-figure supplement 2

Data collection and analysis parameters for cryo-ET and subtomogram averaging.

Method	**Subtomogram Averaging**			
Dataset	***WT***	***RSP3A-KO***	***RSP3B-KO***	***RSP3C-KO***
Microscope	Titan Krios	Titan Krios	Titan Krios	Titan Krios
Electron Detector	Gatan K3	Gatan K3	Gatan K3	Gatan K3
Zero-loss filter (eV)	20	20	20	20
Magnification	42,000	42,000	42,000	42,000
Voltage (keV)	300	300	300	300
Exposure (e/A^2)	160	160	80	160
Defocus (µm)	1.0-3.0	3.5-5.0	3-4	2.5-4.0
Pixel size (Å)	2.12	2.12	2.12	2.12
Tilt range (increment)	-60° - 60° (3°)	-60° - 60° (3°)	-60° - 60° (3°)	-60° - 60° (3°)
Tilt scheme	dose symmetric	dose symmetric	dose symmetric	dose symmetric
Tilt series acquired	58	37	50	38
Subtomo averaged	2608	2099	2093	2790
Symmetry imposed	C1	C1	C1	C1
Map resolution (Å)	19	20	22	17

Figure 4

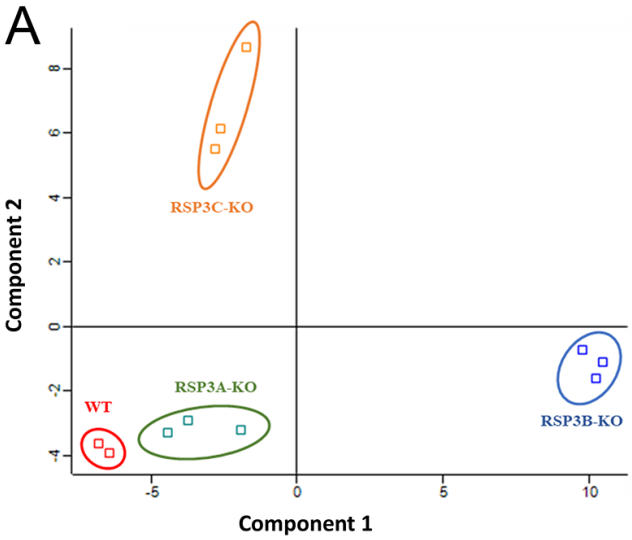
A
RSP3C-KO
RSP3A-KO
WT
RSP3B-KO
Component 1
Component 2

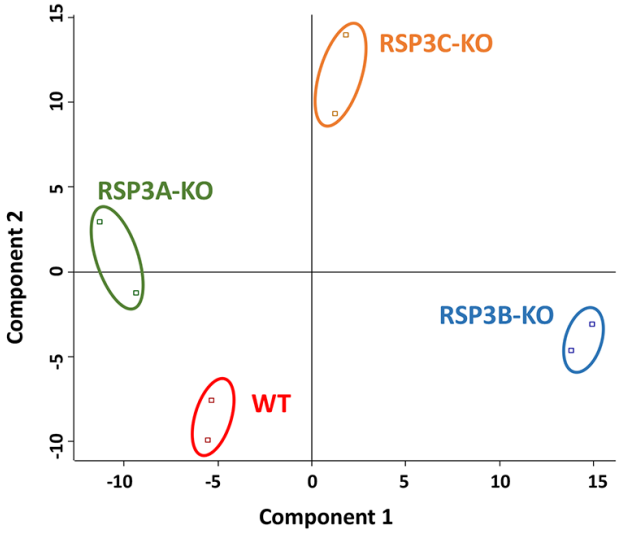
RSP3C-KO
RSP3A-KO
RSP3B-KO
WT
Component 1
Component 2

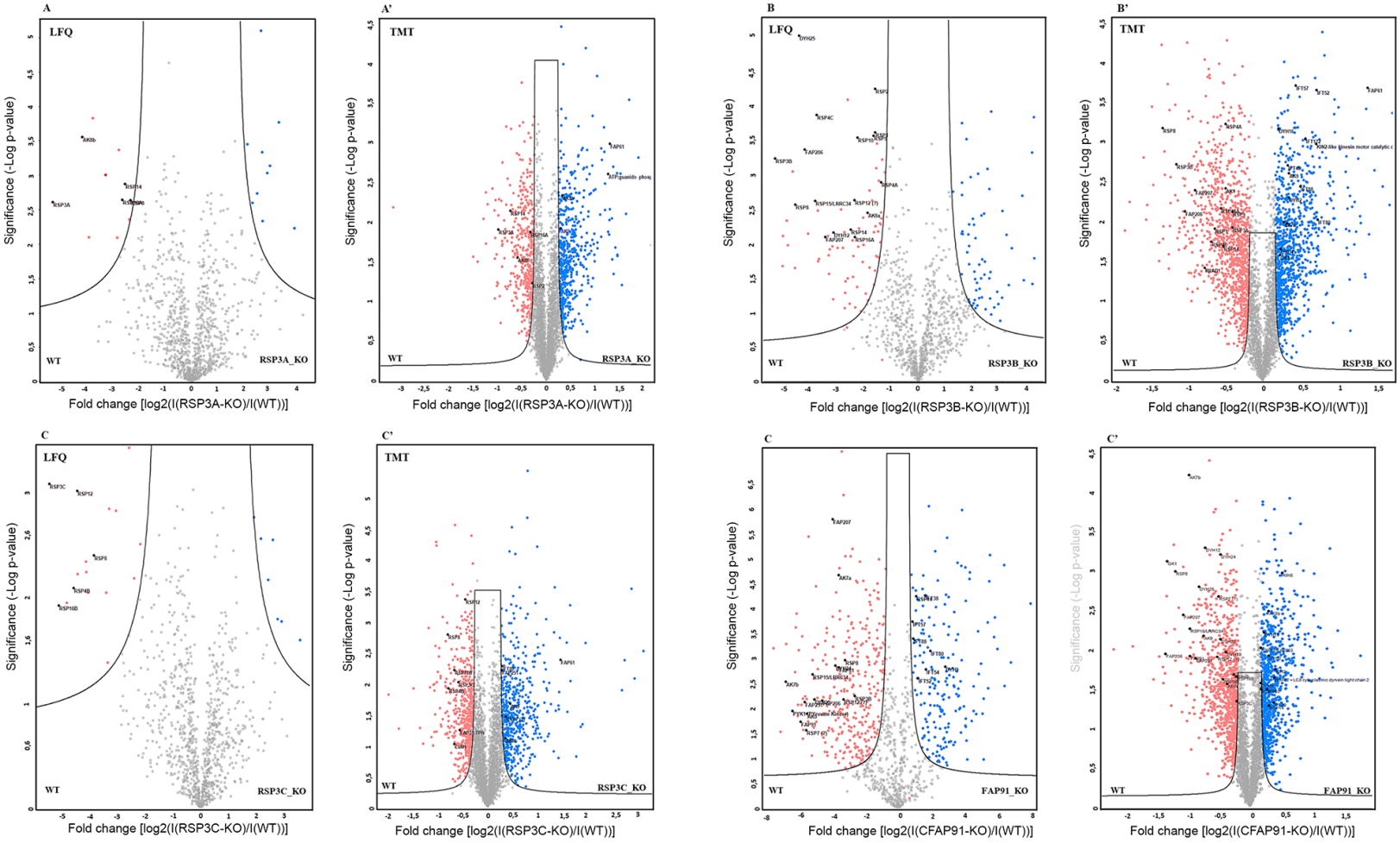
B
A
LFQ
WT
RSP3A_KO
Significance (-Log p-value)
Fold change [log2(I(RSP3A-KO)/I(WT))]
A'
TMT
WT
RSP3A_KO
Fold change [log2(I(RSP3A-KO)/I(WT))]
B
LFQ
WT
RSP3B_KO
Fold change [log2(I(RSP3B-KO)/I(WT))]
B'
TMT
WT
RSP3B_KO
Fold change [log2(I(RSP3B-KO)/I(WT))]
C
LFQ
WT
RSP3C_KO
Fold change [log2(I(RSP3C-KO)/I(WT))]
C'
TMT
WT
RSP3C_KO
Fold change [log2(I(RSP3C-KO)/I(WT))]
C
WT
FAP91_KO
Fold change [log2(I(CFAP91-KO)/I(WT))]
C'
WT
FAP91_KO
Fold change [log2(I(CFAP91-KO)/I(WT))]

Figure 5

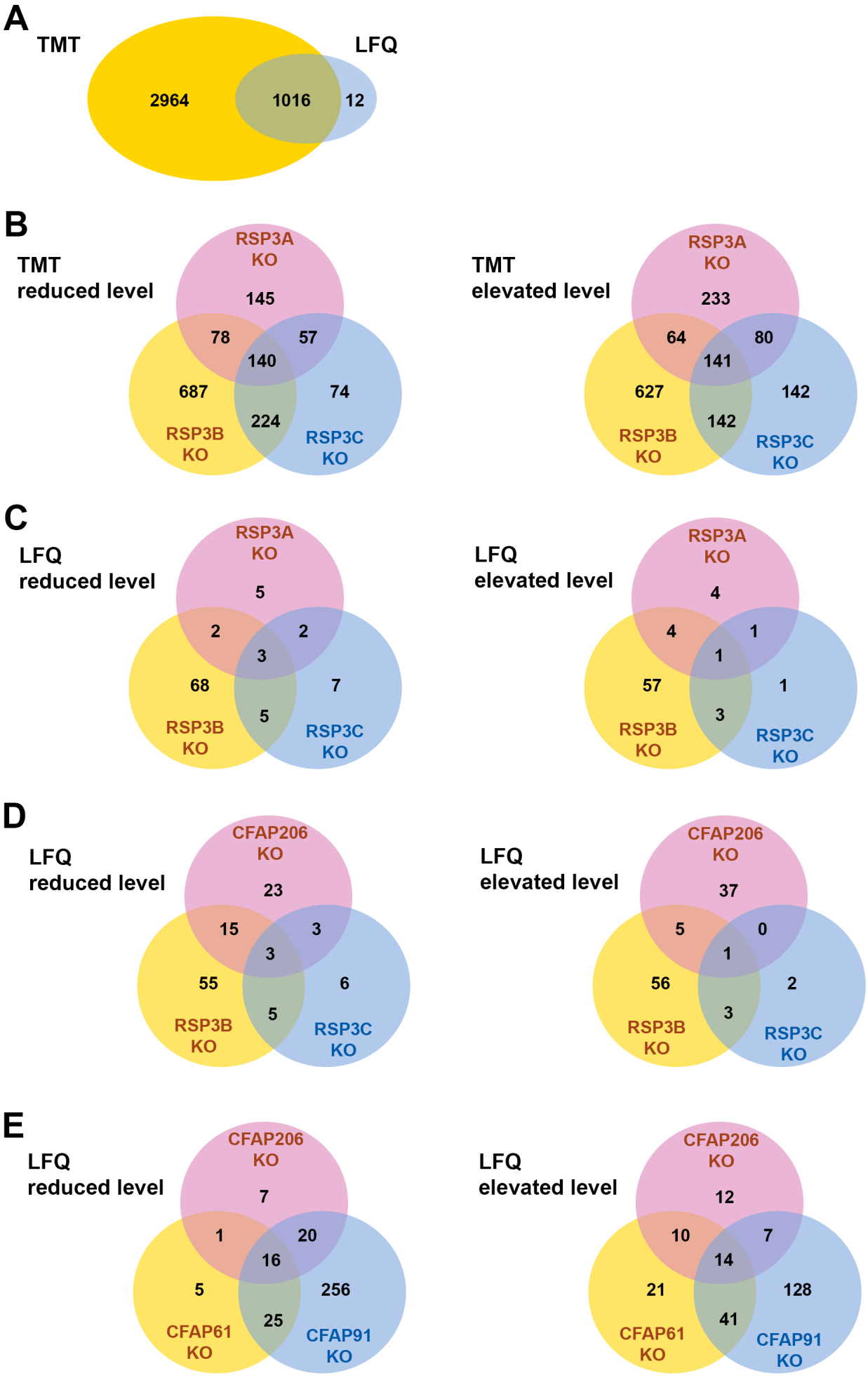
A
TMT
LFQ
2964
1016
12
B
TMT
reduced level
RSP3A KO
145
78
57
140
687
74
224
RSP3B KO
RSP3C KO
TMT
elevated level
RSP3A KO
233
64
80
141
627
142
142
RSP3B KO
RSP3C KO
C
LFQ
reduced level
RSP3A KO
5
2
2
3
68
7
5
RSP3B KO
RSP3C KO
LFQ
elevated level
RSP3A KO
4
4
1
1
57
1
3
RSP3B KO
RSP3C KO
D
LFQ
reduced level
CFAP206 KO
23
15
3
3
55
6
5
RSP3B KO
RSP3C KO
LFQ
elevated level
CFAP206 KO
37
5
0
1
56
2
3
RSP3B KO
RSP3C KO
E
LFQ
reduced level
CFAP206 KO
7
1
20
16
5
256
25
CFAP61 KO
CFAP91 KO
LFQ
elevated level
CFAP206 KO
12
10
7
14
21
128
41
CFAP61 KO
CFAP91 KO

Figure 6

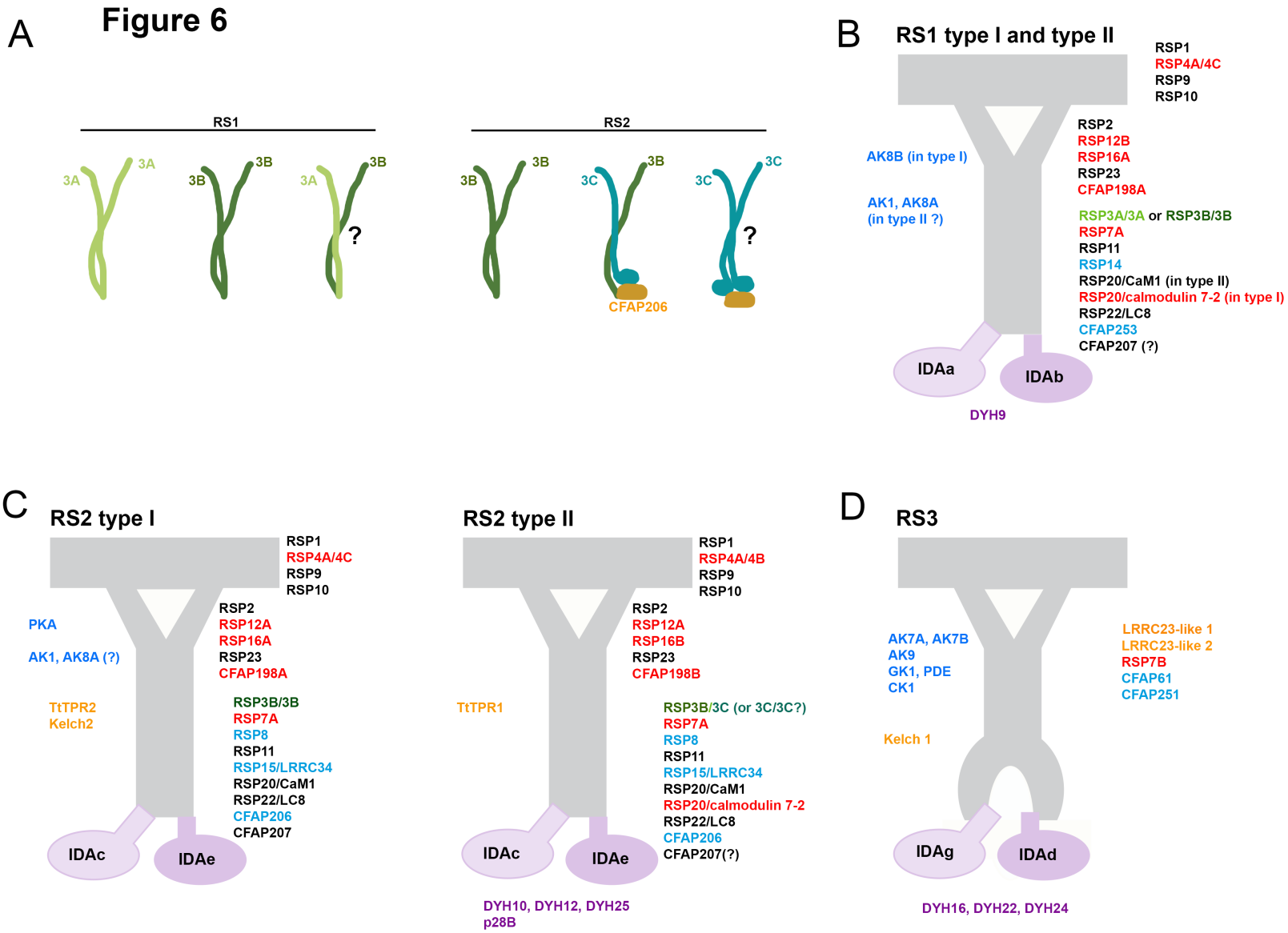
A
RS1
3A
3A
3B
3B
3A
3B
?
RS2
3B
3B
3C
3B
3C
3C
?
CFAP206
B
RS1 type I and type II
RSP1
RSP4A/4C
RSP9
RSP10
RSP2
RSP12B
RSP16A
RSP23
CFAP198A
AK8B (in type I)
AK1, AK8A
(in type II ?)
RSP3A/3A or RSP3B/3B
RSP7A
RSP11
RSP14
RSP20/CaM1 (in type II)
RSP20/calmodulin 7-2 (in type I)
RSP22/LC8
CFAP253
CFAP207 (?)
IDAa
IDAb
DYH9
C
RS2 type I
RSP1
RSP4A/4C
RSP9
RSP10
RSP2
RSP12A
RSP16A
RSP23
CFAP198A
PKA
AK1, AK8A (?)
TtTPR2
Kelch2
RSP3B/3B
RSP7A
RSP8
RSP11
RSP15/LRRC34
RSP20/CaM1
RSP22/LC8
CFAP206
CFAP207
IDAc
IDAe
RS2 type II
RSP1
RSP4A/4B
RSP9
RSP10
RSP2
RSP12A
RSP16B
RSP23
CFAP198B
TtTPR1
RSP3B/3C (or 3C/3C?)
RSP7A
RSP8
RSP11
RSP15/LRRC34
RSP20/CaM1
RSP20/calmodulin 7-2
RSP22/LC8
CFAP206
CFAP207(?)
IDAc
IDAe
DYH10, DYH12, DYH25
p28B
D
RS3
AK7A, AK7B
AK9
GK1, PDE
CK1
Kelch 1
LRRC23-like 1
LRRC23-like 2
RSP7B
CFAP61
CFAP251
IDAg
IDAd
DYH16, DYH22, DYH24

Figure 6-figure supplement 1

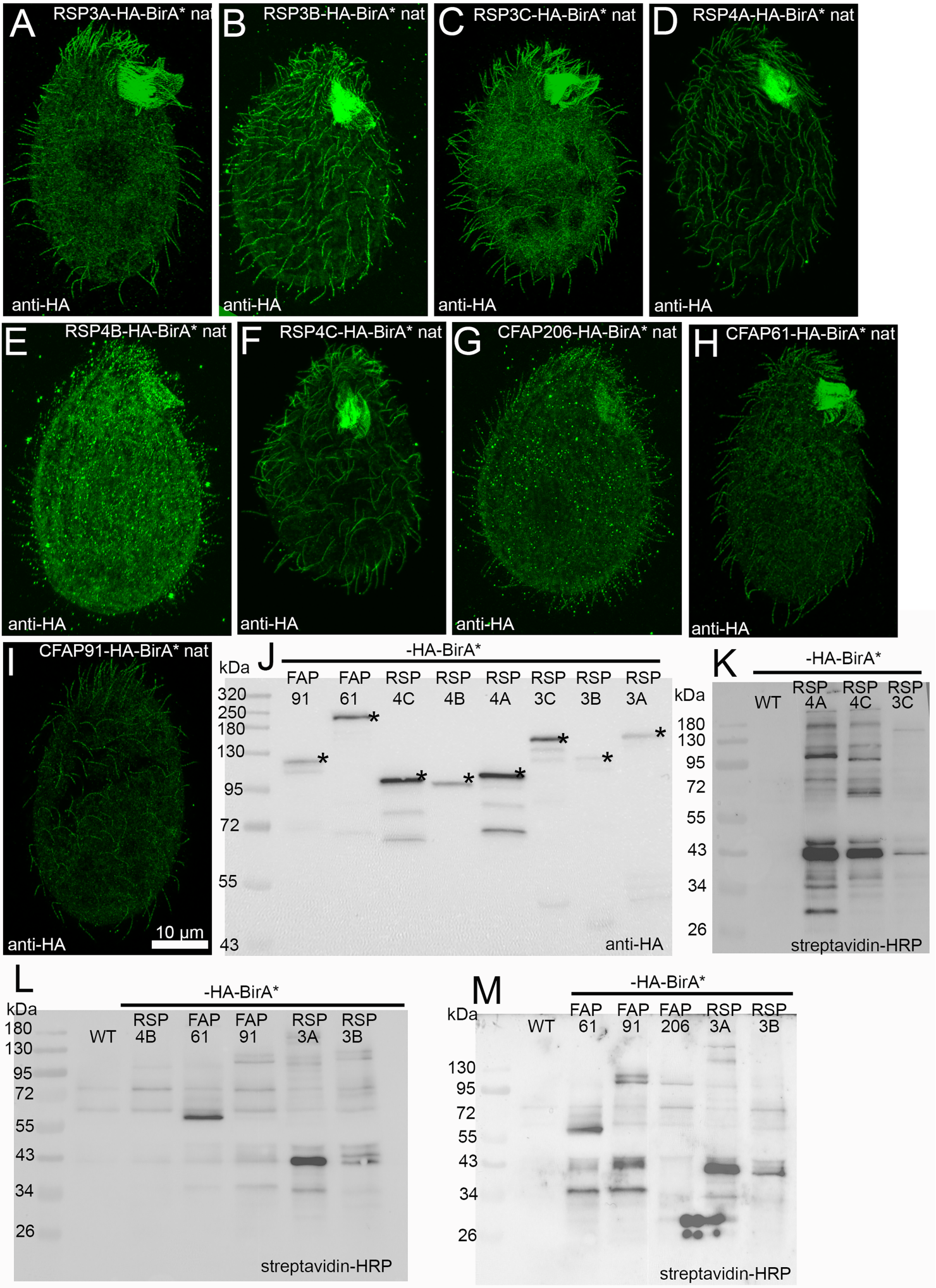

Figure 6-figure supplement 2

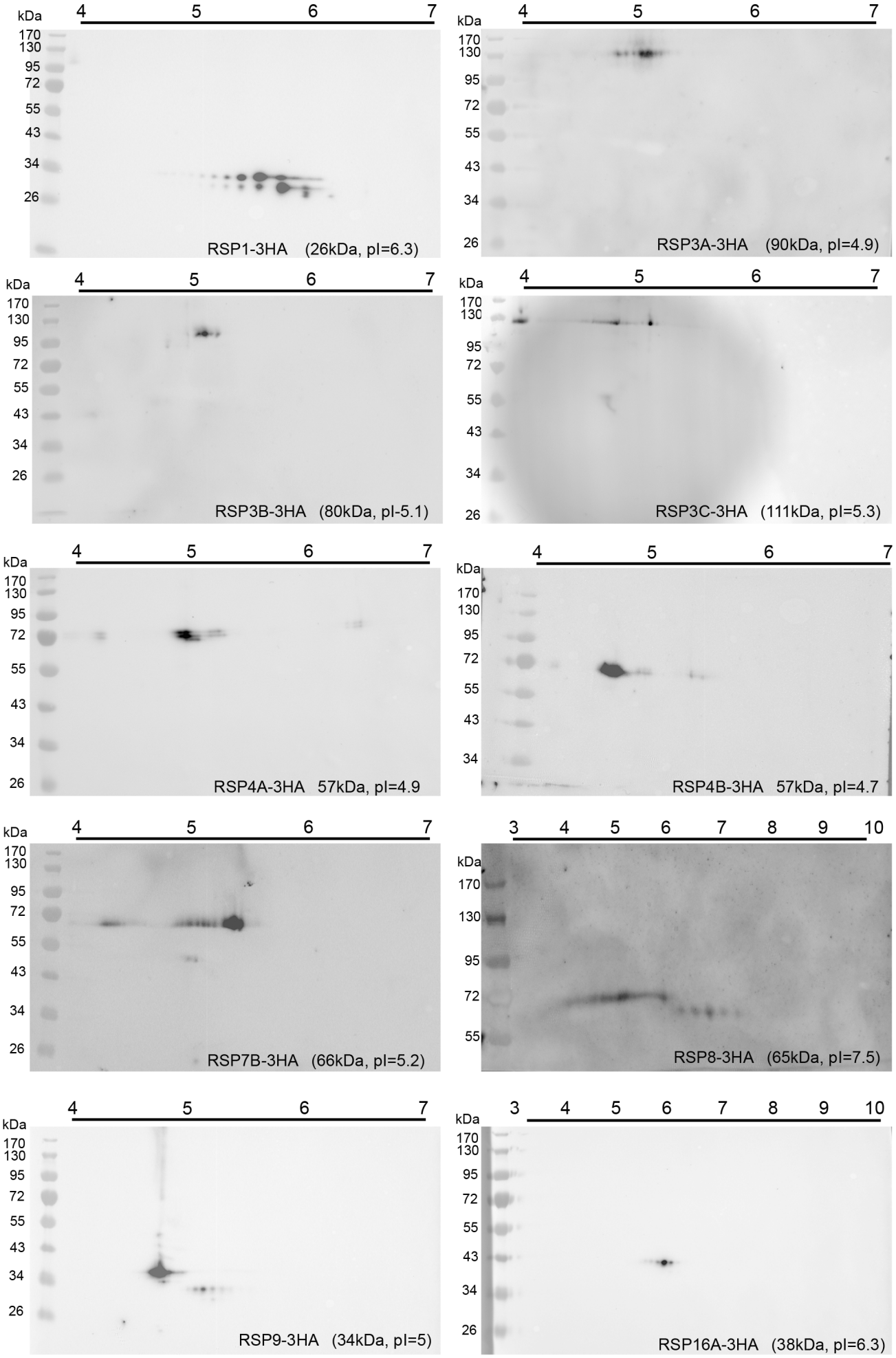

Figure 6-figure supplement 3. Identification of Tetrahymena RSP orthologs

Figure 6-figure supplement 3-Table 1A. List of *Tetrahymena thermophila* radial spoke proteins identified in Tetrahymena Genome Database (TGD, https://tet.ciliate.org) using *Chlamydomonas* RSP proteins as baits. In the case of multiple hits (see details in **Table S1B**), it was analyzed if identified *Tetrahymena* RSP orthologs are present in the *Tetrahymena* ciliomes (Figure 4-Source Data 2'), co-immunoprecipitate with known RSPs (Figure 6-Source Data 1'), or are biotinylated in cilia of cells expressing RSP proteins fused with mutated BirA* ligase (Figure 6-Source Data 2'). The identification of *Tetrahymena* orthologous proteins was verified by a reverse blast search against *Chlamydomonas reinhardtii* proteins (https://blast.ncbi.nlm.nih.gov). Domains were identified using SMART (http://smart.embl-heidelberg.de/) and InterProScan (https://www.ebi.ac.uk/interpro) programs.

RS protein	RS part	domains	MW (kD)	pI	TGD number TTHERM_	% of identity / similarity	E-value (TGD blastp)
RSP1	head	MORN	26	6.3	TTHERM_000196029	31/49	3.19514e-12
RSP2	neck	DPY-30 CC	75	4.7	TTHERM_00394410	37/51 within DPY	0.000540192
RSP3	stalk	AKAP AKAP ARF, AKAP	90 80 111	4.9 5.1 5.3	RSP3A TTHERM_01044600 RSP3B TTHERM_00566810 RSP3C TTHERM_00418270	44/60 41/65 31/54	2.34814e-19 2.1949e-41 8.00525e-20
RSP4 RSP6	head	Unknown Unknown Unknown	57 57 54	4.9 4.7 4.9	RSP4A TTHERM_00427590 RSP4B TTHERM_00502580 RSP4C TTHERM_00444180	23/39 22/43 30/48	1.40043e-13 5.25581e-26 2.00863e-31
RSP5	**not found**						
RSP7	stalk	RIIa, IQ AKAP28, EF hand	39 66	4.7 5.2	RSP7A TTHERM_00670610 RSP7B TTHERM_00492840	50/64 (N-term only) 20/38	3.31578e-05 6.65092e-05
RSP8	stalk	ARM-like	65	7.5	TTHERM_00313520	30/47	4.89747e-16
RSP9	head	unknown	34	5	TTHERM_00430020	26/43	6.28284e-12
RSP10	head	MORN	27	5.3	TTHERM_00378600	36/49	1.78444e-19
RSP11	stalk	RIIa	9	7.9	TTHERM_00540090	60/72	1.62388e-11
RSP12	stalk near neck	Pro-isomerase Fructose-1,6-bisphosphatase	126	9.3	RSP12A TTHERM_01018330	37/58 (cover 11%)	2.06701e-19
RSP12	stalk near neck	Pro-isomerase Fructose-1,6-bisphosphatase	102	9.0	RSP12B TTHERM_00466090	33/49	3.9832e-18
RSP13	**no Chlamydomonas sequence available**						
RSP14	stalk	RPT2, HEAT ARM-like	41	5.7	TTHERM_000773538	20/43	0.481103
RSP15	stalk	LRR	47	5.7	LRRC34 TTHERM_00695730	28/46	5.12592e-19
RSP16	neck	DNAJ/DNAJ-C DNAJ/DNAJ-C	38 39	6.3 6.2	RSP16A TTHERM_00471260 RSP16B TTHERM_00238810	36/53 32/51	1.2198e-43 3.53246e-40
RSP17	**not found**						
RSP18	RS2,	FAP91 domain	76	7.3	CFAP91 TTHERM_00578560	33/53	2.20388e-19

	RS3 adaptor	CC					
RSP19	RS3 stalk	DUF4821 FAD/NAD(P) binding CC	198	5.4	CFAP61 TTHERM_00641200	25/42	4.98635e-36
RSP20	stalk	EF hand	17	4	Calmodulin TTHERM_00630500	88/95	7.17305e-92
RSP20 (?)	stalk?	EF hand	24	4.8	CaM 7-2 TTHERM_00549500	25/54	4.0036e-14
RSP21	**no Chlamydomonas sequence available**						
RSP22	stalk	LC8	10	6.8	TTHERM_000649439	85/92	7.13575e-57
RSP23 CFAP67B	neck	nucleoside diphosphate kinase 6	43	6.2	TTHERM_000372529	49/61	8.23531e-33
FAP206	RS2 adaptor	FAP206 domain	74	6.03	TTHERM_00820660	33/53	1.47723e-10
FAP251	RS3 base	WD40, EF hand	114	4.8	TTHERM_01262850	29/50	1.27034e-122
FAP198	stalk	Cyt-b5 Cyt-b5	28 28	5.1 5.1	FAP198A TTHERM_01092470 FAP198B TTHERM_00476710	49/69 47/65	1.3317e-53 1.872e-48
FAP207	RS1, RS2 base	MORN	48	4.9	TTHERM_00529880	41/52	2.76951e-48
FAP253/ IQUB/ CMUB116	RS1 base	IQ	49	9	TTHERM_00316930	52/69	4.36935e-87

AKAP - A-kinase anchoring protein; ARF - ADP-ribosylation factor; ARM - armadillo repeat; CC – coiled coil; Cyt-b5 - Cytochrome b5; DNAJ - Hsp40 type protein; DPY-30 – domain found in the Dpy-30 proteins; DUF- domain of unknown function; EF hand - calcium-binding; HEAT - tandemly repeated, amino acid module present in huntingtin, elongation factor 3, alpha regulatory subunit of PP2A, and TOR1; IQ - calmodulin-binding motif; LRR – leucine-rich repeat; ; MORN - Membrane Occupation and Recognition Nexus motif ; RIIa - Regulatory subunit portion of type II PKA R-subunit; WD40 - WD-40 repeats;

Figure 6-figure supplement 3-Table 1B. *Tetrahymena* RSP orthologs identified with multiple hits in TGD. In cases when numerous proteins were identified with similar scores in blastp search of *Tetrahymena* total proteome (TGD) using *Chlamydomonas* RSP as a bait, it was analyzed which of those proteins are present in *Tetrahymena* ciliome (Tables S3 and S4) and either co-immumoprecipitate (co-IP, Table S5) with known RSPs or are biotinylated (BioID, Table S6) in cells expressing known RS proteins as fusions with mutated BirA* ligase. Arrows indicate if there was a significant change (↑ increase or ↓ decrease) in the protein level in studied knock-out mutants (based on TMT analyses, Table S4). ns – change not significant, nd – protein not detected in the *Tetrahymena* ciliome.

		E-value (TGD blastp)	In TMT ciliome	In co-IP or BioID	RSP3A-KO	RSP3B-KO	RSP3C-KO	FAP91-KO

RSP1	**TTHERM_000196029**	1.78444e-19	yes	coIP 3A (1) Bir 3A, 3B, 4A, 4C	ns	↓	ns	ns
RSP10	**TTHERM_00378600**	1.90468e-19	yes	coIP 4A (5/5) Bir 3A, 3B, 4A, 4C	ns	↓	ns	ns
	TTHERM_00338260	7.69708e-19	no	-	-	-	-	-
	TTHERM_00561720	4.08366e-17	yes	nd	ns	ns	ns	ns
	TTHERM_00086700	3.34742e-16	yes	Bir 3B (1), 4A (1)	ns	↓	↓	↓
	TTHERM_00940320	4.65599e-16	no	-	-	-	-	-
	TTHERM_00471440	3.45586e-15	no	-	-	-	-	-
	TTHERM_00522150	6.02902e-15	no	-	-	-	-	-
	TTHERM_00013150	6.59314e-15	no	-	-	-	-	-
	TTHERM_00122390	1.03558e-14	no	-	-	-	-	-
	TTHERM_01044720	4.35786e-14	no	-	-	-	-	-
	TTHERM_00058629	8.15103e-14	yes	nd	ns	↓	ns	ns
	TTHERM_00047490	8.87354e-14	yes	nd	↑	ns	ns	↓
	TTHERM_00080020	1.83831e-13	yes	nd	ns	ns	ns	ns
	TTHERM_00138540	1.85468e-13	no	-	-	-	-	-
	TTHERM_00133460	4.62151e-13	no	-	-	-	-	-
	TTHERM_00149910	5.33197e-13	no	-	-	-	-	-
	TTHERM_00691730	6.19233e-13	no	-	-	-	-	-
	TTHERM_00142460	6.24492e-13	no	-	-	-	-	-
	TTHERM_01248870	6.40885e-13	no	-	-	-	-	-
	TTHERM_00724730	1.06173e-12	no	-	-	-	-	-
	TTHERM_00078940	1.13884e-12	yes	nd	ns	↓	ns	ns
	TTHERM_00685930	1.18943e-12	yes	nd	ns	↓	↓	↓
	TTHERM_00509110	2.45575e-12	yes	nd	ns	ns	↑	ns
	TTHERM_00486410	4.33653e-12	yes	nd	ns	ns	ns	ns
	TTHERM_00590130	5.60043e-12	yes	nd	ns	↓	↓	↓
	TTHERM_00077350	6.44267e-12	yes	nd	ns	ns	ns	ns
	TTHERM_00329860	6.74109e-12	no	-	-	-	-	-
	TTHERM_01084140	8.55508e-12	no	-	-	-	-	-
	TTHERM_00637100	8.74526e-12	no	-	-	-	-	-
	TTHERM_00196080	1.13797e-11	yes	nd	↓	↓	↓	↓
	TTHERM_00766490	1.31424e-10	yes	nd	↓	↓	↓	↓
	TTHERM_00584930	1.95024e-10	yes	nd	↑	↑	ns	↓
	TTHERM_00732890	3.04534e-10	yes	nd	ns	ns	ns	ns
RSP5	TTHERM_00962090	none	yes	nd	↑	ns	↑	↑
	TTHERM_00338200	none	yes	nd	↑	ns	ns	↓
	TTHERM_01080330	none	yes	nd	↑	↑	ns	ns
	TTHERM_00058260	none	yes	nd	↑	↑	ns	ns
	TTHERM_00526310	none	yes	nd	↑	↑	↑	ns
	TTHERM_00300640	none	yes	nd	↑	ns	ns	ns
	TTHERM_00300630	none	yes	nd	ns	↓	↓	ns
	TTHERM_00526449	none	yes	nd	ns	ns	↑	↓
	TTHERM_00274520	none	yes	nd	ns	↓	↓	↓
	TTHERM_00266330	none	yes	nd	ns	↓	ns	ns
	TTHERM_00300620	none	yes	nd	ns	ns	ns	↑

	TTHERM_00703880	none	yes	nd	ns	↑	↑	ns
	TTHERM_01002600	none	yes	nd	ns	ns	↓	↓
RSP7	TTHERM_00353490	7.66049e-13	yes	nd	ns	↑	ns	↑
	TTHERM_00686010	2.22411e-09	no	-	-	-	-	-
	TTHERM_00384910	5.51363e-09	yes	nd	↓	ns	ns	↑
	TTHERM_00632950	1.57971e-08	no	-	-	-	-	-
	TTHERM_00486220	8.14257e-08	no	-	-	-	-	↑
	TTHERM_00523059	1.054e-07	yes	nd	↓	ns	↓	-
	TTHERM_00059190	1.12651e-07	yes	nd	↓	↓	↓	↓
	TTHERM_00668030	2.30983e-07	yes	nd	ns	ns	ns	ns
	TTHERM_000442899 (STK36-like)	4.65608e-07	yes	co-IP RSP4C (1) Bir RSP4A (1-2), 3B (1) 4B (3/3)	ns	↑	ns	↑
	TTHERM_00300120	6.8876e-07	yes	nd	ns	↑	ns	ns
	TTHERM_00630500 (CAM1)	9.98653e-07	yes	Bir 4A (2-3), 3B (1-11) F206 (1)	ns	↓	↓	ns
	TTHERM_00622900	2.83945e-06	no	-	-	-	-	-
	TTHERM_00267880 (BBC37)	4.07889e-06	yes	coIP 3A(1), 4A(4)	ns	↓	↓	↑
	TTHERM_00194410	5.09536e-06	no	-	-	-	-	-
	TTHERM_00616570	5.2479e-06	yes	nd	↓	ns	ns	ns
	TTHERM_00218310	9.61136e-06	yes	nd	ns	↓	↓	↓
	TTHERM_00589960	1.36054e-05	yes	nd	ns	ns	ns	ns
	TTHERM_00899430	1.57e-05	no	-	-	-	-	-
	TTHERM_00495950	1.90483e-05	yes	nd	↑	ns	ns	↑
	TTHERM_01052880	2.2429e-05	yes	nd	ns	↓	ns	↑
	TTHERM_00670610 (RSP7A)	3.31578e-05	yes	co-IP 4A(2), 4B(2), 4C(1), 3A(8) Bir 3A(1-5), 3B(4-13), 3C(11), 4A(14-16), 4C(1-3), 206 (4)	ns	↓	ns	↓
	TTHERM_00637390	4.33175e-05	yes	nd	↑	↓	ns	↓
	TTHERM_000841299	5.08855e-05	no	-	-	-	-	-
	TTHERM_00147620	6.24849e-05	yes	nd	ns	ns	ns	ns
	TTHERM_00492840 (RSP7B)	6.65092e-05	yes	coIP 3A (4), 4A(4), 4B (1) Bir 3B(2), 3C(1), 4A(1), 206(1), 61(3-5)	↑	↑	↑	↓
	TTHERM_00136380	0.00013603	no	-	-	-	-	-
	TTHERM_00079490	0.00017402	yes	nd	ns	↑	ns	ns
	TTHERM_00013440	0.00017893	no	-	-	-	-	-
	TTHERM_00371010	0.00021959	yes	nd	ns	↓	ns	ns
RSP12	TTHERM_00051740	1.0883e-25	yes	Bir 3 A(1 pep)	ns	↑	ns	ns
	TTHERM_00997720	1.64934e-25	no	-	-	-	-	-
	TTHERM_00890120	2.17043e-25	yes	nd	↑	ns	↑	↑
	TTHERM_00243800	1.07131e-22	no	-	-	-	-	-

	TTHERM_00118710	5.99925e-22	yes	nd	ns	↓	↓	ns
	TTHERM_00492720	6.01654e-22	no	-	-	-	-	-
	TTHERM_00548130	4.03513e-21	yes	nd	ns	↓	↓	↑
	TTHERM_01018330	2.06701e-19	yes	coIP 3a (1) BioID4B (4)	ns	↓	↓	↓
	TTHERM_00865350	5.9945e-19	yes	nd	↑	↓	ns	ns
	TTHERM_00877050	1.9254e-18	no	-	-	-	-	-
	TTHERM_00466090	3.9832e-18	yes	Bir 4a (1)	↓	↓	ns	ns
	TTHERM_00075590	7.37871e-18	no	-	-	-	-	-
	TTHERM_00772040	1.51296e-17	no	-	-	-	-	-
	TTHERM_00538480	7.1862e-15	no	-	-	-	-	-
	TTHERM_00757550	0.00121392	no	-	-	-	-	-
	TTHERM_00770670	0.82296	yes	coIP 3A (5/2) 4A (4/4) 4B (2/2) 4C (1/1) FAP251(1-2/1-2)	ns	ns	ns	↓
RSP22	**TTHERM_000649439**	7.13575e-57	yes	coIP 3A (11/5) Bir 3A, 3B, 4A, 4C	ns	↓	ns	ns
	TTHERM_000463528	2.6695e-36	yes	nd	ns	ns	ns	ns
	TTHERM_00449029	7.66385e-31	yes	Bir (1/1)	ns	ns	ns	↓
	TTHERM_000756449	4.69204e-27	yes	nd	ns	ns	ns	ns
	TTHERM_00971840	2.90049e-24	yes	Bir (1/1)	ns	ns	ns	ns
	TTHERM_01079060	8.79124e-21	yes	nd	↓	ns	ns	↑
	TTHERM_00716250	3.10027e-13	yes	Bir (1/1)	ns	ns	ns	ns
	TTHERM_00023950	2.90337e-11	yes	Bir (1/1)	ns	ns	ns	↑
	TTHERM_000442909	5.67464e-07	yes	(1/1) coIP, Bir	ns	ns	ns	ns
FAP207	**TTHERM_00529880**	2.76951e-48	yes	coIP 3A, 4A, 4B, BioID 3A, 4A	ns	↓	ns	↓
	TTHERM_00584930	1.54591e-31	yes	nd	↑	↑	ns	↓
	TTHERM_00047490	1.45891e-27	yes	nd	↑	ns	ns	↓

RSP1 and **RSP10** – proteins contain multiple MORN domains. Using *Chlamydomonas* RSP1 as a bait, *Tetrahymena* RSP1 and RSP10 were identified as a 9th and 36th hits, using *Chlamydomonas* RSP10 as a bait, *Tetrahymena* RSP1 and RSP10 were identified as a 1st and 2nd hits (shown in the Table S1B). The MORN domain-containing **TTHERM_00086700** was reduced in mutants with *RSP3B*, *RSP3C*, or *CFAP91* deletion but was identified among biotinylated proteins only by a single peptide.

RSP5 has a **aldo-keto reductase** domain. The orthologous proteins were not identified in *Tetrahymena* proteome. Table S1B shows analyses of other (non-homologous) proteins described as aldo-keto reductases present in *Tetrahymena* ciliome.

RSP7 – predicted *Tetrahymena* RSP11 is significantly smaller than *Chlamydomonas* paralog, similarity was detected only within N-terminal proteins' region.

RSP12 - **Peptidyl-prolyl cis-trans isomerase**. 8th hit (TTHERM_01018330) has the higher similarity in reverse blastp to *Chlamydomonas* RSP12. Protein TTHERM_00770670 highly reduced in CFAP91-KO cilia, was found in co-IP and BirA* assays but has no similarity to RSP12 in reverse blastp

Figure 6-figure supplement 3-Table 2. Comparative analyses of the levels of the radial spoke proteins in wild-type cells and radial spoke mutants

Radial spoke proteins	Acc numer in TGD	co-IP	BioID	RSP3A-KO/WT				RSP3B-KO/WT				RSP3C-KO/WT				CFAP206-KO/WT		CFAP61-KO/WT		CFAP91-KO/WT			
				LFQ		TMT		LFQ		TMT		LFQ		TMT		LFQ		LFQ		LFQ		TMT	
				q-value	diffe-rence	q-value	diffe-rence	q-value	diffe-rence	q-value	diffe-rence	q-value	diffe-rence	q-value	diffe-rence	q-value	diffe-rence	q-value	diffe-rence	q-value	diffe-rence	q-value	diffe-rence
RSP1	TTHERM_000196029	yes	yes	0.7795	-0.15	0.2168	-0.13	0.0171	-1.54	0.0016	-0.64	0.8424	-0.12	0.5512	-0.07	0.3602	-0.37	0.9789	-0.01	0.6253	0.21	0.1372	-0.13
RSP2	TTHERM_00394410	yes	yes	0.4621	-0.50	0.0414	-0.29	0.0196	-1.54	0.0012	-0.59	0.3111	-0.74	0.3073	-0.13	0.3215	-0.42	0.4980	0.24	0.6309	-0.21	0.5120	-0.05
RSP3A	TTHERM_01044600	yes	yes	0.0025	-5.23	0.0124	-0.99	0.0748	-1.12	0.0029	-0.40	0.7104	-0.22	0.6405	0.05	0.3774	-0.41	0.9426	0.02	0.8836	-0.08	0.0548	0.18
RSP3B	TTHERM_00566810	yes	yes	0.4992	0.41	0.3772	-0.09	0.0010	-5.10	0.0019	-1.15	0.6048	0.30	0.8883	0.02	0.0768	-1.05	0.5058	-0.24	0.0040	-2.61	0.0041	-0.43
RSP3C	TTHERM_00418270	yes	yes	0.9072	-0.06	0.8769	0.02	0.2197	-0.53	0.1760	-0.10	0.0009	-5.47	0.0044	-0.59	0.0085	-3.39	0.3490	0.43	0.0554	-1.69	0.0399	-0.21
RSP4A	TTHERM_00427590	yes	yes	0.7013	-0.20	0.3759	-0.08	0.0320	-1.32	0.0011	-0.49	0.9359	-0.05	0.4944	0.07	0.1033	-0.83	0.7104	0.12	0.2889	-0.40	0.2864	-0.08
RSP4B	TTHERM_00502580	yes	yes	0.3863	-0.80	0.9895	0.002	0.2212	-0.75	0.9626	0.00	0.0082	-4.58	0.0125	-0.79	0.0954	-0.94	0.9786	0.01	0.0484	-2.05	0.0219	-0.26
RSP4C	TTHERM_00444180	yes	yes	0.3744	-0.74	0.1361	-0.18	0.0003	-3.62	0.0017	-0.68	0.5952	-0.27	0.5776	0.07	0.9839	-0.01	0.9724	0.01	0.8082	-0.11	0.6438	-0.03
RSP7B AKA28, EF hand	TTHERM_00492840	yes	yes	0.5596	-0.30	0.0471	0.25	0.7444	-0.16	0.0031	0.35	0.6300	-0.27	0.0271	0.36	0.0815	-3.00	0.3705	-0.42	0.0043	-5.51	0.0020	-0.51
RSP7A RIIAD1/IQ	TTHERM_00670610	yes	yes	0.4480	0.61	0.0700	-0.29	0.0441	-2.04	0.0019	-0.77	0.4556	0.57	0.8805	0.02	0.0963	-1.34	0.8033	-0.08	0.0248	-1.16	0.0044	-0.48
RSP8	TTHERM_00313520	yes	yes	0.0444	-2.31	0.2889	-0.11	0.0180	-4.38	0.0006	-1.34	0.0040	-3.86	0.0017	-0.80	0.0247	-2.51	0.0381	1.12	0.0056	-3.19	0.0006	-1.21
RSP9	TTHERM_00430020	yes	yes	0.7701	-0.15	0.4773	-0.08	0.0190	-1.59	0.0024	-0.40	0.6139	-0.27	0.1883	0.16	0.4841	-0.30	0.3612	-0.37	0.1901	-0.57	0.5680	0.04
RSP10	TTHERM_00378600	yes	yes	0.3694	-0.78	0.4403	-0.08	0.0148	-2.16	0.0012	-0.58	0.3030	-0.79	0.7289	-0.04	0.5293	-0.23	0.7611	0.10	0.6808	-0.18	0.2148	-0.11
RSP11	TTHERM_00540090	yes	yes	0.2115	-1.53	0.0307	-0.31	0.0111	-4.64	0.0011	-0.49	0.0869	-2.04	0.0367	-0.35	0.5919	1.14	0.1085	2.76	0.6309	1.01	0.0548	-0.20
RSP12A	TTHERM_01018330	no	no	0.9256	0.05	0.2392	0.11	0.0161	-2.27	0.0079	-0.29	0.0010	-4.46	0.0118	-0.45	0.0096	-2.20	0.5560	-0.26	0.0036	-3.28	0.0019	-0.53
RSP12B	TTHERM_00466090	no	yes	nd		0.0102	-0.48	nd		0.0000	-0.68	nd		0.0807	0.24	nd		nd		nd		0.5789	0.04
RSP14	TTHERM_000773538	yes	yes	0.0377	-2.51	0.0045	-0.74	0.0146	-2.40	0.0010	-0.52	0.3733	-0.65	0.8355	0.02	0.6305	-0.24	0.1018	0.72	0.0130	1.08	0.0172	0.31
RSP15/LRRC34	TTHERM_00695730	yes	yes	0.2194	-1.21	0.5601	-0.06	0.0120	-3.67	0.0019	-0.86	0.1759	-1.49	0.2321	-0.17	0.0080	-2.91	0.3356	-0.88	0.0042	-5.13	0.0038	-0.97
RSP16A	TTHERM_00471260	yes	yes	0.0406	-2.62	0.0253	-0.33	0.0216	-2.25	0.0013	-0.56	0.0968	-1.59	0.5844	-0.07	0.3365	-0.51	0.2292	0.54	0.4597	0.35	0.4636	0.05
RSP16B	TTHERM_00238810	yes	yes	0.8796	-0.08	0.3494	0.10	0.3395	-0.40	0.6381	0.03	0.0121	-5.13	0.0064	-0.67	0.0092	-1.92	0.8685	-0.05	0.0078	-1.24	0.0354	-0.22
RSP20/CaM1	TTHERM_00630500	no	no	nd		0.1719	-0.20	nd		0.0240	-0.32	nd		0.0117	-0.67	0.1659	-2.02	0.0406	1.00	0.0049	-3.10	0.3203	0.10
calmodulin 7-2	TTHERM_00549500	yes	yes	0.0484	-2.36	0.0186	-0.38	0.1804	-0.83	0.3745	-0.06	0.0061	-4.45	0.0130	-0.44	0.6666	-0.22	0.9592	0.02	0.8873	-0.08	0.1067	0.14
RSP22/LC8	TTHERM_000649439	yes	yes	0.0666	-2.53	0.4513	-0.08	0.0439	-1.62	0.0027	-0.42	0.0461	-3.36	0.2872	0.11	0.0952	-1.00	0.2773	0.5	0.4440	-0.38	0.2457	0.08
RSP23B/FAP67B	TTHERM_000372529	yes	yes	0.6087	-0.29	0.9553	-0.01	0.7482	-0.16	0.6381	0.03	0.6874	-0.26	0.6799	0.04	0.5172	-0.25	0.5812	0.19	0.9600	0.03	0.0188	0.27
RSP19/FAP61	TTHERM_00641200	yes	yes	0.5334	-0.39	0.0010	1.32	0.5872	-0.23	0.0002	1.41	0.5468	-0.36	0.0044	1.46	0.6809	-0.16	0.0128	-3.60	0.0044	-3.56	0.1182	0.13
FAP251	TTHERM_01262850	yes	yes	0.7834	-0.15	0.3688	0.09	0.6187	-0.23	0.4797	0.04	0.9708	-0.02	0.0437	0.28	0.3754	-0.34	0.9176	-0.03	0.0049	-5.61	0.0095	-0.88
RSP18/FAP91	TTHERM_00578560	yes	yes	0.6777	-0.21	0.3425	0.10	0.2540	-0.54	0.1045	-0.13	0.5640	-0.34	0.2188	0.14	0.3221	-0.40	0.7473	-0.10	0.0035	-5.85	0.0089	-0.97
FAP206	TTHERM_00820660	yes	yes	0.8793	-0.08	0.4950	0.07	0.0008	-4.04	0.0074	-1.04	0.6660	-0.22	0.3175	-0.16	0.0139	-4.67	0.2723	-0.46	0.0041	-4.55	0.0083	-1.37
FAP253	TTHERM_00316930	yes	yes	0.6415	-0.24	0.3314	-0.09	0.8457	-0.09	0.1084	0.12	0.5416	-0.36	0.4070	0.09	0.5152	-0.45	0.3267	0.55	0.6564	0.27	0.0557	0.18
FAP207	TTHERM_00529880	yes	yes	0.8223	-0.12	0.5520	0.06	0.0137	-3.31	0.0040	-0.90	0.5665	-0.32	0.9967	0.00	0.0157	-3.76	0.4082	-0.29	0.0177	-3.93	0.0024	-1.08
FAP198A/CYB5D1	TTHERM_01092470	yes	yes	0.8513	-0.09	0.0085	-0.55	0.4064	-0.34	0.0004	-0.98	0.0889	-2.42	0.0710	0.25	0.3138	-0.76	0.2017	-1.37	0.5137	0.84	0.0423	0.20
FAP198B/CYB5D1	TTHERM_00476710	yes	yes	0.8513	-0.09	0.0927	0.23	0.4064	-0.34	0.4849	0.05	0.0889	-2.42	0.0177	-0.45	0.1449	-1.85	0.2997	-1.01	0.0467	-1.51	0.1430	-0.14
FAP296	TTHERM_01016220	no	no	nd		0.2675	-0.13	nd		0.4282	-0.06	nd		0.4993	0.08	nd		nd		nd		0.2818	-0.09
FAP299	TTHERM_00427460	yes	yes	0.8343	0.12	0.2473	0.12	0.5220	0.27	0.0305	0.21	0.6862	0.24	0.0518	0.27	0.3679	-0.38	0.868026	-0.05	0.9871	0.01	0.0982	0.15

Significant reduction or increase of the protein level are marked in red or blue, respectively; TGD – Tetrahymena Genome Database; LFQ – label-free quantification, TMT- tandem mass tag 10-plex isobaric mass tagging approaches.

Figure 6-figure supplement 3-Table 3. Comparative analyses of the levels of potential radial spoke-associated proteins in wild-type cells and radial spoke mutants

Protein name	Acc number in TGD	Co-IP	BioID	RSP3A-KO/WT				RSP3B-KO/WT				RSP3C-KO/WT				CFAP206-KO/WT		CFAP61-KO/WT		CFAP91-KO/WT			
potential RS-associated proteins				LFQ		TMT		LFQ		TMT		LFQ		TMT		LFQ		LFQ		LFQ		TMT	
				q-value	diffe-rence	q-value	diffe-rence	q-value	diffe-rence	q-value	diffe-rence	q-value	diffe-rence	q-value	diffe-rence	q-value	diffe-rence	q-value	diffe-rence	q-value	diffe-rence	q-value	diffe-rence
TtTPR1	TTHERM_00623040	yes	yes	0.4441	-0.77	0.6006	-0.05	0.1834	-0.66	0.9062	-0.01	0.0091	-3.42	0.0116	-0.56	0.0256	-2.01	0.7405	0.14	0.0683	-1.95	0.1189	-0.14
TtTPR2	TTHERM_00221090	yes	yes	0.9944	0.01	0.8607	0.02	0.0192	-2.31	0.0035	-0.34	0.4491	-0.66	0.1096	0.20	0.1426	-1.10	0.3186	-0.52	0.0033	-2.22	0.0821	-0.16
kelch-motif containing 1	TTHERM_00760390	yes	yes	0.9112	0.06	0.8595	0.02	0.8452	-0.09	0.1661	0.11	0.9543	-0.04	0.2436	0.14	0.6226	-0.23	0.5444	0.23	0.0053	-3.87	0.0017	-0.52
kelch-motif containing 2	TTHERM_00532180	no	yes	0.3220	-1.39	0.8817	0.02	0.0135	-3.18	0.0099	-0.30	0.2992	-1.49	0.8341	-0.02	0.1784	-1.51	0.4491	0.71	0.0646	-1.85	0.9241	-0.01
LRRC23A	TTHERM_000703669	yes	yes	0.2089	-1.02	0.0663	0.23	0.3478	-0.45	0.0339	0.21	0.2615	-1.73	0.0178	0.42	0.2243	-1.41	0.7830	-0.10	0.0035	-4.12	0.0014	-1.16
LRRC23B	TTHERM_00105260	yes	yes	0.7001	-0.22	0.6874	0.04	0.3550	-0.40	0.1415	0.12	0.4826	-0.45	0.0131	0.46	0.1661	-0.60	0.0477	-0.94	0.0034	-6.02	0.0003	-1.12
LRRC45	TTHERM_01220370			0.5447	-0.36	0.9962	0.00	0.4854	-0.30	0.1142	0.13	0.4139	-0.64	0.7251	0.04	0.3822	-0.39	0.5476	0.20	0.7461	-0.14	0.1612	0.12
LRR-containing	TTHERM_01084360	no	no	0.5992	0.27	0.0605	0.26	0.1355	-0.95	0.0019	-0.40	0.4602	-0.45	0.0285	0.34	0.0682	-2.21	0.0770	-1.45	0.0085	-1.27	0.0132	-0.32
CCDC104/FAP36	TTHERM_00557860	yes	yes	0.6816	0.46	0.0116	-0.72	0.0646	-1.20	0.0006	-1.27	0.6020	0.45	0.0017	-0.77	0.1204	1.10	0.0180	1.68	0.0083	-2.01	0.0017	-0.84
sperm-tail PG-rich repeat protein 1	TTHERM_00549640	no	no	0.8430	0.16	0.0267	-0.36	0.0337	-1.43	0.0170	-0.29	0.9056	0.08	0.0044	0.81	0.1105	-0.94	0.0546	-1.59	0.0147	-3.47	0.0354	-0.90
sperm-tail PG-rich repeat protein 2	TTHERM_00420710	no	no	0.5100	0.64	0.1000	-0.20	0.1549	-0.77	0.0028	-0.38	0.3054	1.02	0.1326	-0.18	0.0186	-3.18	0.1492	-0.64	0.0089	-3.72	0.1069	-0.14
EF-hand protein	TTHERM_00637390	no	no	0.4234	-0.75	0.0310	0.31	0.1381	-1.27	0.0278	-0.22	0.5102	-0.62	0.8047	0.03	0.3778	0.83	0.1814	1.43	0.0249	-2.21	0.0026	-0.46
EF-hand protein	TTHERM_00649260	yes	yes	0.5110	-0.39	0.8682	0.02	0.2456	0.48	0.0146	0.27	0.9841	-0.01	0.3052	0.11	0.9272	-0.05	0.2987	0.43	0.7630	-0.17	0.7626	-0.02
EF-hand protein	TTHERM_00193760	yes	yes	0.4058	-0.77	0.5332	-0.06	0.2303	-0.68	0.1101	-0.12	0.3828	-0.76	0.3680	-0.10	0.4723	-0.26	0.6762	0.13	0.0364	-0.93	0.0834	0.15

Significant reduction or increase of the protein level are marked in red or blue, respectively; TGD – Tetrahymena Genome Database; LFQ – label-free quantification, TMT- tandem mass tag 10-plex isobaric mass tagging approaches.

Figure 6-figure supplement 3-Table 4. Comparative analyses of the levels of proteins with an enzymatic activities in radial spoke mutants

Enzyme name	Acc numer in TGD	Co-IP	BioID	RSP3A-KO/WT				RSP3B-KO/WT				RSP3C-KO/WT				CFAP206-KO/WT		CFAP61-KO/WT		CFAP91-KO/WT			
ATP homeostasis				LFQ		TMT		LFQ		TMT		LFQ		TMT		LFQ		LFQ		LFQ		TMT	
				q-value	diffe-rence	q-value	diffe-rence	q-value	diffe-rence	q-value	diffe-rence	q-value	diffe-rence	q-value	diffe-rence	q-value	diffe-rence	q-value	diffe-rence	q-value	diffe-rence	q-value	diffe-rence
ENO1	TTHERM_00486480	no	no	0.8338	-0.23	0.0188	0.42	**0.0195**	**-1.96**	**0.0113**	**-0.29**	0.3673	-1.58	0.5140	0.08	0.0981	-0.80	**0.0662**	**-2.76**	**0.0045**	**-3.83**	**0.0015**	**-0.49**
PYK1 (PYruvate Kinase)	TTHERM_00118600	no	no	0.3864	1.07	**0.0089**	**0.59**	**0.0526**	**-1.93**	**0.0081**	**-0.31**	0.2726	-2.11	0.1047	-0.22	0.1606	-0.72	**0.0176**	**-1.77**	**0.0042**	**-6.35**	0.2339	-0.09
adenylate kinase 1, AK1	TTHERM_00317200	yes	yes	0.2096	-1.03	0.2215	-0.12	**0.0186**	**-1.50**	**0.0010**	**-0.49**	0.2443	-0.93	0.4282	-0.09	0.3223	-0.43	0.4288	0.29	0.2574	-0.43	**0.0346**	**-0.22**
adenylate kinase 7A, AK7A	TTHERM_00558060	yes	yes	0.9677	-0.02	0.0706	0.23	0.2455	-0.51	0.6449	0.03	0.9148	-0.06	0.0778	0.24	0.3148	-0.43	0.2183	-0.45	**0.0095**	**-3.57**	**0.0089**	**-0.37**
adenylate kinase 7B, AK7B	TTHERM_000569069	yes	yes	0.6181	-0.27	0.0196	0.33	0.3412	-0.42	0.0116	0.28	0.5422	-0.36	0.0306	0.35	0.3047	-0.42	0.1970	-0.53	**0.0048**	**-6.74**	**0.0000**	**-0.99**
adenylate kinase 8A, AK8A	TTHERM_00227800	yes	yes	0.5095	-0.41	0.4586	0.07	**0.0181**	**-1.80**	**0.0111**	**-0.28**	0.2103	-1.10	0.6136	-0.05	0.1451	-0.69	0.1838	0.54	0.6095	0.22	0.1733	-0.11
adenylate kinase 8B, AK8B	TTHERM_00455540	yes	yes	**0.0003**	**-4.12**	**0.0065**	**-0.60**	0.1562	-0.73	0.0723	-0.16	0.8016	0.14	0.2832	0.12	0.5638	-0.25	0.5959	0.18	0.2885	0.41	**0.0134**	**0.31**
adenylate kinase 9, AK9	TTHERM_00148750	yes	yes	0.4987	-0.40	0.0318	0.30	0.2744	-0.44	0.0031	0.35	0.4566	-0.48	0.0129	0.45	0.4154	-0.30	0.1851	-0.49	**0.0034**	**-5.47**	**0.0047**	**-0.76**
arginine kinase 2, AK2	TTHERM_00151390	no	no	0.3877	-1.80	0.0025	1.28	**0.0016**	**-4.46**	**0.0009**	**-0.54**	0.0910	-2.16	0.0083	0.66	**0.0171**	**-6.23**	**0.0107**	**-5.07**	**0.0034**	**-5.39**	**0.0020**	**-0.61**
cGMP -related enzymes																							
guanylate kinase 1	TTHERM_00781030	yes	yes	0.5794	-0.30	0.8152	0.02	0.3717	-0.41	0.0244	0.23	0.5953	-0.33	0.0659	0.25	0.4619	-0.33	0.4632	-0.31	**0.0048**	**-4.83**	**0.0004**	**-1.35**
3'5'-cyclic nucleotide phosphodiesterase	TTHERM_00293350	no	yes	0.4822	-0.50	0.0101	0.53	0.3325	-0.43	0.0011	0.55	0.5061	-0.49	0.0201	0.75	0.7072	-0.18	**0.0107**	**-4.61**	**0.0053**	**-5.50**	**0.0040**	**-0.65**
NDK, nucleoside diphosphate kinase	TTHERM_000160999	no	no	0.3841	1.98	0.0450	0.32	0.2471	-1.28	**0.0013**	**-1.07**	0.9015	0.21	**0.0136**	**-0.51**	0.9075	0.07	0.2269	-0.56	0.0076	-1.45	0.8180	0.02
Ser/thre kinases																							
caseine kinase 1, CK1,	TTHERM_00938880	yes	yes	0.3214	-1.20	0.0153	0.43	0.1869	-0.79	0.0009	0.48	0.3032	-0.90	0.0172	0.47	0.3752	-0.42	**0.0398**	**-1.77**	**0.0040**	**-3.45**	**0.0215**	**-0.32**
calcium/calmodulin-dependent protein kinase	TTHERM_01344710	no	no	0.9064	-0.07	0.2161	-0.129	**0.0317**	**-1.283**	**0**	**-0.88**	0.4734	-0.65	**0.011**	**-0.47**	**0.038**	**-2.17**	0.154	-0.63	**0.0075**	**-4.29**	**0.0016**	**-0.47**
STK36-like	TTHERM_000442899	yes	yes	0.4018	-0.8	0.3671	0.096	0.5252	0.28	**0.0028**	**0.44**	0.5808	-0.29	0.6694	0.05	0.0774	1.13	0.0835	0.87	**0.0078**	**1.48**	**0.0469**	**0.23**
cAMP-dependent kinase catalytic subunit	TTHERM_00433420	yes	yes	0.7840	0.21	0.6428	-0.04	0.0831	-1.36	**0.0000**	**-0.98**	0.5403	-0.59	**0.0000**	**-0.61**	0.9273	-0.05	0.2436	0.49	0.0206	-1.50	**0.0037**	**-0.38**
cAMP-dependent kinase catalytic subunit	TTHERM_00658860	no	no	0.5455	-0.68	0.1637	-0.16	0.1845	-1.16	**0.0019**	**-0.63**	0.3813	-1.09	0.1141	-0.23	0.2830	0.55	0.3487	0.43	0.0075	-3.58	0.7250	0.03
cAMP-dependent kinase regulatory protein	TTHERM_00623090	yes	yes	0.8422	0.18	0.3634	-0.09	**0.0103**	**-3.57**	**0.0035**	**-1.04**	0.8085	0.19	**0.0120**	**-0.47**	0.0945	-0.96	0.6476	-0.16	**0.0073**	**-3.93**	**0.0186**	**-0.27**

Significant reduction or increase of the protein level are marked in red or blue, respectively; TGD – Tetrahymena Genome Database; LFQ – label-free quantification, TMT- tandem mass tag 10-plex isobaric mass tagging approaches.